AD-A096 167 HUGHES AIRCRAFT CO FULLERTON CA GROUND SYSTEMS GROUP F/G 17/1
ADAPTIVE TRACKING SYSTEM STUDY.(U)
OCT 80 P L FEINTUCH, F A REED, N J BERSHAD N00024-79-C-6405
UNCLASSIFIED HAC-FR81-11-70 NL

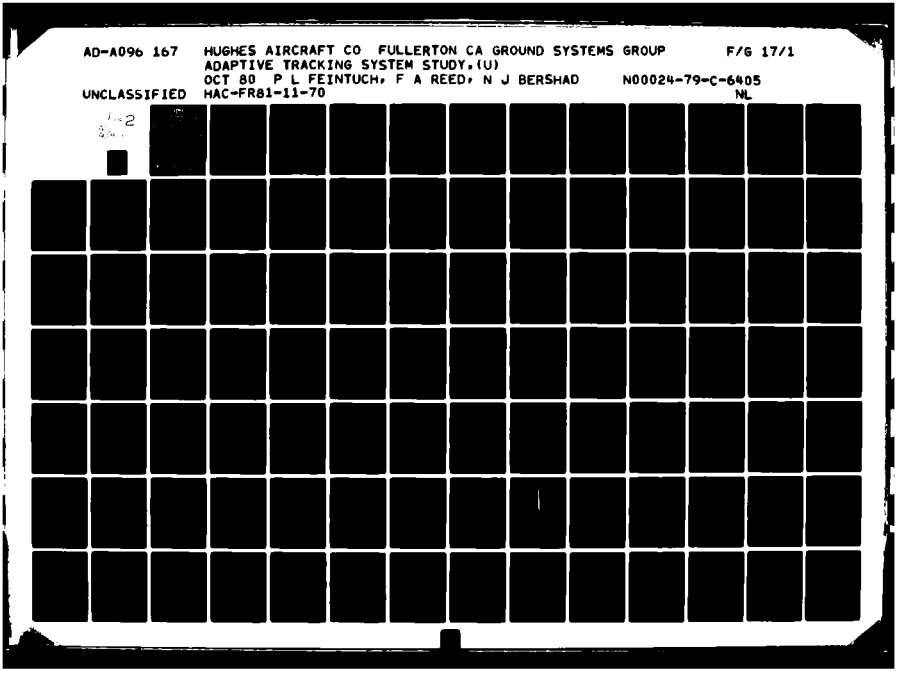

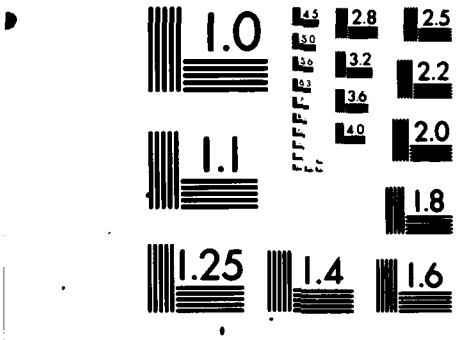

FR81-11-70

FINAL REPORT ON PHASE 3

OF THE

ADAPTIVE TRACKING SYSTEM STUDY

October 1980

Prepared Under

Contract Number N00024-79-C-6405

For The

Naval Sea Systems Command Code 63R

Hughes Aircraft Company
Ground Systems Group
Fullerton, California

FR81-11-70

FINAL REPORT ON PHASE 3
OF THE
ADAPTIVE TRACKING SYSTEM STUDY

OCTOBER 1980

Prepared Under

Contract Number N00024-79-C-6405

For the

Naval Sea Systems Command 63R

By

P. L. Feintuch
F. A. Reed
N. J. Bershad
C. M. Flynn

Hughes Aircraft Company
Ground Systems Group
Fullerton, California

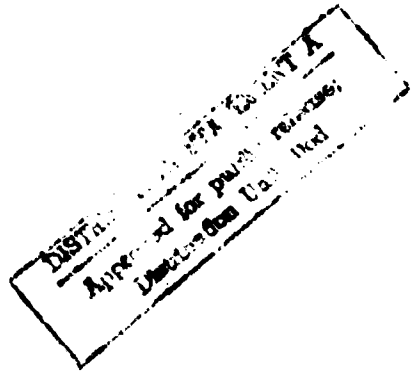

FOREWORD

This report, and the associated Secret Supplement, documents the third phase of the effort performed for the Naval Sea Systems Command Code 63R-11 under Contract N00024-79-C-6405, and covers the period from October 1979 to October 1980. This study has as its goal the examination of adaptive filters to passive sonar bearing tracking. This has been accomplished via statistical modeling and analysis, with verification by simulation on computer generated data and data recorded at sea.

ACKNOWLEDGEMENTS

This work was directed by Mr. Daniel E. Porter of NAVSEA Code 63R. The studies were performed at Hughes by the principal investigator, Dr. Paul L. Feintuch, with the major analytic support of Mr. Francis A. Reed. Consulting services were provided by Dr. N. J. Bershad, and the computer simulations were performed by Mr. Curtis M. Flynn

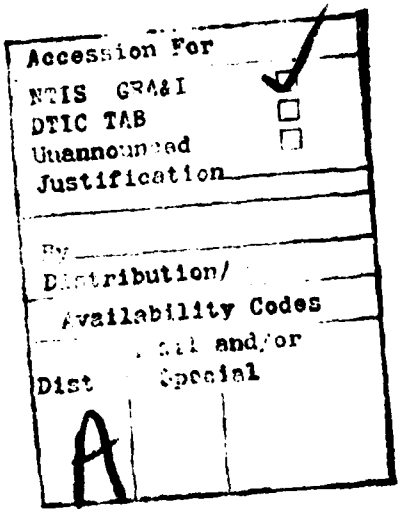

TABLE OF CONTENTS

SECTION 1.0

INTRODUCTION

1.0 INTRODUCTION

This is the Final report on phase three of the Adaptive Tracking System Study, which considers the application of adaptive filtering to passive sonar bearing estimation. The study was initiated because the adaptive filter structure seemed well suited to bearing estimation problems involving unknown input statistics and dynamic targets. In particular, (a) an adaptive filter does not require a priori power spectral information on signal and noise fields, (b) because it is iterative, it can track non-stationary inputs while preserving its underlying minimum mean square optimality criterion, and (c) since all the correlation information between adaptive filter inputs is contained in the filter weights, the potential exists to perform both broadband and narrowband tracking simultaneously.

The first phase of this study [1] addressed the feasibility of such a tracker using the Least Mean Square (LMS) adaptive filter algorithm, and developed the tracker structure of Figure 1. In this structure, the two beamformed split array outputs are provided as the two inputs to an LMS adaptive filter configured as a canceller. The output of one half array, processed by a non-recursive adaptive filter, is subtracted from the other half array to yield an error signal. The error signal is then used to recursively update the adaptive filter weights, or impulse response, such that the mean square error is minimized. If x(nTs) and d(nTs) are the two inputs, with T_s the sample rate and n the time index, the adaptive filter stores the data vector

$$\underline{X}(n) = \left[x\left[nTs\right], x\left[(n-1)Ts\right], \ldots x\left[(n-M+1)Ts\right]\right]^T \quad (1)$$

where $\underline{X}^T$ denotes $\underline{X}$ transpose. The output of the adaptive filter is

$$y(n) = \underline{W}^T(n)\underline{X}(n) \quad (2)$$

where $\underline{W}(n)$ is a vector of M weights at time nT_s. The error output is therefore

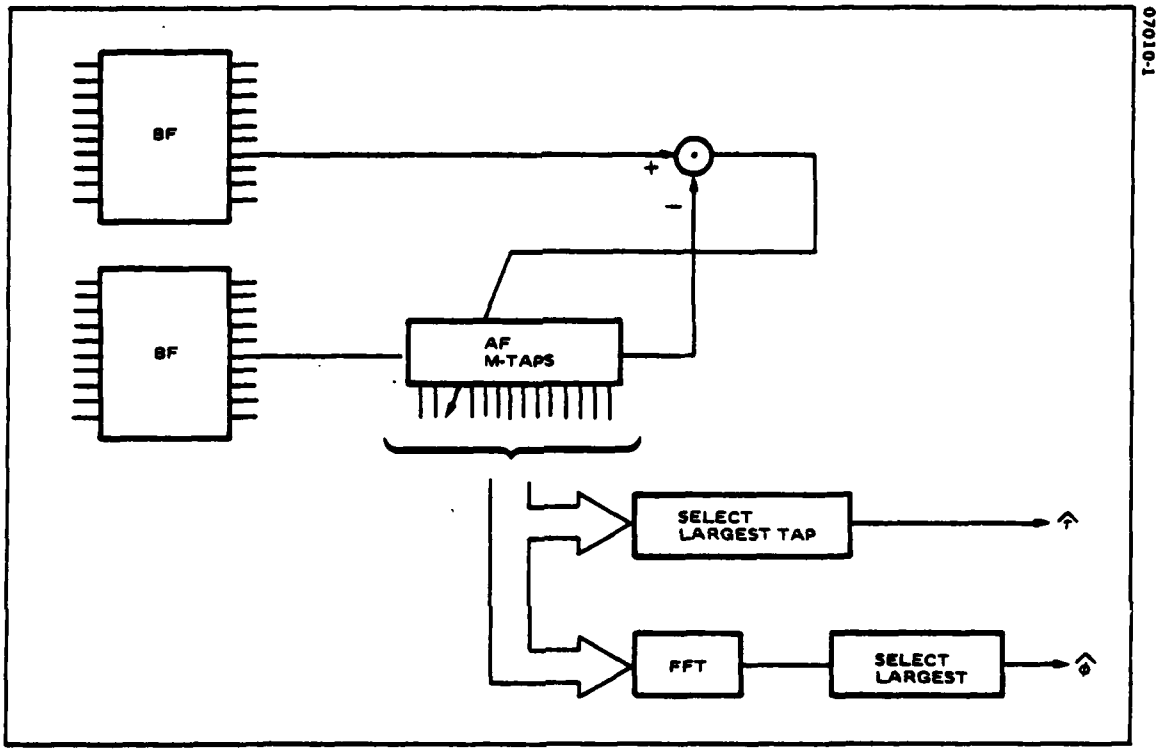

Figure 1. Adaptive Tracker Structure

Figure 1. Adaptive Tracker Structure

$$\epsilon(n) = d(n) - \underline{W}^T(n)\underline{X}(n). \quad (3)$$

The LMS algorithm updates the weight vector on each iteration as

$$\underline{W}(n+1) = \underline{W}(n) + \mu\, \epsilon(n)\underline{X}(n) \quad (4)$$

where μ is a weight update coefficient. This parameter controls the rate of convergence, algorithm noise, and, ultimately, the stability of the algorithm.

In converging to minimize the mean square error between half array outputs, the adaptive filter must incorporate any time delay (or for narrowband sources, phase shift) between its inputs in the weight vector. For broadband inputs, the weights have the same shape as the signal autocorrelation function with the peak located at the delay between the phase centers. Hence, the tracker must determine the location of the peak of the weights, using interpolation between discrete taps if necessary. For sinusoidal inputs, the weights converge to a sinusoid with phase equal to the phase shift between array halves. The tracker then determines the phase shift by means of spectrum analysis of the weight vector. Either the time delay or phase shift is easily converted to a bearing estimate.

The first phase of the study also provided many of the analytical techniques required for analysis of the adaptive tracker. In particular, it provided the frequency domain model for the adaptive tracker shown in Figure 2. In the frequency domain version, the two inputs are Fast Fourier Transformed (FFT'd) and a single tap, complex LMS adaptive filter performed independently to the time domain filter, both in transient and steady state operation, under certain conditions on the filter design parameters. The primary advantage of the frequency domain model is that both the mean and variance of the weights can be predicted. By careful selection of filter parameters, this model can then be used to predict the variance of the time domain weights, which cannot be obtained by analysis in the time domain.

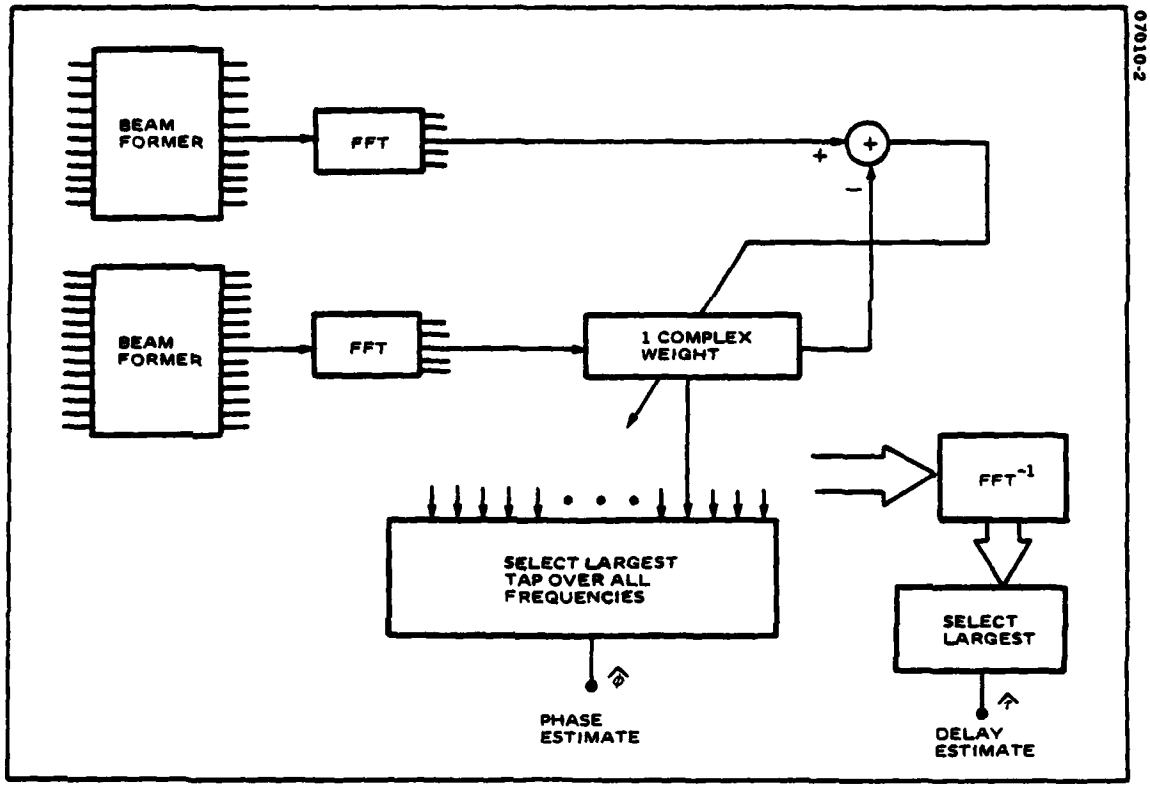

Figure 2. Frequency Domain Model for the Adaptive Tracker

Figure 2. Frequency Domain Model for the Adaptive Tracker

Given the statistics of the time and frequency domain weights, it was possible to obtain predictions of the bearing estimate statistics for broadband inputs. A continuous broadband adaptive tracker was shown to perform within 0.5 dB of the Cramer-Rao Lower Bound on the variance of all unbiased estimators. Performance results were also derived for a practical realization of the tracker, operating at a reasonable sampling rate with interpolation between samples providing fine delay (hence bearing) resolution. These results were shown to be comparable to a conventional tracker. The first phase of the study also developed the mean weight of the adaptive filter with dynamic broadband and narrowband inputs. The results were applied in Phase Two in the analysis of the tracker performance for dynamic targets. Finally, the first phase developed extensive simulation programs for the tracker structure, which were used to validate the analyses, and provide an initial look at dynamic tracking performance.

The second phase of the study [2] considered in detail the potential advantages of the adaptive tracker with combined broadband and narrowband inputs, unknown a priori input spectra, and dynamic targets. The bearing estimate variance was determined analytically for narrowband targets, combined narrowband and broadband targets, and narrowband targets in the presense of a broadband interference. For a high signal to noise ratio narrowband target, the adaptive tracker was shown to perform within 0.5 dB of the Cramer-Rao lower bound on the variance of any unbiased estimator operating on the same observations. It was also shown that in the presense of interference, the bias of the estimate dominates the bearing error for low SNR targets.

The adaptive tracker was compared to a conventional split bearing tracker when the a priori assumptions on the input spectra were incorrect. The adaptive tracker

was shown to be significantly more tolerant of changes in the input spectra than conventional trackers. Whether this advantage can be realized in actual practice will depend upon the degree to which input spectra vary in actual sonar environments.

An analysis comparing the adaptive tracker and a conventional split bearing tracker with moving targets was also performed. For a specific input correlation function, the adaptive tracker was shown to be about 1.6 dB bettern than the conventional tracker.

The third phase of the study concentrated in three areas. It continued the analytical evaluation of the tracker to include such effects as multipath, arrays, and use of adaptive cancellers prior to the tracker to reject interferences. Secondly, it considered the implementation and operation of the tracker in a sonar environment, addressing an improved interpolator, multi-target tracking, beam-to-beam handover, and combined broadband and narrowband tracking. Finally, it utilized sea tape data to evaluate tracker performance of the broadband and narrowband trackers with actual targets.

This report is organized into five sections, including this introduction. Section 2.0 discusses the system aspects of applying the adaptive tracker in an actual sonar environment and considers the efficient implementation of the algorithm. An overall systems block diagram of a potential adaptive tracking system is developed. Section 3.0 summarizes the results of the performance analyses and simulations done during the third phase. These are presented without detailed descriptions and derivations, which are included as appendices. Section 4.0 presents the results of simulations with sea tapes of broadband targets. Section 5.0 provides an overview of the three phases of the Adaptive Tracking System Study and presents

conclusions resulting from the results of all three phase. In addition to these five sections, there is a classified supplement to this report which deals with simulation of the tracker with classified sea tapes.

SECTION 2.0

SYSTEMS CONSIDERATION FOR ADAPTIVE TRACKER IMPLEMENTATION

2.0 SYSTEMS CONSIDERATIONS FOR ADAPTIVE TRACKER IMPLEMENTATION

Most of the analyses and simulations of the adaptive tracker to date have attempted to isolate the sensitivities of the tracker to various input parameters by considering relatively simple input signals, such as pure broadband, single sinusoid, broadband plus a single sinusoid, etc. In processing sea tape data, however, the inputs are not controlled, and the tracker must accommodate the range of signal and noise environments that would be encountered by an operational tracker. These include combined broadband and narrowband targets, broadband and narrowband interferences, multiple targets, multipath arrivals from a given target, and beam-to-beam handover of moving targets. These issues are simplified significantly by first considering the function of the tracker and the way in which it would be used operationally.

Inherent in the function of a tracker is the assumption that a source of interest has been detected, and that the tracker is assigned, by an operator, to track that source. For the broadband tracker, this implies that the nominal source bearing is known, so that the split beams can be steered such that the peak of the weight vector appears in a relatively short adaptive filter. The actual detection and determination of the approximate bearing will have been made by an available search sonar. Assignment of a narrowband tracker requires not only detection and nominal bearing of a source, but knowledge that the source radiates a narrowband component. This knowledge implies detection of the narrowband component and the availability of its approximate frequency. The narrowband tracker is then assigned to given narrowband components by providing the tracker with this coarse frequency estimate, as well as the bearing required to steer the split beams. If multiple lines or multiple targets are present, the operator

selects which of these is appropriate for tracking, and assigns the tracker according to his judgment. Multiple target and line considerations are of interest only in that they may interfere with the ability of the tracker to maintain track on the source to which it was assigned. There is no need for the tracker to determine the presence of multiple targets or to choose among those present.

With this bit of philosophy in mind, issues of interest in the practical implementation of the tracker are discussed below.

2.1 Combined Implementation of a Broadband and Narrowband Tracker

One of the attractive features of the adaptive tracker is its ability to track, via the weight vector, narrowband and broadband signal components simultaneously. To extract the bearing related to a broadband component, the peak of the time domain weight vector is located, and its time coordinate converted to a bearing. For the narrowband signal, the weight vector is Fast Fourier Transformed (FFT'd) and the phase of the bin with the largest magnitude is converted to a bearing. This assumes that the FFT has sufficient resolution that the narrowband component is approximately bin centered.

Two avenues are possible to provide increased resolution in time delay, hence, increased bearing accuracy for broadband targets; use of a high sampling rate, many times the Nyquist rate, or interpolation between discrete taps at a sample rate only slightly above the Nyquist rate (some oversampling is required to produce correlated samples so that the interpolator will work). The high computational cost of the LMS algorithm makes use of a high sample rate impractical. This combined with the computational efficiency and performance of the quadratic interpolator makes the choice of a lower sample rate obvious.

The ability to operate near the Nyquist rate may, in fact, be an advantage of the adaptive tracker over other methods.

In the narrowband tracker, frequency resolution serves two functions. It provides sufficient gain against the broadband background noise to allow extraction of a high quality estimate of both the signal phase and frequency as needed for determination of bearing. Analogous to the broadband case, this could be provided by high resolution in the frequency domain weight vector, or by interpolating between somewhat coarser frequency bins. In simulations to date, the resolution has been provided by using narrow frequency cells in the frequency domain weight vector. For these purely narrowband simulations, the total bandwidth has been relatively narrow, so this approach has not led to large filter lengths. In a system for combined broadband and narrowband use, this will not be the case, however. Consider a system with total bandwidth, B_t, and sample rate kB_t. For the sonar to have a beamwidth of θ_B, the array aperture must be nominally

$$L = \frac{50}{\theta_B/\lambda} \tag{5}$$

where λ is the wavelength at the design frequency. Let

$$\lambda = \frac{c}{B_t}$$

so that the design frequency coincides with the high end of the band, so

$$L = \frac{50\ c}{\theta_B B_t} \tag{6}$$

The maximum propagation time between array phase centers (corresponding to a target that is endfire relative to those phase centers) is then

$$\tau_{max} = \frac{L}{2c} = \frac{25}{\theta_B B_t} \tag{7}$$

In practice the actual maximum will be much less because a single beam will not track over the entire range of broadside to endfire. The number of taps must provide $\pm \tau_{max}$ seconds,

$$2\tau_{max} = MTs$$

or

$$M = \frac{2\tau_{max}}{T_s} = \frac{50/\theta_B B_t}{1/kB_t} = \frac{50k}{\theta_B} \tag{8}$$

If k is on the order of 3 to 5, then in most sonars, less than 50 taps would be required. On the other hand, if a frequency resolution of F_r is required, then

$$F_r = \frac{1}{MT_s} = \frac{kB_t}{M} \tag{9}$$

so

$$M = \frac{kB_t}{F_r} \tag{10}$$

It is not at all uncommon for B_t/F_r to be 1000 or more in narrowband detection systems, so clearly if the filter size is used to provide resolution then the frequency domain estimator is the primary determinant of M, and the time extent of the filter, MTs, will be much larger than is required for the broadband tracker.

The primary computational load of the adaptive tracker is the LMS algorithm itself, particularly if it is implemented in the time domain. The number of computations in the LMS algorithm is proportional to the length of the adaptive filter, M, so that the large filter sizes needed to provide frequency resolution over the entire input band will drive the computational cost far beyond that required by the broadband tracker. This can be mitigated somewhat by a frequency domain implementation of the LMS algorithm, but as discussed in the following section, this is not always practical.

The size of the adaptive filter not only impacts the computational cost per iteration of the tracker. The algorithm noise is directly proportional to the filter length, so that providing the longer adaptive filters necessary for narrowband tracking will reduce the performance of the tracker unless this noise is reduced by decreasing μ. However, decreasing μ, which increases the time constant of the filter, degrades the performance of the tracker in the presence of target dynamics or changing spectra. Further, use of small values of μ may require higher precision in the implementation of the device.

Given the effects of the filter length, M, on the computational cost and performance of the adaptive tracker, it makes sense to maintain as coarse a resolution as possible in the computation of the frequency domain weight vector. Then, using the approximate value of the frequency of the narrowband component provided in the assignment of the tracker, some method of interpolation could hopefully be used in that vicinity to provide higher resolution over a limited band.

In Appendix A of [2], the mean and variance of the frequency domain weight vector were derived for a sinudoid embedded in white noise. The steady state mean weight in the k^{th} FFT bin is

$$E\{W_k(\omega)\} = \frac{|G(k,\omega_o)|^2 \sigma_s^2}{|G(k,\omega_o)|^2 \sigma_s^2 + M\sigma_n^2} e^{-j\omega_o \frac{d}{c} \sin\theta} \qquad (11)$$

where

$$|G(k,\omega_o)|^2 = \frac{\sin^2\left|\frac{M}{2}\left(\frac{2\pi}{M} k - \omega_o T_s\right)\right|}{\sin^2\left|\frac{1}{2}\left(\frac{2\pi}{M} k - \omega_o T_s\right)\right|} \qquad (12)$$

and

ω_o = sinusoid radian frequency

d = distance between array phase centers

c = speed of sound

θ = bearing of target

σ_s^2 = signal power

σ_n^2 = noise power

From (11), it can be seen that once it has reached steady state, the adaptive filter produces a d.c. component in the frequency domain weight vector for a static sinusoidal input. Further, each bin responding to the signal has the correct phase, $\phi = (\omega_o d/c) \sin\theta$. This suggests that additional FFT resolution can be provided by processing each frequency domain weight sequence, $W_k(m)$, with a d.c. centered FFT bin, that is, compute

$$\tilde{W}_k(\ell) = \sum_{m=0}^{N-1} W_k(\ell N - m) \qquad (13)$$

Note that this is a coherent sum in which real and imaginary parts are summed separately so that the phase information is maintained. Due to the recursive nature of the LMS algorithm, the fluctuating part of the sequence, $W_k(m)$, is somewhat correlated from sample to sample, so the sequence is not spectrally white. Consequently, the combination of an M point adaptive tracker with the post processing of (13) is not equivalent to an MN point adaptive tracker in terms of resolution.

This post-processing can be used to substantially reduce the computational load of the narrowband tracker as shown in Figure 3. The adaptive filter size, M, is selected to give reasonable computational requirements, providing much coarser resolution in frequency for the frequency domain weight vector. Given assignment of the narrowband tracker to a given line component, the post-processing of (13) is implemented in the vicinity of the line, probably several FFT bins to either side of the frequency domain weight known to contain the signal. Once sufficient post-processing has been performed, the $\tilde{W}_k(\ell)$ will be narrow bandwidth, high SNR FFT bins with the frequency spacing of the original M point FFT. From these several bins, the $\tilde{W}_k(\ell)$'s, the one with the largest magnitude and the two adjacent bins are selected. The phase is extracted from the largest $\tilde{W}_k$, and a quadratic interpolation on the three W_k selected is used to estimate the line frequency, ω_o. From Appendix E, where the quadratic interpolator was used to determine delay,

$$\hat{\omega}_o(\ell) = \frac{|\tilde{W}_{M-1}(\ell)| - |\tilde{W}_{M+1}(\ell)|}{|\tilde{W}_{M-1}(\ell)| + |\tilde{W}_{M+1}(\ell)| - 2|\tilde{W}_M(\ell)|} \frac{\pi}{MTs} \qquad (13)$$

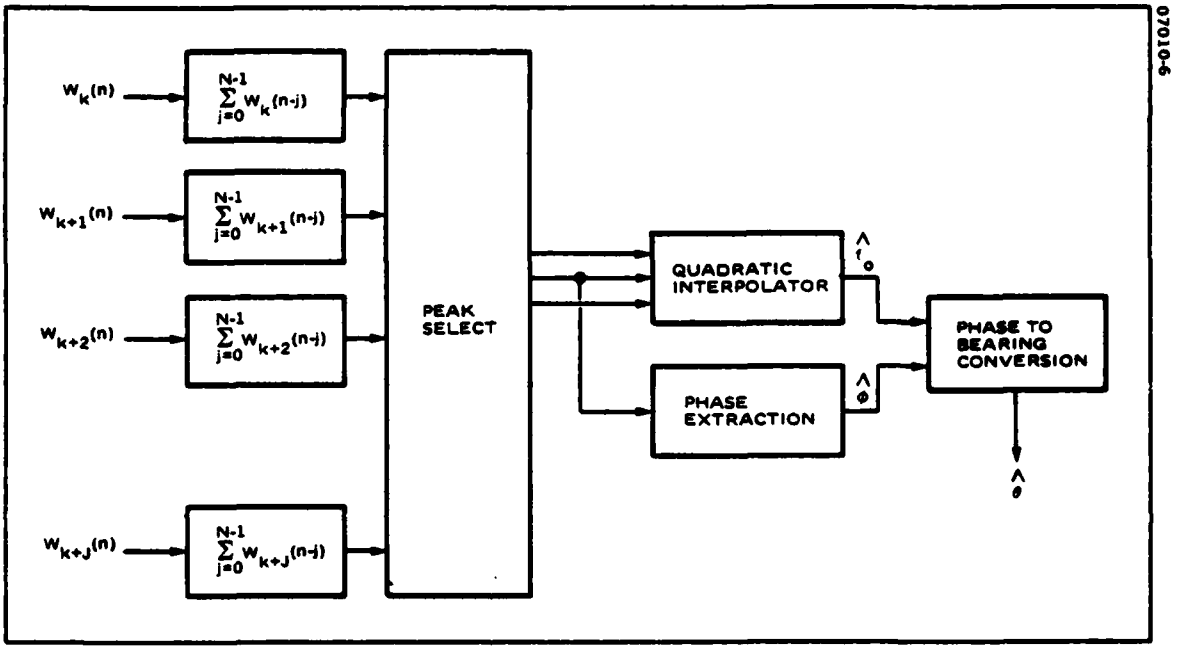

Figure 3. Post Processing Vernier for Narrowband Adaptive Tracker

where $\hat{\omega}_o(\ell)$ is the frequency estimate on the ℓ^{th} post processor output, $\tilde{W}_M(\ell)$ is the processed weight with the largest magnitude, T_s is the adaptive filter sample interval, and M the adaptive filter length. The bearing estimate is then given by

$$\hat{\theta} = \sin^{-1}\left[\frac{c}{\hat{\omega}_o D}\hat{\phi}\right] \tag{15}$$

where $\hat{\phi}$ is the phase of the largest FFT bin.

2.2 Time Domain Versus Frequency Domain Implementation

During the first phase of the tracker study [1], a time and a frequency domain algorithm for the LMS adaptive filter were developed. In the frequency domain version of an M tap time domain filter, the time series is passed through a M point FFT and a single, complex tap adaptive filter implemented in each frequency bin. If the time domain filter was real, only M/2 single tap filters need be implemented in the frequency domain since the FFT bins are conjugate symmetric. The time domain weight vector is obtained by inverse transforming the complex weights across the M frequency bins.

The frequency domain algorithm is analytically attractive in that it allows computation of both the mean and variance of the frequency domain weights under certain assumptions [1]. In many practical cases, this can be used to determine the statistics of the time domain weight vector, which is not possible with signal present by direct time domain methods. Even more significantly, however, the frequency domain algorithm provides substantial reduction in computational cost relative to the time domain algorithm. At each iteration, the frequency domain algorithm requires one complex multiply for each real multiply in the time domain, equivalent to four real multiplies. However, since only M/2 bins

are computed, the frequency domain approach requires nominally twice as many multiplies per iteration as the time domain algorithm. If the FFT is computed without redundancy and with no gaps in the input time series, the frequency domain algorithm iterates only 1/M times as often as the time domain algorithm. Therefore, the M iterations, the frequency domain algorithm requires approximately 2/M times the number of multiplications of the time domain approach. To this, the computations of the two forward FFTs and the inverse FFT must be added. In fact, if both time and frequency domain weights are needed, the inverse FFT in the frequency domain implementation requires the same number of multiplies as the forward FFT needed to obtain the frequency domain weights from the time domain. Therefore, letting $N_T(M)$ be the number of real multiplies for an M point time domain algorithm, the number of real multiplies for the frequency domain implementation, N_F, is

$$N_F \approx M \log_2 \frac{M}{2} + \frac{2}{M} (N_T(M)) \tag{16}$$

This produces sizeable reductions for even modest M.

Unfortunately, the frequency domain algorithm is not an exact realization of the time domain LMS algorithm. It is subject to windowing effects due to the block processing in the FFT. For a broadband signal, this effect can only be regarded as insignificant if [2]

$$M >> \Delta \tag{17}$$

where Δ is the delay in the signal between adaptive filter inputs in sample intervals. In a broadband tracker implemented in the time domain, it is desirable to keep M small and place the peak near the center of the adaptive filter

when the target is on the split beam MRA, so that $\Delta/M=1/2$. If this tracker were to be implemented in the frequency domain, M would have to be increased substantially to reduce windowing effects, offsetting some of the computational advantages of the frequency domain algorithm, and increasing algorithm noise. On the other hand, for a combined narrowband and broadband system that uses large M to achieve frequency resolution, by the results of the preceding section, the total time delay needed for the broadband signal is a small fraction of the filter length. By placing the peak near the front of the adaptive filter for all bearing angles, it can then be assured that (17) is true, so window effects will be negligible.

It has been shown that the variance of the time domain weight vector obtained via the two implementations is the same for broadband inputs at low signal-to-noise ratio whenever $M >> 2$. Simulations appear to support this at higher signal to noise ratios as well. However, it is possible, given a particular desired time constant, for the filter to be stable in the time domain but unstable in the frequency domain. The time constant, in iterations of the time domain filter is

$$\tau_{tI} = \frac{1}{2\mu P_{in}} \tag{18}$$

where P_{in} is the input power. Due to the gain of the FFT, the time constant of the frequency domain filter is

$$\tau_{fI} = \frac{1}{2\mu M P_{in}} \tag{19}$$

where it is assumed that the input power is primarily broadband. Since the frequency domain implementation iterates only 1/M times as often, the two filters have the same time constant in seconds. However, the time constant for the frequency domain implementation is much smaller, i.e., closer to the unstable region. If, for example, the system required $\tau_{tl} = 256$ and $M = 1024$, then $\tau_{fl} = 1/4$ for equal response in seconds, and the frequency domain implementation is unstable.

The choice of frequency or time domain implementation must therefore be made on a case by case basis, taking into account the above considerations. For broadband only trackers, the increased filter size necessary to use a frequency domain implementation will offset some of its computational advantages. For purely narrowband applications, the frequency domain approach should be used if the combination of M and the desired time constant do not lead to unstable or near unstable operation. Implementation of the tracker for combined broadband and narrowband targets must consider both factors.

2.3 Tracking of Multiple Targets

Typically, the sonar environment will consist of a number of directional sources, some of which will be targets of interest, others interferences. Often, the nature of some contacts will be unknown, and targets of interest will be differentiated from interferences only after tracking for some period of time. The adaptive tracker structure must therefore have the capability of tracking in this multi-contact environment.

At the outset, multiple contact tracking is simplified by the spatial response of the split beams. Given two contacts of similar strength that are

separated in bearing by more than a beamwidth, the output of a beam steered at one can essentially be regarded as containing the single contact, since the other is in the sidelobes and severely attenuated. Therefore, a tracker structure operating on the largest peak or largest line in the weight vector will almost always track the target of interest. Multiple tracking will then consist of assigning a second split-beam pair and adaptive tracker to the other contact. Hence, for contacts of approximately the same radiated noise level separated by more than a beamwidth, the multiple target tracking problem reduces to multiple single-target trackers.

The problem is complicated somewhat when one contact is much stronger than the other, and it is desired to track the weaker of the two. Even though the stronger contact is in the sidelobes of a beam steered at the weaker one, it may be sufficiently strong to produce a peak of nearly equal or greater amplitude in the weight vector. If the adaptive tracker merely picks the largest peak, then the tracker will operate on the target that is in the sidelobes whenever its amplitude exceeds that of the target of interest. This problem can be eliminated by restricting the choice of the largest weight to that range of delays that would occur for targets in the mainlobe, say $\pm T_{max}$, where

$$T_{max} = \frac{d}{c} \sin\frac{\theta_o}{2} \tag{20}$$

with θ_o the beamwidth of the split beams. This is most efficiently done from a computational point of view by restricting the length of the adaptive filter to $2T_{max}$, and providing bulk delay to place a target on the beam maximum response axis (MRA) at the center of the weight vector, as shown in Figure 4.

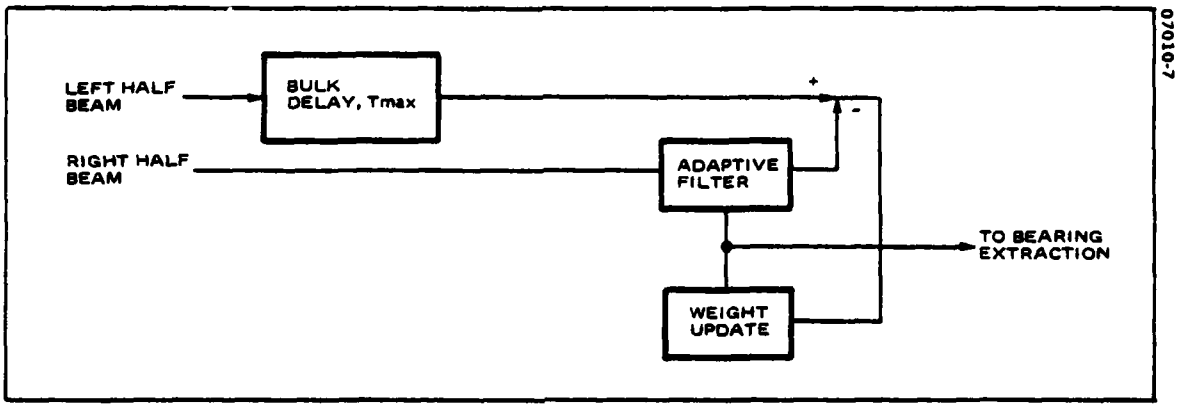

Figure 4. Use of Bulk Delay to Center Peak in the Adaptive Filter

In implementations for combined broadband and narrowband tracking (see Section 2.2), the adaptive filter length may be required to provide frequency resolution. In that case, the restriction to $\pm T_{max}$ is made by limiting the taps used in the broadband estimator rather than shortening the time domain weight vector. Note, however, that the presence of the strong contact may still bias the location of the peak, or even mask its location. This situation is best handled by use of a sidelobe canceller prior to the tracker. The stronger contact is then treated as an interference, and handled as in Section 3.5

If the target is narrowband, the estimate of bearing is based upon the phase of a line component radiated by the contact. Restriction of the length of the adaptive filter will not change the effects of a strong contact in the sidelobes. In assigning the narrowband tracker, though, a particular frequency will have been selected for tracking so that the narrowband estimate can be restricted to the vicinity of that line in the FFT of the weight vector. Unless a line radiated by the sidelobe contact is close to the chosen line from the contact of interest, this will allow the tracker to operate on the weaker contact. This should be taken into account in the choice of a line for assignment to the tracker. A line from a sidelobe contact that is too close to a line of interest may be treated as an interference and rejected by sidelobe cancellation (see Section 3.5). A strong broadband contact in the sidelobes may bias the narrowband estimate, as discussed in [2], but the sidelobe cancellation methods can also be used to eliminate the effects.

The most severe case of multiple target tracking occurs when multiple targets appear within the mainlobe of a single beam. This will occur most often when two targets originally in separate beams cross in bearing, and therefore

appear in the same beam for some period of time. The problem is then twofold; maintain contact with both targets while they are in the same beam, and discriminate between the two targets so that the individual tracks may be maintained. The effects of such an encounter depends upon whether broadband or narrowband tracking is being used on each of the two contacts.

a. Both Narrowband Targets: If the lines used to track the two targets are sufficiently far apart in frequency with respect to the resolution of the frequency domain weight vector, then the two tracks can be maintained. However, if their frequencies are indistinguishable by the algorithm, they will appear as a single target while they are in the main lobe.

b. Broadband Target and Narrowband Target; It is unlikely that the narrowband target would be sufficiently strong to appreciably affect the peak of the time domain weights, so it will be possible to maintain track on the broadband target with little degradation. As shown in Appendix D of [2], the broadband target will bias the narrowband estimate and increase its variance. If the broadband target were very strong, the narrowband estimator could track the broadband target instead of the line to which it was assigned.

c. Both Broadband Targets: When the peaks in the weight vector corresponding to each target are close together, their locations become biased toward the other target, eventually becoming a single peak, indistinguishable from a single target without the use of prior history of the tracks.

These considerations are very much the same as those involved in the use of conventional trackers in a multi-target environment.

In conventional broadband trackers, the time delay estimate is generally based upon the determination of the location of the peak of the cross-correlation function between the split array outputs (or, alternatively, the zero crossing of its derivative). The correlation function is computed at a single value of delay and τ varied to maximize the cross-correlation function. This is done as shown in Figure 5, in which a variable delay is inserted in one line of the tracker to control the point at which the derivative of the cross-correlation function is computed. The sign of the derivative determines the direction in which the value of the current τ is incremented, with equilibrium occurring when τ is at the zero crossing. Typically, the output of the correlator, y(n), is fed back through some type of tracking logic which controls how τ is modified for a given value of y(n). In most systems, the tracking logic includes smoothing, and a first order update of the delay, that is

$$\tau(n+1) = \tau(n) - \alpha Y_s(n) \tag{20}$$

where

$\tau(n)$ = n^{th} value of delay

and

$Y_s(n)$ = n^{th} smoothed value of y

Higher order tracking loops vary $\tau(n)$ based on not only the value of y(n), but its derivatives (actually, higher order differences in a discrete system).

The incorporation of such loops into the tracker provides the tracker with the ability to follow dynamic signals. For example, the first order loop can follow a linearly changing delay with a fixed lag error (the lag being dependent upon the gains incorporated in the loop). However, the tracking loop serves

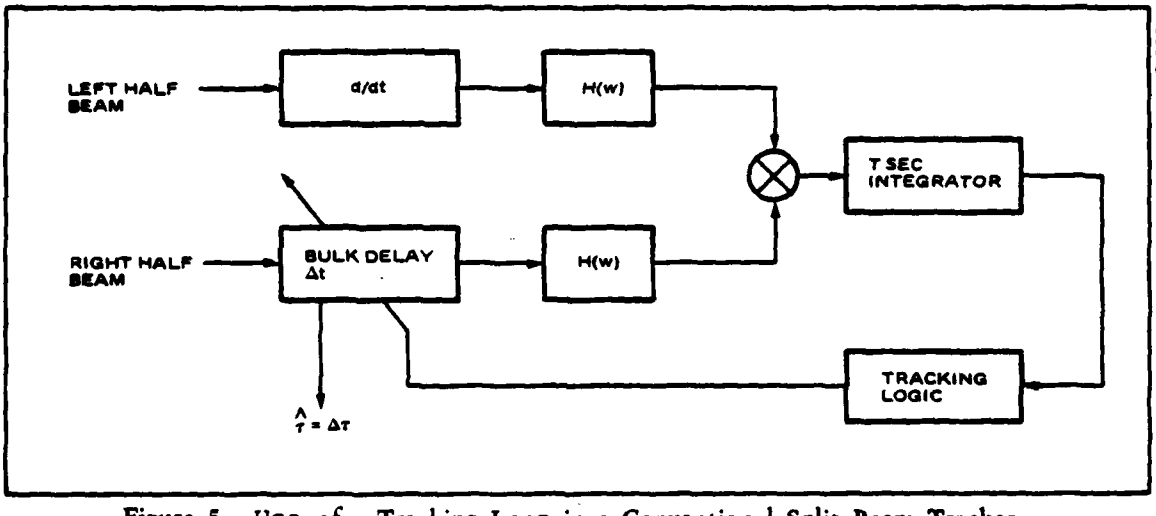

Figure 5. Use of a Tracking Loop in a Conventional Split Beam Tracker

another function whenever two targets cross in bearing, that of allowing the tracks to be maintained using the past dynamics of the target. Clearly, if one of the targets changes its dynamics during the time in which the zero crossings in the derivative are indistinguishable, then loss of track may occur.

A similar approach can be applied to the adaptive tracker to handle the case when two broadband targets appear in one beam. A relatively narrow window is placed about the current peak in the weight vector, and the peak selection is only allowed to occur within the window. For example, if the current delay estimate from the interpolator is $\hat{\tau}(m)$, then on the (m+1)th iteration the peak (which provides the starting point for the interpolator) will be the largest weight within $\pm\tau_{max}$ of $\hat{\tau}(m)$. This prevents the interpolator from jumping to another target more than τ_{max} from the current location. Clearly, if the window is too narrow (τ_{max} too small) then the dynamics of the source can carry the peak out of the window between iterations, and track will be lost, so the window width must take into account the maximum rate of change of delay.

If the current estimate, $\hat{\tau}(m)$, were used to control the next location of the window, then whenever the fluctuations in $\hat{\tau}(m)$ were large in comparison to τ_{max}, then a single fluctuation could move the window away from the peak, and again track would be lost. This can be prevented by passing the estimate $\hat{\tau}(m)$ through tracking logic prior to moving the window, just as is done in conventional trackers. The width of the window then must consider the signal dynamics and the fluctuations in the output of the tracking logic. The simplest tracking logic would simply smooth the sequence $\hat{\tau}(m)$, but in order to maintain track using

target dynamics, higher order differences of the smoothed delay, $\hat{\tau}_s(m)$, are used to update the current window location, as shown in Figure 6. A first order loop on the window would compute the new window location as

$$T_w(m) = \hat{\tau}_s(m) - \alpha T_w(m-1)$$

for example. Now, when two windows overlap, only a single estimate would be supplied to the loops controlling the windows analogous to the conventional tracking loops. If the targets do not execute maneuvers during the period when the windows overlap, the loop will allow maintenance of the two tracks.

Use of the loops to control the location of windows operating on the weight vectors instead of varying a bulk delay prior to the input of the adaptive filter has the advantage of decoupling the tracking loop from the dynamic behavior of adaptive filter. If the loop controlled a delay prior to the tracker, as shown in Figure 6, then the dynamic behavior of the combination of the tracking loop and adaptive filter (which exhibits its own first order behavior in the weight updates) would be extremely difficult to quantify given the nonlinear properties of the adaptive filter. By using the windowing scheme, the dynamics and statistics of the adaptive tracker estimate can be characterized using the methods developed in [1] and [2], then the response of the loop to these input statistics analyzed by linear system theory. This of course assumes that the window is sufficiently wide that it does not affect the statistical behavior of the interpolator. It has been shown in [2] that the adaptive tracker can follow a linearly changing delay with a fixed lag. Therefore, a first order loop would simply introduce an additional lag in the window location. Taking this into account in the width of the window would allow the estimator to track a ramp input without any additional lag, since

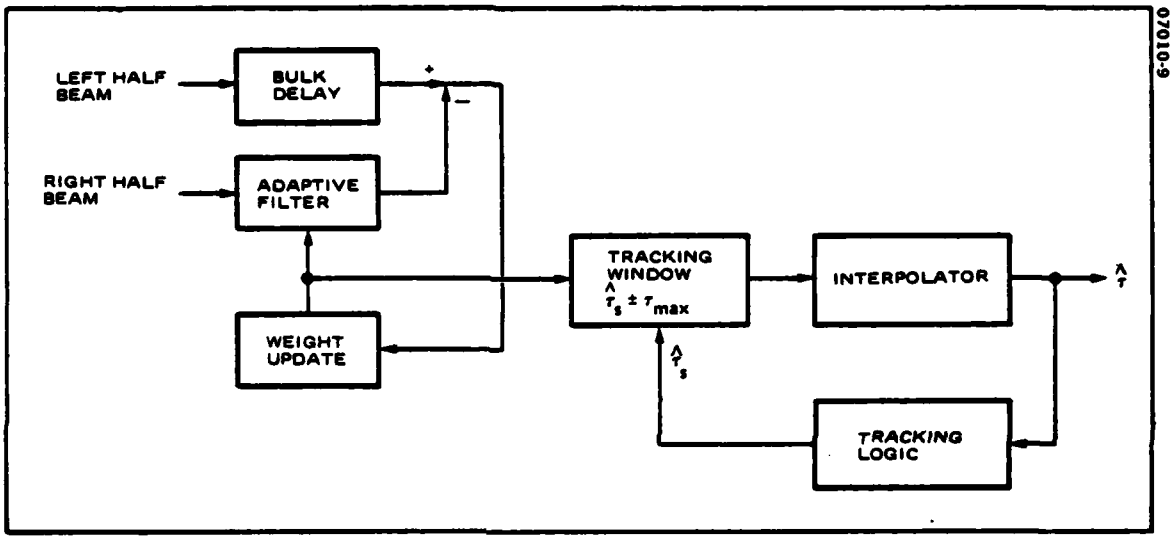

Figure 6. Delay Windowing with a Tracking Loop

the window lag does not affect the estimate (unless it becomes too great, so that track is lost). Use of a second order loop would allow tracking of a ramp input without accounting for any lag in the window width, although some accounting for the increased fluctuations in the current window center would be necessary. It must be noted that because the behavior of the adapter filter and the window tracking loop are decoupled, the order of the combination is limited by that of the adaptive tracker. That is, use of a higher order loop in the windowing does not give higher order behavior for the tracker since the adaptive filter is first order.

2.4 Beam-to-Beam Handover of Dynamic Targets

Whenever split array beamformers are used to provide the input to the adaptive tracker, the potential exists for moving targets to move out of the main lobe of the split beam, resulting in *loss of track.* Two methods of maintaining track are steering of the split beams to maintain contact, or handover of the tracking function to an adjacent fixed beam. Steering of the split beams requires a beamformer structure that is dedicated to the tracker and capable of relatively high resolution steering. It also requires incorporation of a tracking loop to control the steerable beam. Beam-to-beam handover applies when the tracker is used as an add-on to a preformed beam sonar, and minimizes the cost of the tracker itself. This is the configuration that is considered here.

Suppose a dynamic target is passing through a beam to which the adaptive tracker is assigned. The goal of the beam-to-beam handover is to reassign the tracker to the next beam before it is sufficiently attenuated to lose track. Since the array pattern is known, the bearing angle corresponding

to, say, a X dB attenuation can be determined as a potential handover point. When the bearing estimate reaches this point, then handover is initiated. Several factors must be taken into account in implementation of the handover, however;

a. The bearing estimate from the tracker is random, and as such, subject to fluctuations. When the target is in the vicinity of the handover point, the estimate may fluctuate back and forth about the desired point. To avoid rapid handover of the target back and forth during this time, the handover algorithm must include some hysteresis. The simplest means of doing this is to designate a different value for handover when the target passes to or from a beam. For example, let ϕ_i and ϕ_{i+1} be the location of two adjacent beams, and let the desired handover point be

$$h_d = \frac{\phi_i + \phi_{i+1}}{2} \tag{22}$$

Then when a target passes from beam i to beam i+1, the actual handover is performed when the bearing estimate, ϕ, reaches

$$h_d(i, i+1) = h_d + \delta_d \tag{23}$$

while, when it passes from beam i+1 to beam i, it occurs when ϕ reaches

$$h_d(i+1, i) = h_d - \delta_d \tag{24}$$

There is therefore a "dead zone" of $2\delta_d$ degrees over which the estimate can fluctuate after beam handover that will not initiate another handover back to the original beam. If δ_d is sufficiently large with respect to the fluctuations in ϕ, the problem of jittering at handover will be eliminated.

b. Since the target is dynamic, the estimate ϕ will lag the actual bearing of the target, Φ, so that handover will actually occur later than desired if ϕ is used to initiate the process. This is compounded by the fact that incorporation of the "dead zone" in (a) makes handover occur later than the desired point, h_d, anyway. In many sonars, the beam spacing will be sufficiently fine (i.e., beam crossover points not highly attenuated) compared to lag that this effect will not be a problem. If the lag is a problem, a possible solution is to estimate the lag from the bearing rate and add it to ϕ prior to comparison to the beam handover point.

c. The beam handover process should include the handover of bearing information from the original beam to the new beam. In the adaptive tracker, this information is in the adaptive filter weight vector. The actual shape of the weight vector should not change drastically, since the spectrum of the source remains the same, with any changes due to the difference in the frequency response of the beams. The primary change will be in the form of a delay in the weights corresponding to the change in the delay between phase centers for the two beams. Because the phase centers are known

for each of the fixed beams, hence, their separation, d_i, the time delay for the new beam can be estimated from the bearing estimate. Let the index k denote the beam from which the target is being handed and k+1 denote the new beam, and

ϕ_{k+1} = bearing of beam j

d_{k+1} = effective distance between phase centers for beam j

$\hat{\tau}_{k+1}$ = estimate of delay between phase centers for beam j

$\hat{\phi}$ = current bearing estimate

Then

$$\hat{\tau}_{k+1} = \frac{d_{k+1}}{c} \sin (\hat{\phi} - \phi_{k+1})$$

where c is the speed of sound. The weight vector for the new beam is therefore approximately the weight vector for the original beam shifted by $(\hat{\tau}_{k+1} - \hat{\tau})$, which would be quantized to the sample rate for implementational simplicity.

Two alternatives exist for inserting this shift, actually time shifting the time domain weight vector or by incorporating a phase shift corresponding to this delay in each FFT bin of the frequency domain weight. Implemented in the time domain, the initial weight vector for the new beam would be

$$\hat{W}_{k+1}(i) = W_k\left(i - \left\lfloor \frac{\hat{\tau}_{k+1} - \hat{\tau}_k}{T_s} \right\rfloor\right), \quad 1 \le i - \left\lfloor \frac{\hat{\tau}_{k+1} - \hat{\tau}_k}{T_s} \right\rfloor \le M \qquad (26)$$

where

$\hat{W}_{k+1}$ = i^{th} initial weight for new beam

$W_k(i)$ = i^{th} weight from original beam

$\lfloor X \rfloor$ = largest integer $\le X$

This leaves $M - \left\lfloor \frac{\hat{\tau}_{k+1} - \hat{\tau}_k}{T_s} \right\rfloor$ weights undefined. Possible alternatives for these weights are an end around shift of the weight vector or arbitrary assignment of these weights to zero. If the length of the adaptive filter is judiciously chosen, the shift will be valid in the vicinity of the peak of the time domain weight vector, hence acceptable in terms of the broadband estimator. However, either end around shift or arbitrary zero assignment of the weights near the end of the filter will reduce the coherence of any narrowband components. The end around shift will minimize this degradation.

If $F_k(i)$ is the i^{th} frequency domain weight of the original beam and $\hat{F}_{k+1}(i)$ is the i^{th} initial frequency domain weight for the newest beam, then the phase shift method gives

$$\hat{F}_{k+1}(i) = F_k(i)\, e^{-j \frac{2\pi}{M} i \left\lfloor \frac{\hat{\tau}_{k+1} - \hat{\tau}_k}{T_s} \right\rfloor} \qquad (27)$$

This produces exactly the end around time shift described above.

SECTION 3.0

SUMMARY OF PERFORMANCE ANALYSIS

3.0 SUMMARY OF PERFORMANCE ANALYSIS

This section summarizes the results of the performance analyses performed during the third phase of the Adaptive Tracking System Study. Section 2.1 considers the effects of multipath on the adaptive tracker, particularly as they relate the multipath effects in conventional trackers. Section 2.2 discusses the effects of arrays on tracking of both static and dynamic targets. This extends results of the first two phase of this study, which considered each half of the split array as a point omnidirectional hydrophone.

In Section 2.3, estimators are developed for tracking of targets which have both broadband and narrowband components. Several structures are developed which require differing amounts of a priori knowledge of the signal and noise characteristics. Section 2.4 described a simplified interpolator for the broadband tracker, and analyzes its performance relative to the sin x/x interpolator used in [1]. Section 2.5 analyzes the effects of using adaptive cancellers on the split beam outputs prior to tracking. Finally, Section 2.6 summarizes the results of simulations of the adaptive tracker and a conventional tracker with moving targets.

3.1 Effects of Multipath on the Adaptive Tracker. The presense of multipath propagation causes multiple delayed and attenuated replicas of the target waveform to appear at the split beam output. It is shown in Appendix A that these multiple arrivals can result in displacement and broadening of the peak of the adaptive tracker weight vector for broadband targets, and may produce ambiguous peaks. These effects will depend upon the particular propagation path lengths involved and upon the arrival angles in both bearing and depression/elevation (d/e). The potential effects of multipath therefore include bias in the estimate due to displacement of the peak or selection of an ambiguous peak, and increased variance due to peak

broadening. These effects are not readily generalized since they apply to each specific multipath structure. However, it is shown that the broadband adaptive tracker is affected by multipath in the same way as conventional trackers.

Similarly, it is shown that multipath produces multiple sinusoids of differing phase in the weight vector. In dynamic situations, it may be possible to resolve these multiple sinusoids by means of differing doppler of different vertical arrival angles. Such lines produce ambiguities analogous to multiple peaks in the broadband tracker. Lines that are not resolvable by the narrowband tracker will produce a biased phase estimate from the FFT bin, and will cause increased variance due to interference of the sinusoids. Again, the quantitative effects depend upon the specific multipath structure present, but it is shown that the adaptive tracker is affected in the same way as conventional trackers.

3.2 Effects of Arrays on the Adaptive Tracker. Throughout the first two phases[1,2] of this study, the inputs to the adaptive tracker have been assumed to come from two omnidirectional hydrophones separated by a distance, d. It was assumed that arrays could replace the omnidirectional hydrophones with minimal modification to the results. This section considers the effects of such arrays on previous analyses in both the static and dynamic cases.

In the static case, it is shown in Appendix B that the addition of arrays produces the equivalent model of the adaptive tracker shown in Figure 7. The results developed for the omnidirectional hydrophones can therefore be extended by replacing the half arrays and beamformers with linear filters, $H_x(\omega)$ and $H_d(\omega)$, i.e., simply by modifying the input spectra in previous results. Most significantly, it is shown that when the two split arrays are identical with identical shading, the equivalent model is as in Figure 8. Therefore, the analyses using omnidirectional

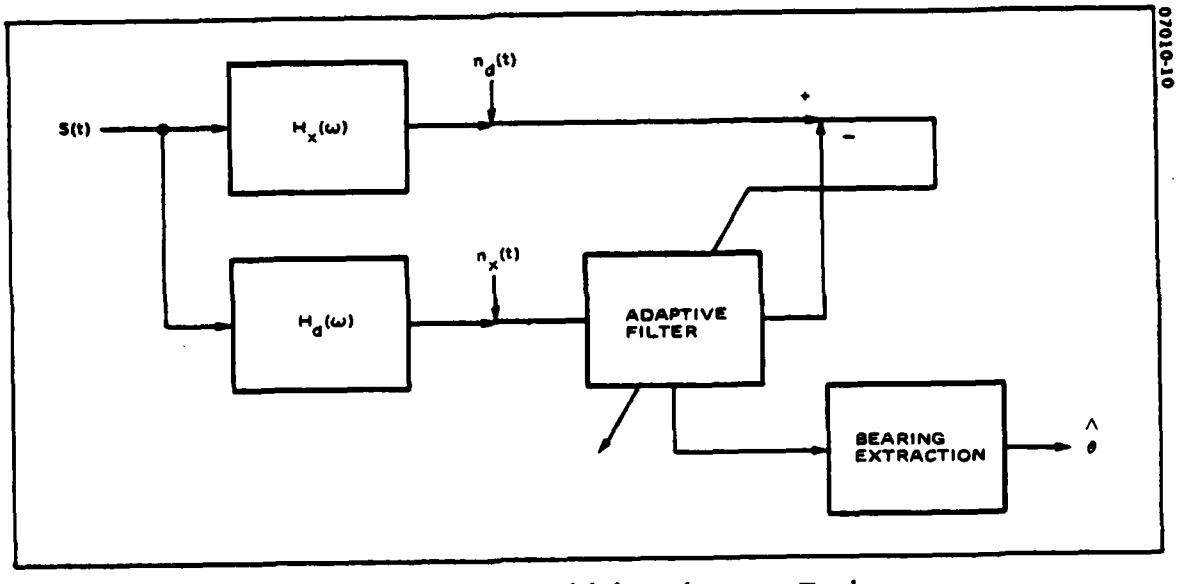

Figure 7. Equivalent Model for Split Array Tracker

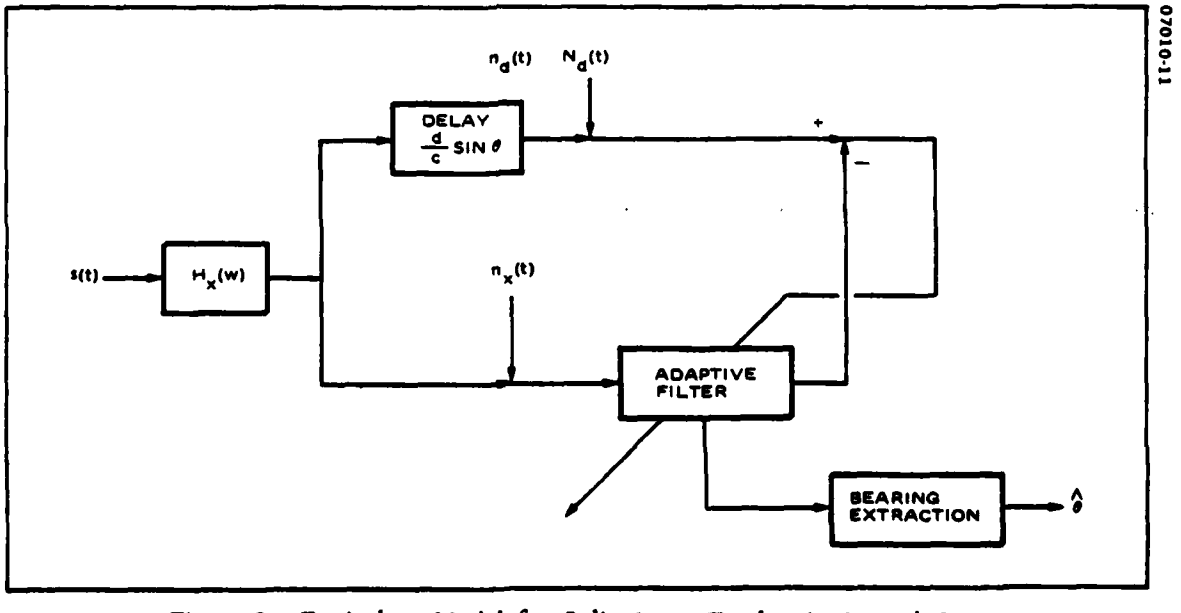

Figure 8. Equivalent Model for Split Array Tracker in Special Case

hydrophones in [1] and [2] can be applied when arrays are used with static targets by modifying the signal spectrum by the transfer function, $H_x(\omega)$, and letting d be the distance between split array phase centers.

Analysis of the dynamic case, in which the delay associated with the target changes linearly with time, is complicated by the fact that the target will eventually leave the main beam, making steady state analysis impossible. This was overcome by making the time delay periodic across the main beam, performing a steady state analysis, then identifying and removing terms associated with the periodicity in the results. It is shown that the lag in the peak of the weights at low SNR, corresponding to the lag in the bearing estimate is

$$\text{Lag} \approx \frac{rc\delta}{(\mu\sigma_n^2 - br\delta)d}\left\{\frac{0.69 + 2\ln M}{M}\right\} \tag{28}$$

where

M = number of hydrophones in half array

r = linear rate of change of delay

δ = algorithm sample rate

b = bandwidth of input processes

μ = feedback coefficient of the adaptive algorithm

σ_n^2 = noise power.

This agrees with the omnidirectional hydrophone case derived in [2] when M = 1. Asymptotically, the lag is directly proportional to lnM/M, thus decreasing with the number of array elements.

3.3 Estimator Structures for Use With Both Broadband and Narrowband Components. As pointed out in the introduction, one of the motivations for use of an adaptive tracker is that it has the potential to track signals using both broadband and narrowband energy simultaneously. Reference [1] developed estimator

structures for use when either broadband or narrowband energy only were present in the radiated noise of the target. References [1] and [2] then analyzed the performance of these two estimators in the presence of targets that are broadband, narrowband, or a combination of the two. However, a means of combining the two estimates, or of performing a different estimate when the target has both broadband and narrowband components was not considered.

In Appendix D, three estimator structures are derived for use when both broadband and narrowband components are present in the target spectrum. These three structures require differing amounts of a priori knowledge as to the signal.

It may readily be argued that the weights of the adaptive filter are gaussian, and an expression for the mean weights with combined narrowband and broadband target was derived in [2]. Further, the results of [2] show that the weight variance is independent of the bearing. With the additional (approximate) assumption that the weights are uncorrelated, it is possible to determine the maximum likelihood (ML) estimator for bearing given the adaptive filter weights. If the broadband and narrowband SNR's are also unknown then they are jointly estimated in the ML structure. The ML estimator maximizes the functional

$$J(\hat{\theta}) = Q_1 f_1(\hat{\theta}) + Q_2 f_2(\hat{\theta}) + Q_2 f_1(\hat{\theta}) f_2(\hat{\theta}) \tag{29}$$

where

$$f_1(\theta) = \left|W_f(\max)\right| \cos\left(\phi_\omega - \hat{\omega}_o \frac{d}{c} \sin\hat{\theta}\right) \tag{30}$$

and

$$f_2(\hat{\theta}) = \sum_{k=0}^{M-1} W(k)\, \rho\left(kTs - \frac{d}{c}\sin\hat{\theta}\right) \tag{31}$$

and where Q_1, Q_2, and Q_3 are constants essentially independent of θ, given in Appendix D. Also

$|W_f(\max)|$ = magnitude of the frequency domain weight with the largest magnitude

ϕ_ω = phase of the frequency domain weight with the largest magnitude

$W(k)$ = k^{th} time domain weight

$\rho(kTs)$ = interpolation function with the shape of the broadband mean weights

M = number of taps in the adaptive filter.

This estimation structure is shown in Figure 9.

If the broadband and narrowband signal to noise ratios are known a priori, or can be estimated from the sonars, then the estimator structure simplifies considerable. The ML estimate then maximizes

$$J_1(\hat{\theta}) = \frac{\gamma_{NB}}{M\gamma_{NB} + \gamma_{BB} + 1} \frac{1}{(\gamma_{BB} + 1)} f_1(\hat{\theta}) + \frac{\gamma_{BB}}{\gamma_{BB} + 1} f_2(\hat{\theta}) \qquad (32)$$

where γ_{NB} and γ_{BB} are the narrowband and broadband signal to noise ratios, respectively. This structure is shown in Figure 10.

An attractive feature of these structures is that they retain elements of the estimators developed in [2] for purely broadband or narrowband signals. In fact, the second estimator reduces the appropriate estimator whenever either γ_{NB} or γ_{BB} is zero. This is a strong justification of the original estimators.

Appendix D also presents an alternate structure which requires no a priori knowledge of the signal and noise characteristics, but combines the broadband and narrowband estimates based upon their estimated variance. The combined estimate is

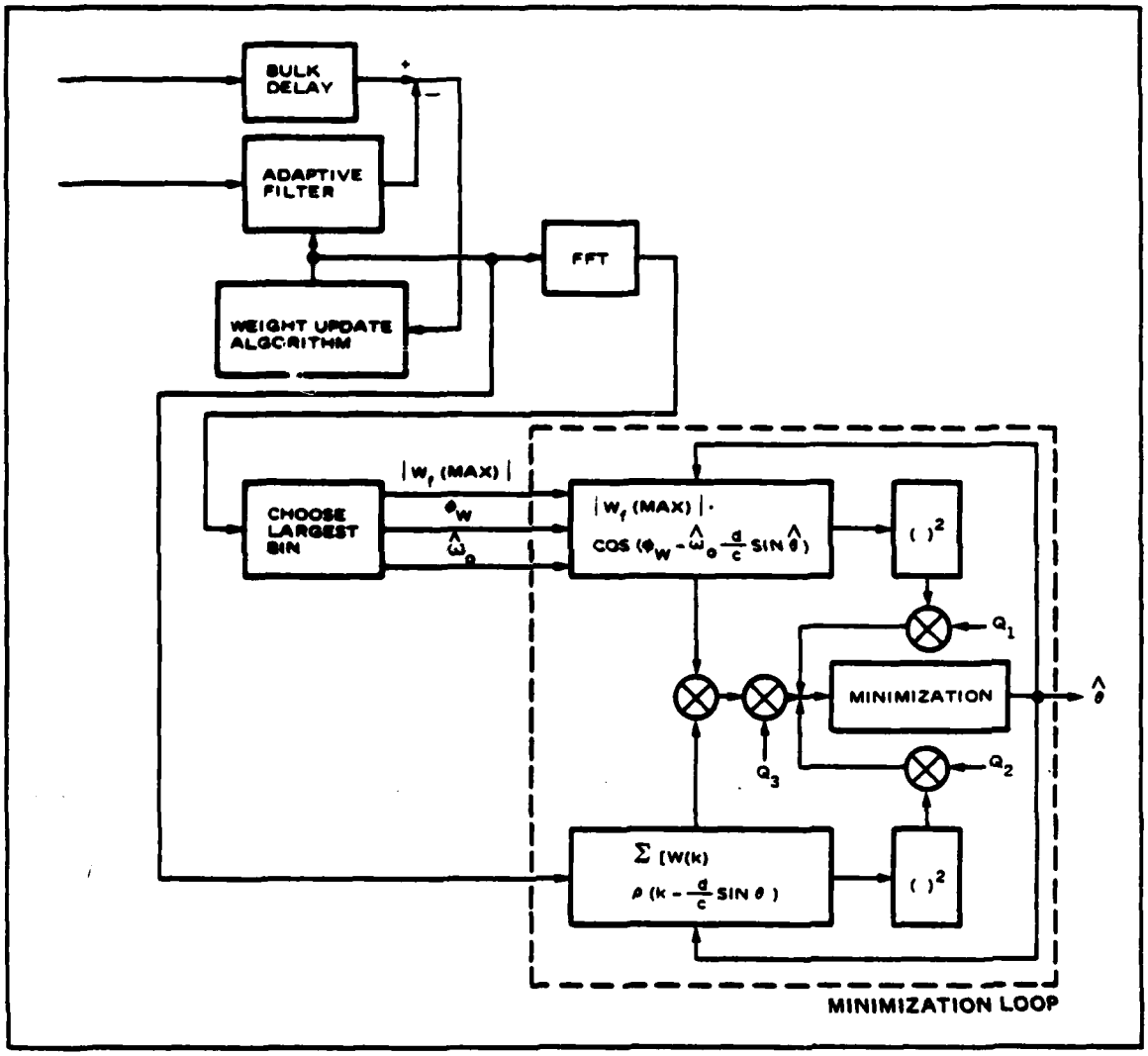

Figure 9. Combined Adaptive Tracking System with Unknown SNRs

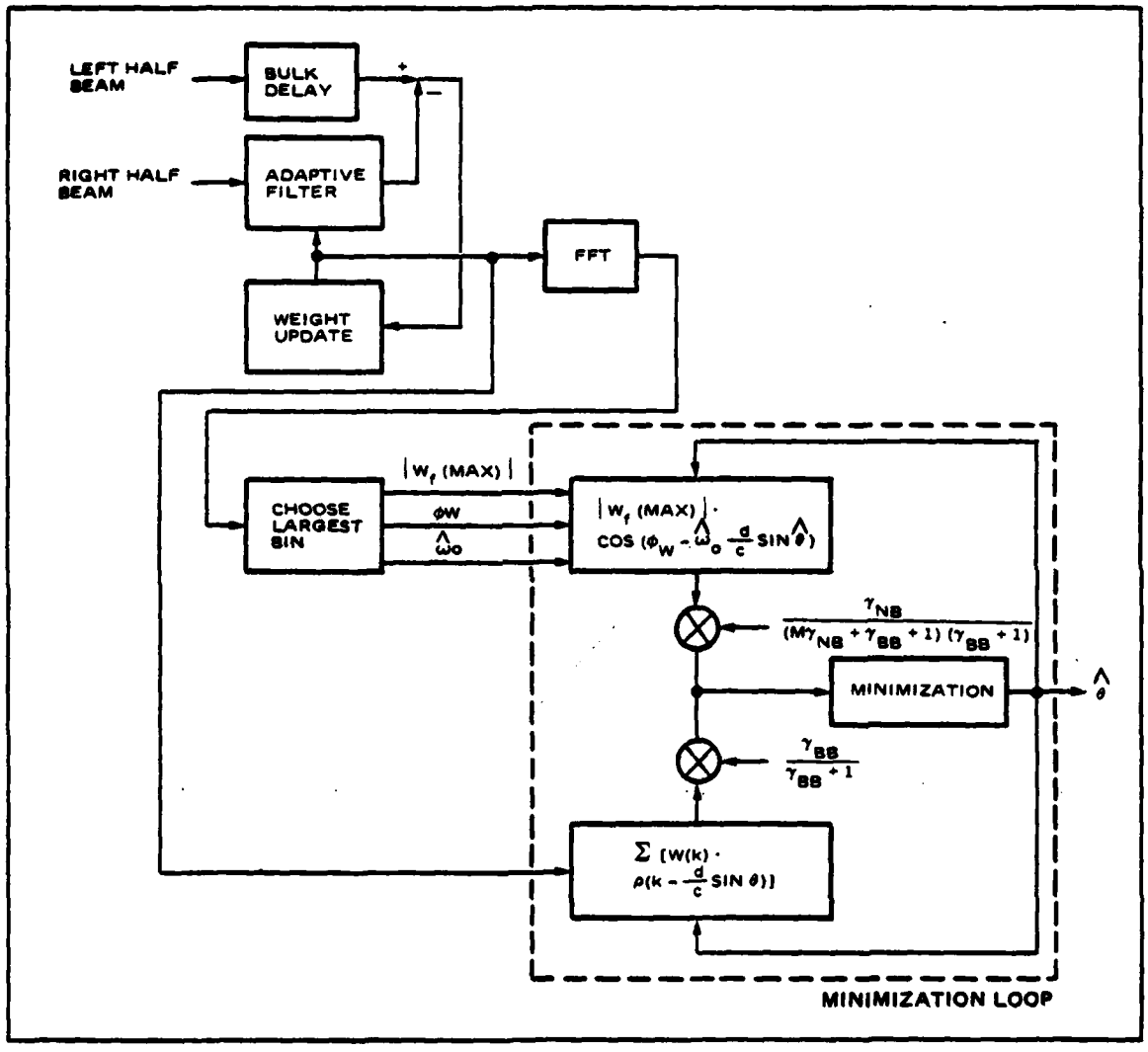

Figure 10. Combined Estimator with Known SNRs

$$\hat{\theta}_c = \frac{\sigma^2_{\hat{\theta}_{NB}}}{\sigma^2_{\hat{\theta}_{NB}} + \sigma^2_{\hat{\theta}_{BB}}} \hat{\theta}_{BB} + \frac{\sigma^2_{\hat{\theta}_{BB}}}{\sigma^2_{\hat{\theta}_{NB}} + \sigma^2_{\hat{\theta}_{BB}}} \hat{\theta}_{NB} \tag{32}$$

where

$\sigma^2_{\hat{\theta}_{NB}}$ = estimated variance of the narrowband estimate

$\sigma^2_{\hat{\theta}_{BB}}$ = estimated variance of the broadband estimate

$\hat{\theta}_{NB}$ = current narrowband estimate

$\hat{\theta}_{BB}$ = current broadband estimate.

The values of $\sigma^2_{\hat{\theta}_{NB}}$ and $\sigma^2_{\hat{\theta}_{BB}}$ are obtained by moving averages over $\hat{\theta}_{NB}$ and $\hat{\theta}_{BB}$.

If the estimator variances were known exactly, and $\hat{\theta}_{BB}$ and $\hat{\theta}_{NB}$ were uncorrelated, this structure would produce a combined estimate with smaller variance than that of $\hat{\theta}_{NB}$ or $\hat{\theta}_{BB}$. The fluctuations in the estimates of $\sigma^2_{\hat{\theta}_{NB}}$ and $\sigma^2_{\hat{\theta}_{BB}}$ will increase this variance. Further, correlation between $\hat{\theta}_{NB}$ and $\hat{\theta}_{BB}$ will increase the variance of the estimate. Appendix D includes an analysis of the sensitivity of this combiner to correlation.

3.4 Analysis of a Simplified Interpolator. The broadband adaptive tracker, as originally described in [1], used a sin x/x interpolator to determine the location of the peak in the weights when it fell between discrete taps. This procedure was computationally inefficient in that it utilized all tracker weights and required an iterative procedure to find the peak. Since many of the weights are dominated by fluctuations, use of all the weights is also a questionable procedure from a performance point of view.

In Appendix E, a method of locating the peak based upon a quadratic fit to the largest weight and the two adjacent weights is described. This interpolator has the computational advantage that the peak is computed directly from the values of the largest weight and the two adjacent weights as

$$\hat{\tau} = \frac{W_{J-1} - W_{J+1}}{W_{J-1} + W_{J+1} - 2W_J} \frac{T_s}{2} + JT_s \tag{34}$$

where W_J is the largest weight, W_{J-1} the adjacent weight with smaller time index, and W_{J+1} the other adjacent weight. Also, J is the time index of the largest weight and T_s the algorithm sample rate. Note that no iterative procedure is needed to find the peak.

The variance of this estimate, $\hat{\tau}$, is then determined analytically using the method used to determine the variance in peak localization in [1] and [2], originally described in [4]. These results are compared to the variance of the estimate using the sin x/x interpolator developed in Appendix V of [1]. The results of the comparison must be evaluated numerically on the computer. Evaluation in several typical cases showed that the variance of the estimate using the sin x/x interpolator was 2 to 3 times that of the quadratic interpolator, in spite of the fact that the quadratic interpolator is much simpler. Both interpolators were used to process sea tape data described in Section 4.0, and the results of this processing supports the analysis.

3.5 Cancellation of Interferences Prior to Tracking. There are basically two approaches to dealing with interference in the adaptive tracking system. One is to depend upon the spatial response of the split arrays and upon the adaptive properties of the tracker to provide relative immunity to the interference. The other approach is to attempt to cancel the interference from the half beam inputs to the

adaptive tracker. It was shown during phase 2 of this study [2] that the primary effect of an interference is to introduce a bias in the bearing estimate, and that this bias, can be quite severe when the signal-to-interference ratio is low at the split array outputs. Under these circumstances, it may be desirable to cancel the interference prior to tracking.

The adaptive noise canceller [5] is often used to eliminate an interference arriving on the sidelobes from a beam output. A reference sensor, for example an omnidirectional hydrophone that is spatially separated from the array, is used as a reference in the LMS canceller configuration of Figure 11. When the interference power dominates, the adaptive filter will spatially reject the interference from the beam output. Depending upon the spacing between the reference hydrophone and array and upon the separation of the target and interference, some rejection of the target signal will occur, but this will usually be acceptable in light of the interference rejection. Figure 12 shows this approach applied to the adaptive tracker. A reference is supplied for each half array and a canceller implemented in each half array output. A convenient choice for a reference may be a single hydrophone located in the opposite half array.

Appendix F considers the possible bias of the broadband and narrowband bearing estimates due to the transfer functions of the adaptive cancellers prior to the tracker in Figure 12. This is done by determining the steady state mean weight of the adaptive trader via a Wiener filter approach. A bias in the broadband estimate is indicated by a shift in the position of the peak of the mean weights, while a bias in the narrowband estimate appears as a bias in the phase of the frequency domain weight containing the signal. It was assumed in all cases that the interference power dominated the signal and background noise, since this is the environment in which the canceller is applied.

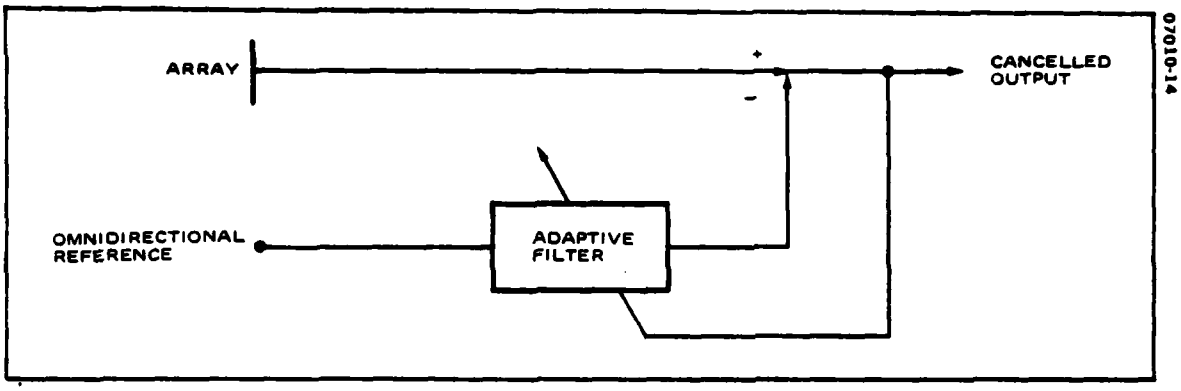

Figure 11. LMS Adaptive Canceller

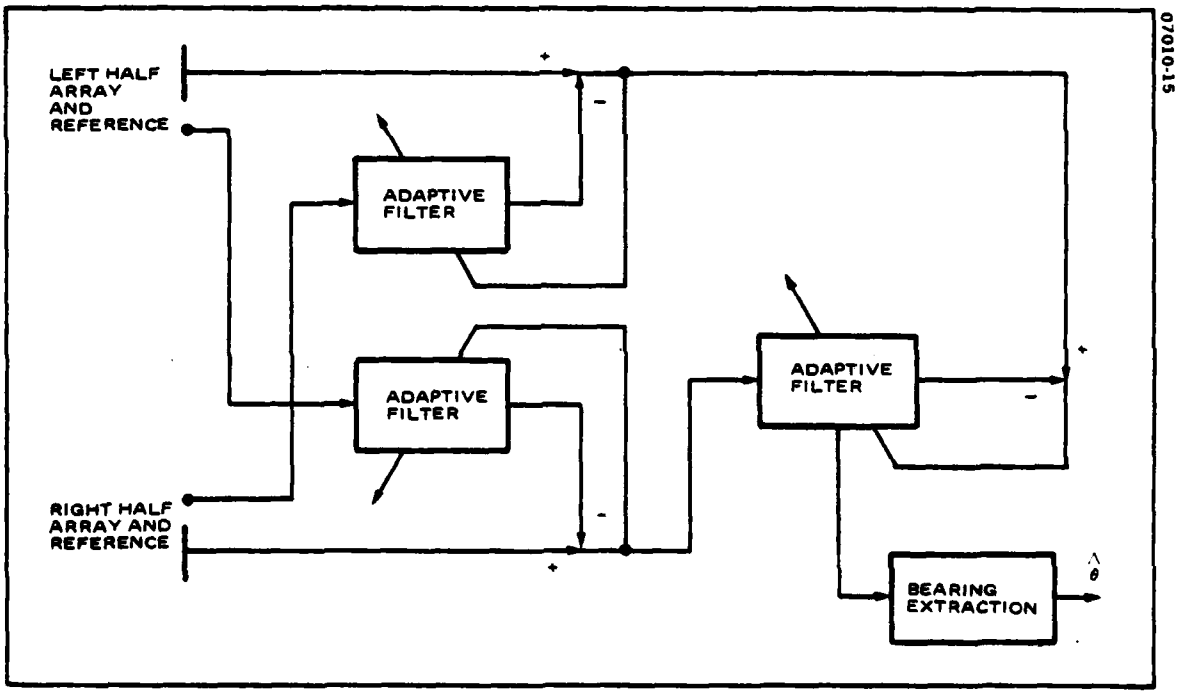

Filter 12. Adaptive Cancellation Applied to the Adaptive Tracker

In the broadband case, Appendix F shows that when the signal to background noise ratio is large (both dominated by interference), the peak in the weights due to the interference is effectively cancelled with no bias in the signal peak, hence, no bias in the broadband bearing estimate. The amplitude of the signal peak after cancelling is essentially that of the interference peak prior to cancelling, and is therefore easily tracked. When the signal to background noise ratio is small, the interference is still effectively rejected, but a small bias is introduced into the signal peak. This results in a delay estimate bias of

$$B_T = -\frac{4D}{c^2} \frac{B_I}{B_S} \left(1 - \frac{d}{D}\right) \left|\sin \theta_S - \sin \theta_I\right| \tag{35}$$

where

B_I = split beam response in direction of the interference (sidelobe response)

B_S = split beam response in direction of the signal

D = distance between split array phase centers

d = distance from split array to its reference

θ_S = signal bearing

θ_I = interference bearing.

C = speed of sound

Since the sidelobe response is small in comparison to the mainlobe response, $B_S >> B_I$, B_T is small. It can be made arbitrarily small by placing the references near the array phase centers so that $d/D \approx 1$. In addition to the bias introduced in the low SNR case the entire weight vector is attenuated proportionally to the SNR at the beamformer output, so longer time constants will be required if degradation in estimation variance is not tolerable.

In the narrowband case, tracking is only possible at relatively high SNR, as shown in [2]. Under this condition, Appendix F shows that the bias in the phase of the frequency domain weight containing the signal is approximately

$$B_{\phi} \approx 4\left[\frac{P_S}{P_I}\frac{d}{D} - \frac{B_I}{B_S}\left(1 - \frac{d}{D}\right)\right]\frac{D}{C^2}\left|\sin\theta_S - \sin\theta_I\right| \qquad (36)$$

with P_S and P_I the signal and interference powers, respectively. Since both P_S/P_I and B_I/B_S are small, the residual bias in the narrowband estimate is small.

3.6 Simulations of an Adaptive and a Conventional Split Beam Tracker With a Moving Target. During the first phase of the adaptive tracker study [1], the adaptive tracker performance was compared to a conventional adaptive tracker described in [6] with static targets Figure 13 shows a block diagram of the tracker. The input signals from the left and right half beams are hard clipped and sampled, with the clipped signal for one side subjected to a variable delay, τ. This delayed signal and the other clipped input are processed by a two point correlator, as shown, which computes the correlation, $\phi(\tau)$, of the clipped signal at τ - T. The value of $\phi(\tau)$ is either +1 or -1 for the clipped inputs. The contents of the delay register, which determines the value of the adjustable delay, is increased by $\Delta\tau$ when +1 occurs on input 2 and -1 on input 1. It is decreased by $\Delta\tau$ when +1 occurs on input 1 and -1 on input 2, with no change in count when the two agree. The tracker is in steady state when $\phi(\tau - T)$ and $\phi(\tau + T)$ are equal (both +1 or both -1). Assuming that the correlation function of the input is symmetrical, this means that the value of t is equal to the delay between the two split beam inputs.

The analytical comparison of the two trackers using the results of [1] and [6] indicated that the variance of the adaptive tracker bearing estimate was nominally a factor of 3 improved over the conventional tracker. This was supported by computer simulations of the two trackers. This appendix repeats these simulations with a dynamic target. The signal has linearly increasing time delay between array halves, which is the same as linearly varying bearing for a target at

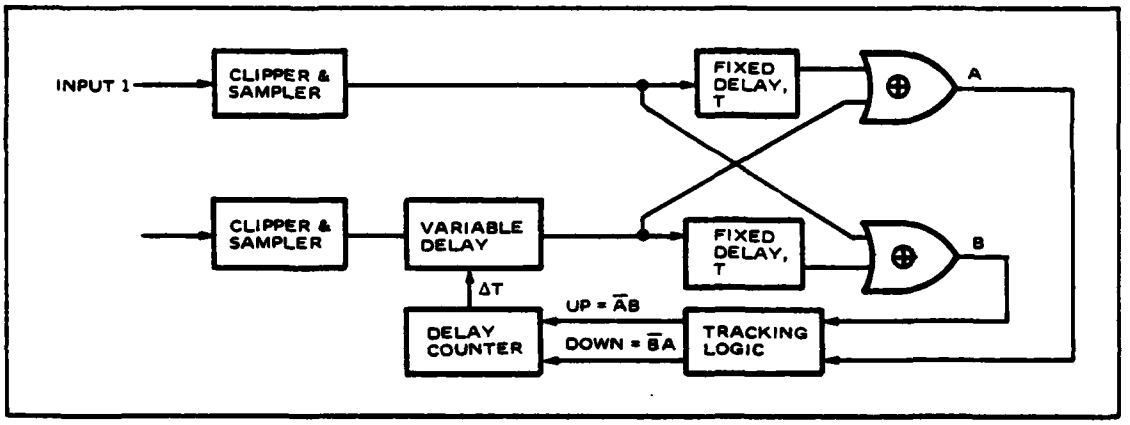

Figure 13. Two Point Correlator Tracker Block Diagram

broadside. Both the target and the background noise are uncorrelated gaussian sequences, and the background noise between the array halves is also uncorrelated. The algorithm sample rate is 24,000 Hz and no interpolation is used between taps of the adaptive filter.

The statistics of the bearing estimate were computed from an ensemble of 10 runs, with time averaging performed over 4.67 seconds in each run of the ensemble. The procedure was as follows. For a given signal-to-noise ratio, a value of the feedback coefficient, μ, was chosen so that the adaptive tracker could acquire and track the signal throughout the duration of the simulation. Since the goal was to compare the trackers during tracking, any runs with spurious loss of track were not used. The 4.7 second time averages of estimate bias and variance were computed for each such run, and an ensemble of ten of these runs averaged to yield a value of bias and variance for a given signal-to-noise ratio and bearing rate.

In order to compare the two-point correlator tracker of [6] to the adaptive tracker, its feedback parameter, Δ, was varied experimentally until the bias of the two-point correlator estimate was approximately the same as that of the adaptive tracker for the given signal-to-noise ratio and bearing rate. As in the case of the adaptive tracker, all statistics for the two point correlator were based upon an ensemble average of simulation runs, with time averaging over 4.67 seconds in each run. Due to greater run-to-run fluctuations in the estimate from the two point correlator, twenty runs were included in an ensemble. With the bias of the two trackers set approximately equal, it is possible to compare the performance based upon bearing estimate variance at a given signal-to-noise ratio, bearing rate, and bias (or lag).

Table 1 shows the results of these simulations for a signal-to-noise ratio of 0 dB and three rates of change in delay between array halves. Table 2 converts these delay rates to bearing rates for two arrays, one with a 7.5 foot baseline and the other with a 75 foot baseline. The feedback coefficient of the adaptive filter, , has been set to 2^{-18} to assure tracking. The standard deviation of the adaptive tracker estimate ranges from 0.751 to 0.975 times that of the two-point correlator. Table 3 shows the same statistics for a -10 dB signal-to-noise ratio, with $\mu = 2^{-18}$. At this lower signal to noise ratio, the advantage of the adaptive tracker is greater, with its standard deviation ranging from 0.535 to 0.73 times that of the two point correlator.

It is interesting to note that the advantage demonstrated by the adaptive tracker in these simulations is quite close to that predicted analytically in

TABLE 1. COMPARISON OF ADAPTIVE TRACKER AND TWO POINT CORRELATOR, SIMULATIONS WITH DYNAMIC TARGET: SNR = 0 dB, $\mu = 2\text{-}16$

Rate	Bias		Standard Deviation		Ratio
μ sec/sec	Adaptive Tracker	Two Point Correlator	Adaptive Tracker, σ_{adt}	Two Point Correlator, σ_{tpc}	$\sigma_{adt}/\sigma_{tpc}$
65.45	6.508×10^{-5}	6.6×10^{-5}	2.369×10^{-5}	2.429×10^{-5}	0.975
130.9	7.846×10^{-5}	7.900×10^{-5}	2.394×10^{-5}	2.804×10^{-5}	0.854
261.8	9.633×10^{-5}	9.241×10^{-5}	2.393×10^{-5}	3.184×10^{-5}	0.751

TABLE 2. CONVERSION OF DELAY RATES TO BEARING RATES FOR TWO HYPOTHETICAL ARRAYS

Delay Rate	Bearing Rate 7.5 ft Baseline	Bearing Rate 75 ft Baseline
65.45 s/s	2.5°/sec	0.25°/sec
130.9 s/s	5°/sec	0.5°/sec
261.8 s/s	10°/sec	1°/sec

TABLE 3. COMPARISON OF ADAPTIVE TRACKER AND TWO POINT CORRELATOR, SIMULATIONS WITH DYNAMIC TARGET: SNR = 10 dB, $\mu = 2^{-18}$

Rate	Bias		Standard Deviation		Radio
μ sec/sec	Adaptive Tracker	Two Point Correlator	Adaptive Tracker, σ_{adt}	Two Point Correlator, σ_{tpc}	$\sigma_{adt}/\sigma_{tpc}$
65.45	8.365×10^{-5}	8.023×10^{-5}	4.590×10^{-5}	8.576×10^{-5}	0.535
130.9	1.239×10^{-4}	1.265×10^{-4}	8.03×10^{-5}	1.422×10^{-4}	0.565
261.8	1.989×10^{-4}	1.954×10^{-4}	8.722×10^{-5}	1.194×10^{-4}	0.730

Appendix G of [2]. For a somewhat different split beam tracker, the adaptive tracker standard deviation was predicted to be 0.831 times that of the split beam tracker under the condition that

$$bc\,\delta \ll \mu\,\sigma^2\,n \ll 1$$

where

b = input bandwidth

c = rate of change in delay

δ = algorithm sample rate

σ_n^2 = input power.

For these simulations, $\mu\sigma_n^2 \ll 1$ and $(bc\delta/\mu\sigma_n^2)$ varies from 0.214 to 3.436. Since the referenced analysis used a bearing deviation indicator structure for the conventional tracker, and an exponential correlation function for the inputs, these simulations should be used only for qualitative validation of the parametric trends in that analysis.

SECTION 4.0

ADAPTIVE TRACKER PERFORMANCE WITH BROADBAND SEA TAPE DATA

4.0 ADAPTIVE TRACKER PERFORMANCE WITH BROADBAND SEA TAPE DATA

As part of the third phase of the adaptive tracker study, several tapes recorded at sea using a towed line array were processed using the broadband adaptive tracker algorithm. These sea tests utilized broadband random noise sources suspended from one or two drifting surface vessels, with the array moving relative to the sources. Two such encounters were processed, a "HOTEL" tape in which only a single source was present, and an "INDIA" tape which included two sources simultaneously. The sources are extremely strong, dominating background and tow ship noise.

The recording consists of 17 hydrophone cluster outputs from the array, with the clusters spaced every 7.25 feet. The hydrophone outputs are bandlimited to 500 Hz and sample at 1 KHz. Figure 14 shows an estimate of the power spectrum of the output of a single hydrophone during the "HOTEL" exercise, averaged over 32.7 seconds. Figure 15 shows the corresponding estimate of the autocorrelation function (ACF) of the hydrophone output. The main peak is only several taps wide (due to sampling at the Nyquist rate with a very sharp bandlimiting filter) and two large negative peaks appear adjacent to the main peak. The shape of the ACF is important in that the weight vector of the tracker will have essentially the same shape, and the bearing estimate is obtained by locating the peak of the weights.

Because of the high signal to noise ratio during the exercises, and the relatively low directivity of the half arrays over much of the band, single hydrophones were used as the inputs to the adaptive tracker rather than split arrays. The hydrophones selected provide a baseline of 72.5 feet. Two types of runs were made with the "HOTEL" data, processing the raw

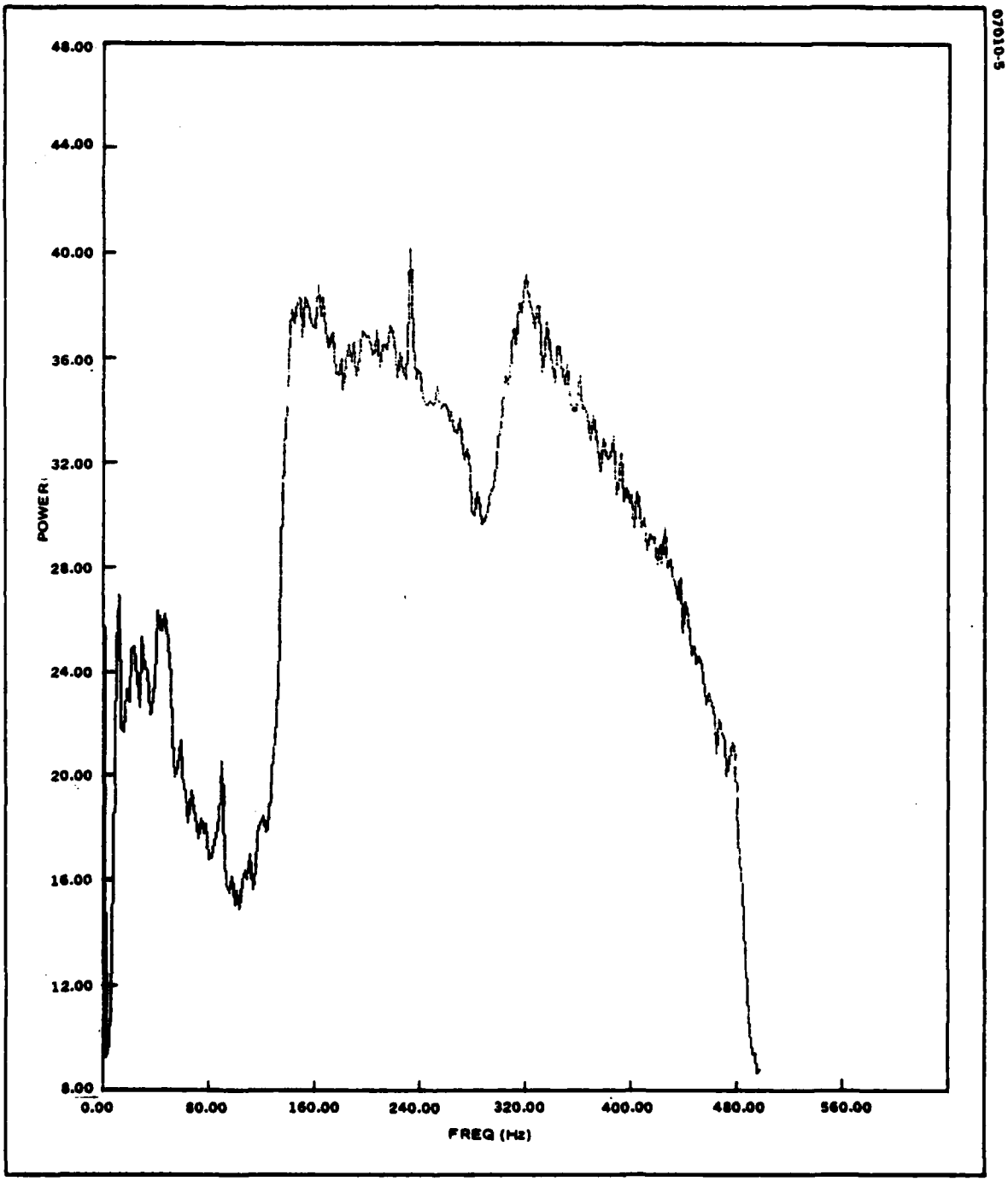

Figure 14. Estimated Power-Spectrum of Hydrophone #4 Output, Exercise HOTEL-1

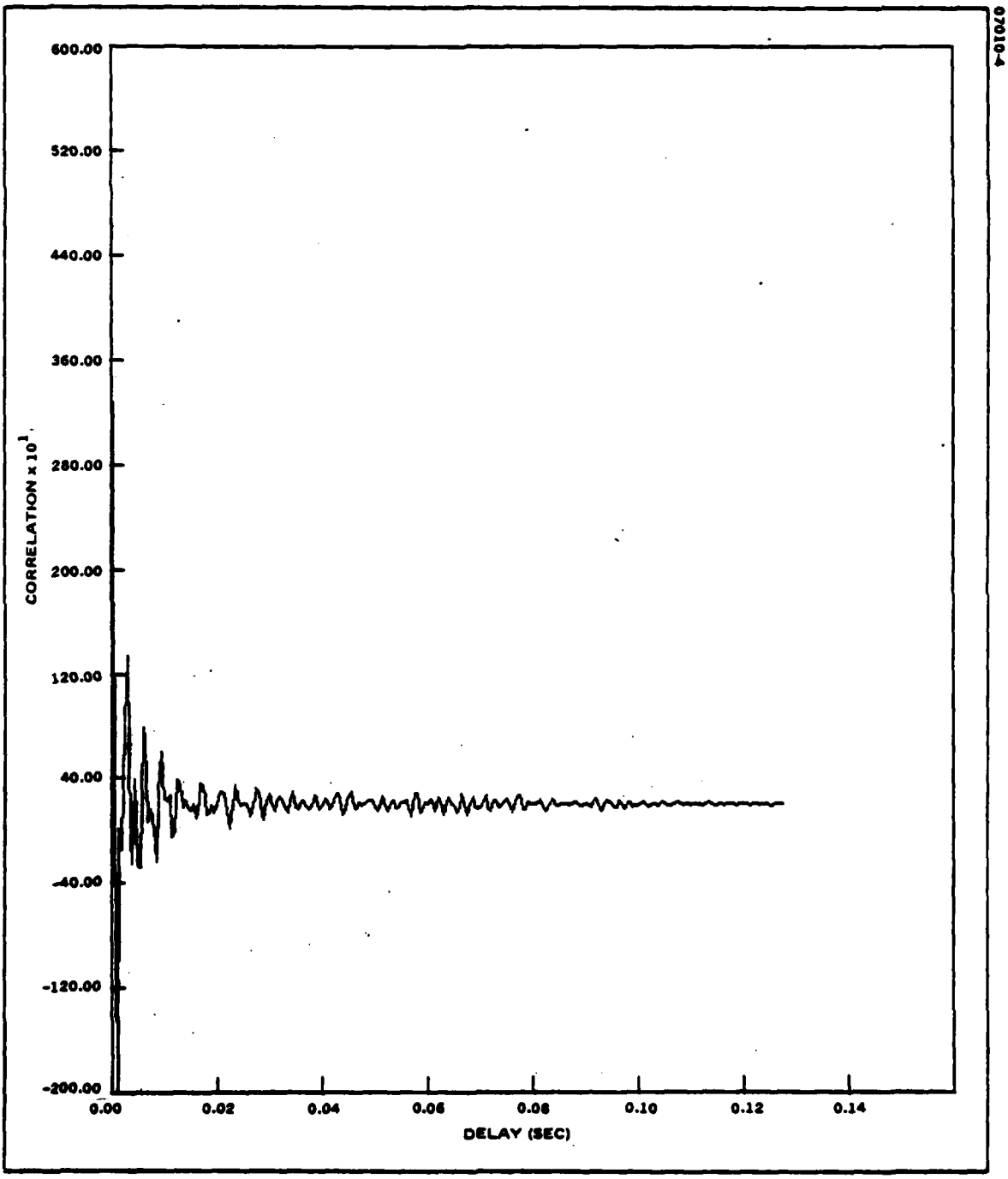

Figure 15. Estimated Autocorrelation Function of Hydrophone #4 Output, Exercise HOTEL-1

hydrophones outputs first, then tracking with additional computer generated noise added to evaluate the tracker at lower signal-to-noise ratios. The "INDIA" encounter was similarly processed.

4.1 Processing of Unmodified "HOTEL" Data. The geometry of the "HOTEL-1" exercise is shown in Figure 16. The array is towed past the noise source at 2.8 knots at a depth of 350 feet. The source is suspended at 100 feet with a nominal spectrum level of 160 dB//μPa at one yard. The closest point of approach is approximately 2214 yards, as shown in Figure 16. Assuming cylindrical spreading and a sea state of between 2 and 3, this would suggest an SNR of 20 to 30 dB at the hydrophones in the 120-480 Hz band.

The bearing estimate vs. time for three segments of the HOTEL-1 tape are shown in Figures 16 through 19. The feedback coefficient, μ, has been set at 2^{-10}, since the signal-to-noise ratio is high. The variance of the estimate is clearly well under 0.1 degrees throughout the exercise, which is not unreasonable given the high signal-to-noise ratio.

Figure 21 shows the weight vector vs. time for a 64 tap adaptive tracker with $\mu = 2^{-10}$ during the period 6:39 to 6:46 of the HOTEL-1 exercise. The track of the noise source is clearly visible. Table 4 compares the estimated bearing of the source from the adaptive tracker with the bearing reconstructed graphically from Figure 16. The "HOTEL-1" tape has also been used to evaluate several beamforming schemes, [7]. Using the result of these tests, given as a BTR plot in Figure 20, the apparent bearing of the target can be seen to be between about 33° and 20° over the same period of time, consistent with the adaptive tracker results. Part of this difference between apparent and reconstructed bearings will be due to the difference in depth between array and source. Reference [7] has also observed a yaw

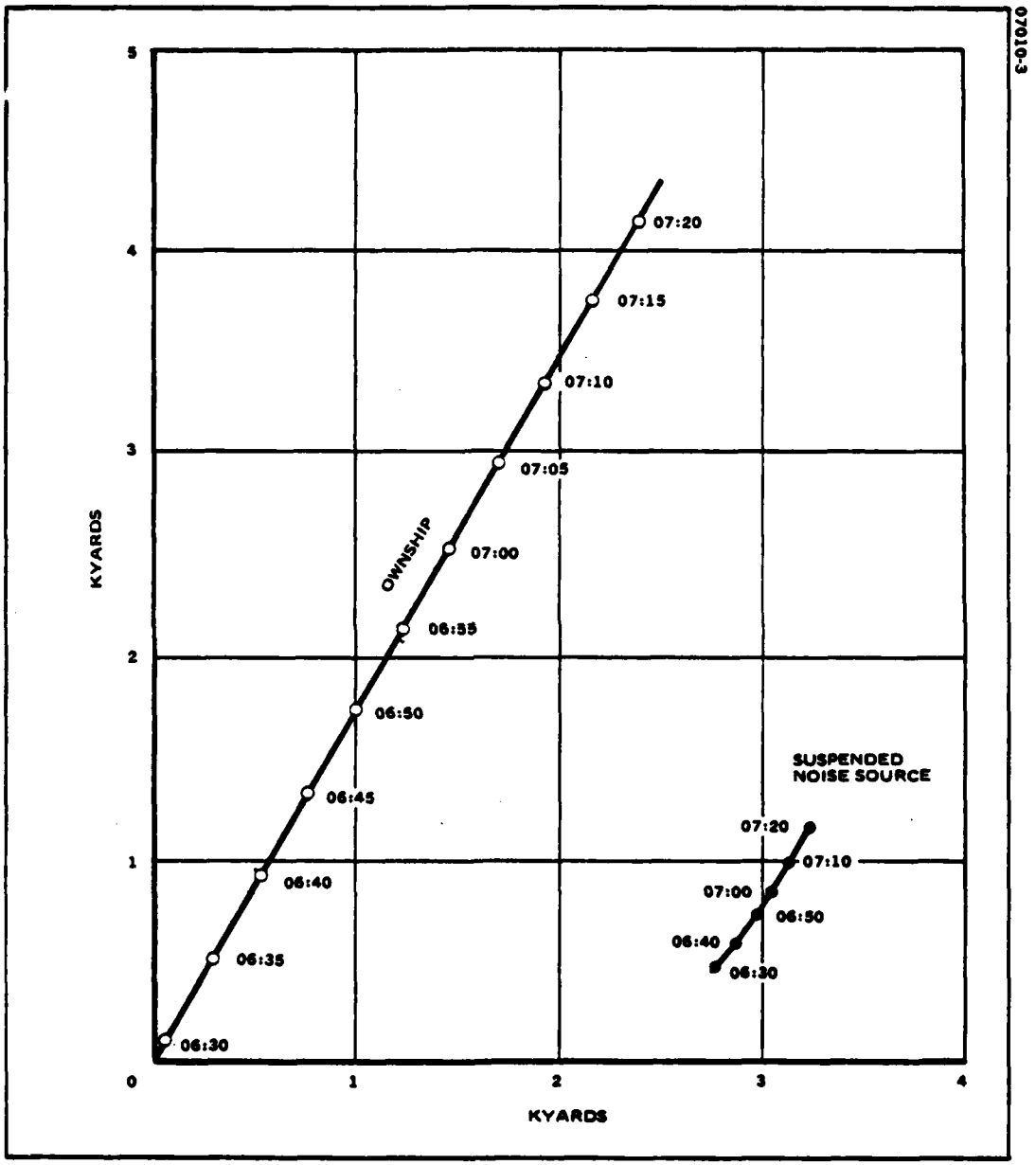

Figure 16. HOTEL Exercise Track Reconstruction

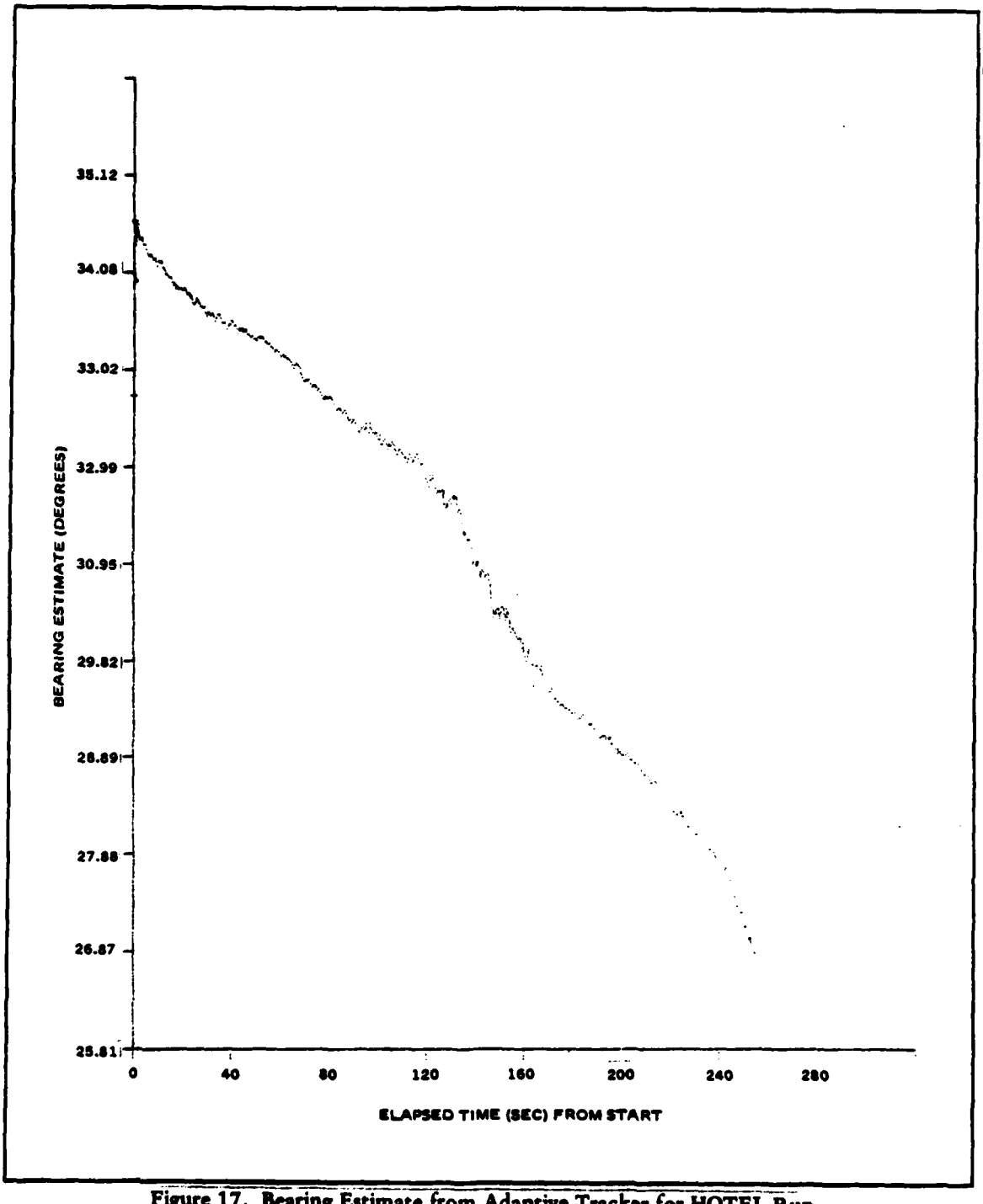

Figure 17. Bearing Estimate from Adaptive Tracker for HOTEL Run
Start of run = 06:39:2.042
End of run = 06:43:18.041

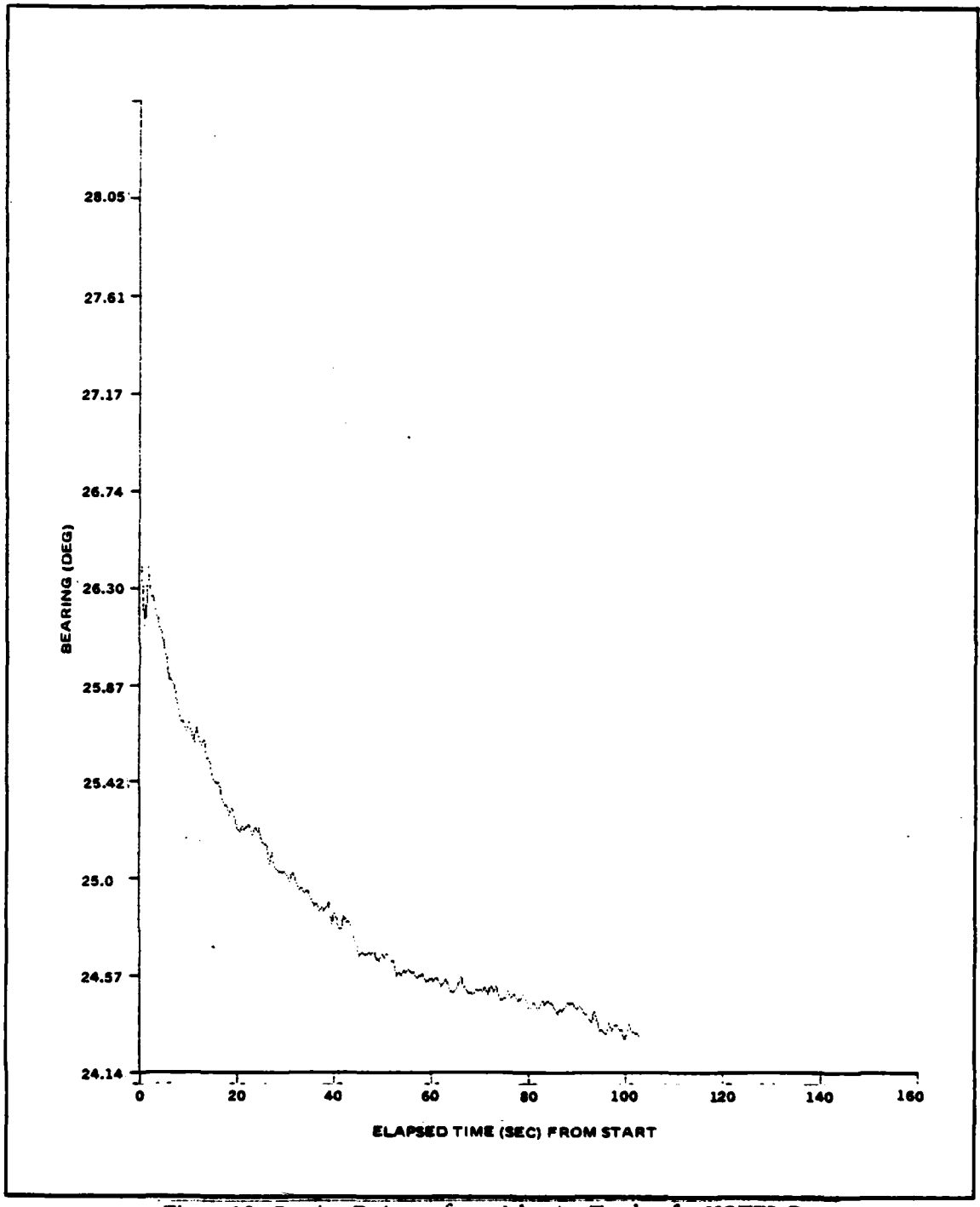

Figure 18. Bearing Estimate from Adaptive Tracker for HOTEL Run
Start of run = 06:43:18.41
End of run = 06:45: 31.00

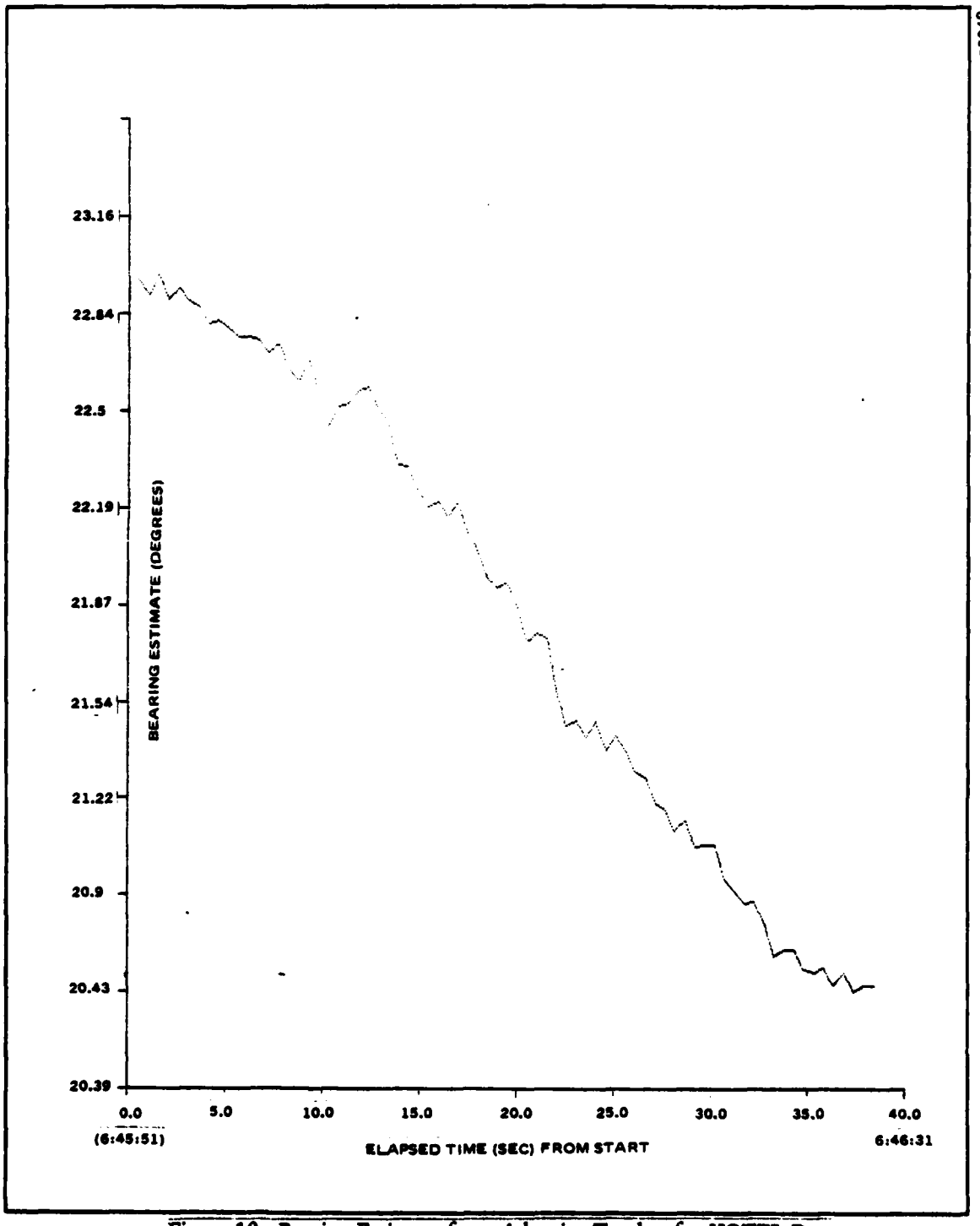

Figure 19. Bearing Estimate from Adaptive Tracker for HOTEL Run
Start of Run = 6:45:51

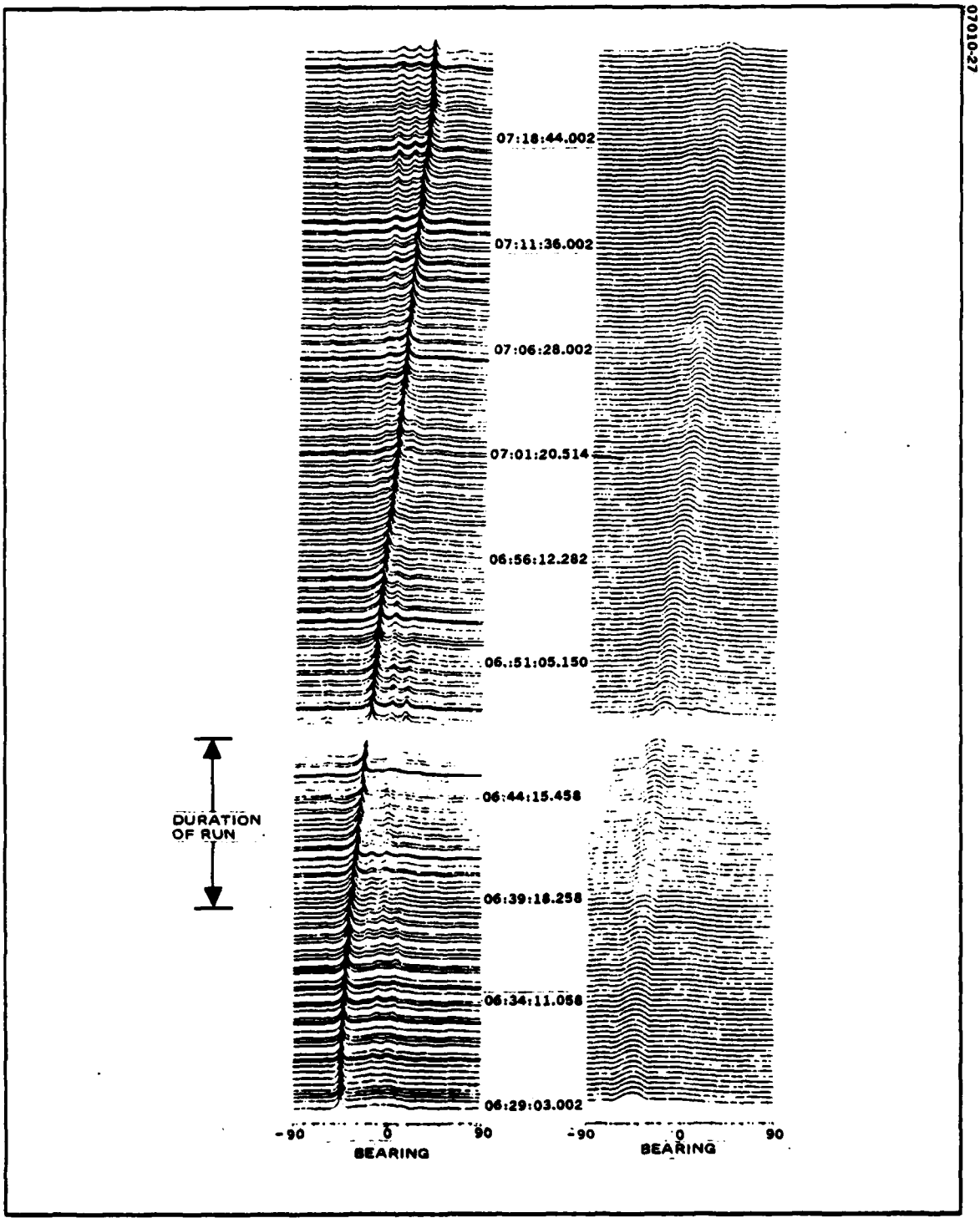

Figure 20. Bearing Time Plot for HOTEL-1 Exercise with Beamforming

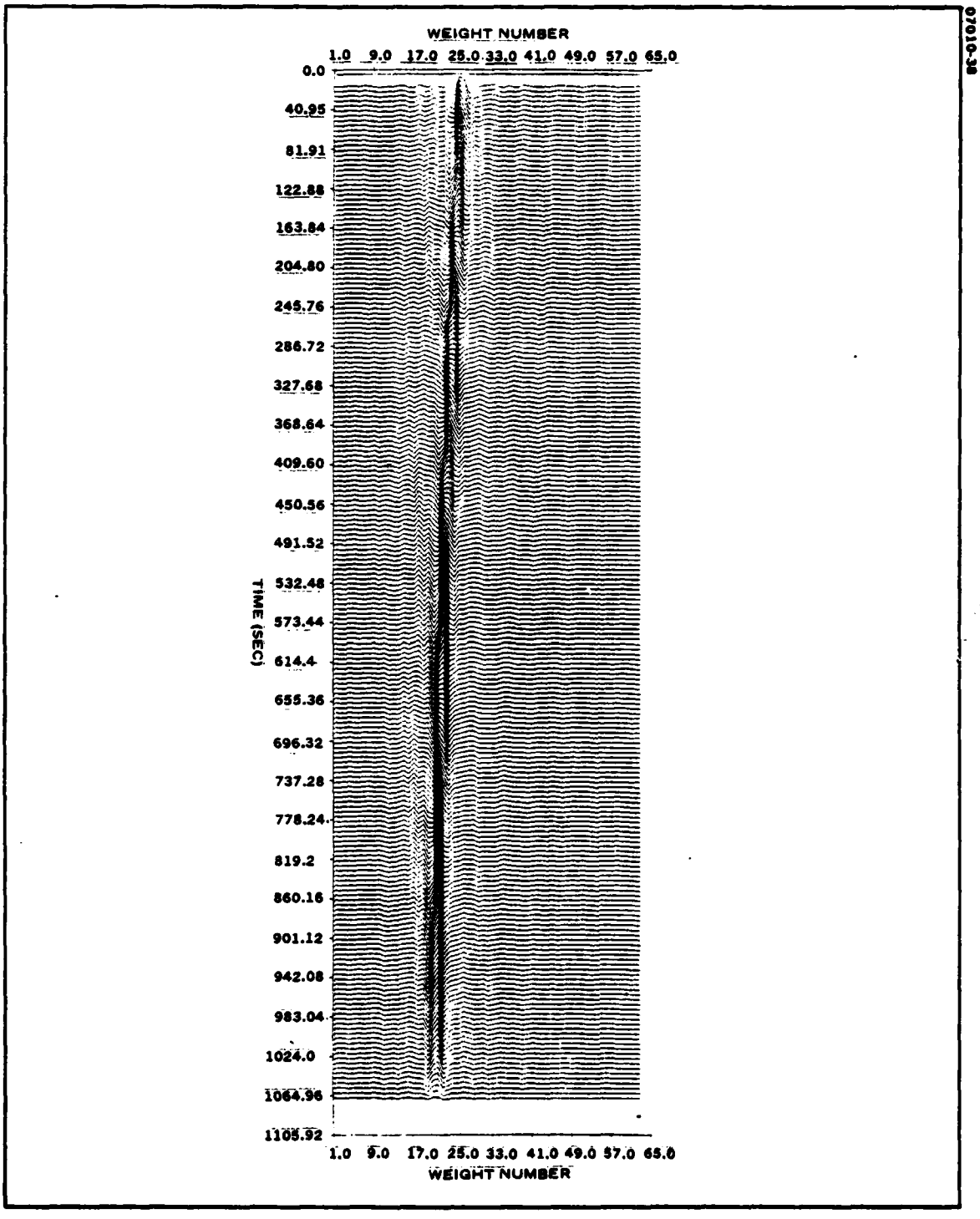

Figure 21. Adaptive Filter Weights vs Time for HOTEL Exercise

angle of 5° - 10° during the test, and indicated the possibility of array pitch and deviation of array depth from the desired value. Further, local variations in array shape, such as array curvature, could cause bearing errors, particularly when only two hydrophones are used in the bearing estimate. By using a different pair of hydrophones with the same spacing as the input to the adaptive tracker with the identical input data, it was shown in the second quarter that array curvature does not seem to be a component in the bearing error, since the bearing estimates were virtually unchanged. This conclusion is reinforced by the agreement between the adaptive tracker results and Figure 17, where the beamforming [7] used all hydrophones, and would be relatively immune to local variations in array shape.

If a fixed bias of about 11° is subtracted from the estimates, as shown in Table 4, excellent agreement is obtained with the reconstructed values. This strongly suggests that a bias of approximately 11° is the combined effect of the above factors.

4.2 Processing of HOTEL Data at Reduced Signal-to-Noise Ratio. In order to use the "HOTEL-1" data at lower signal-to-noise ratios, computer generated Gaussian noise was added to the two hydrophone outputs. The noise is uncorrelated in time and between the two inputs. Since the exact signal-to-noise ratio on the tape is unknown, the power ratio

$$R_p = \frac{P_s + P_n}{P_A} \tag{66}$$

was varied, where P_s is the signal power on the tape, P_n the noise power on the tape, and P_A the additional noise power added. The actual signal-to-noise ratio is then .

$$SNR = \frac{R_p (P_s/P_n)}{(R_p + 1) + (P_s/P_n)} \tag{67}$$

with (P_s/P_n) the unknown signal-to-noise ratio on the tape.

This modified acoustic data was applied to the adaptive tracker structure, again a 64 tap time domain filter, and μ varied from 2^{-10} to 2^{-16}. In addition, the two interpolators analyzed in Appendix E were used so that their performance could be compared with real data. The results were averaged over 26.6 seconds to produce a sample mean and variance for the bearing estimate. Table 5 shows the mean bearing for 7 values of R_p and for values of μ for both the quadratic and sin x/x interpolator, while Table 6 shows the variance for the same runs. The average is over the period of 6:44:38 to 6:45:04 of the exercise during which the reconstructed bearing will be nominally 14°. These results show generally good agreement with the theoretical predictions for a static broadband target developed in Section II. Some deviation from these predictions is to be expected since the target has a slow bearing rate and the spectrum is not exactly white. Also, these runs indicate that the sin x/x interpolator has approximately 1.5 times the variance of the quadratic interpolator, which is in the theoretically predicted range.

Table 6. Mean Bearing Estimates for HOTEL-1 Tape

	Sin(x)/x Interpolator					Quadratic Interpolator				
	10 log R_p					10 log R_p				
μ	-10	0	10	20	∞	-10	0	10	20	∞
2^{-10}	-	24.37°	24.37°	27.38°	27.39°	-	27.39°	24.40°	27.38°	27.38°
2^{-12}	24.46°	24.46°	24.46°	24.51°	24.51°	27.38°	24.46°	24.39°	24.44°	24.44°
2^{-14}	24.65°	24.57°	24.59°	24.61°	24.64°	24.59°	24.51°	24.51°	24.51°	24.51°
2^{-16}	24.98°	24.85°	24.85°	24.83°	24.85°	24.74°	24.72°	24.68°	24.68°	24.68°

Table 5. Standard Deviation of Bearing Estimate for HOTEL-1 Tape

	Sin(x)/x Interpolator					Quadratic Interpolator				
	10 log R_p					10 log R_p				
μ	-10	0	10	20	∞	-10	0	10	20	∞
2^{-10}	-	.186°	.105°	.089°	.089°	-	.115°	.068°	.0536°	.0529°
2^{-12}	.207°	.063°	.0766°	.081°	.078°	.138°	.0488°	.0488°	.0488°	.0488°
2^{-14}	.170°	.098°	.0769°	.0724°	.0756°	.111°	.0834°	.051°	.0462°	.0481°
2^{-16}	.086°	.078°	.079°	.077°	.0756°	.055°	.0529°	.056°	.055°	.054°

Table 4. Comparison of Adaptive Tracker Bearing Estimate and Reconstructed Target Bearing

Time	Graphically Reconstructed Bearing	Bearing Estimate from Adaptive Tracker	Bearing Estimate with 11° Bias Subtracted
0640	22°	33.2°	22.2°
0641	19.5°	31.98°	20.98°
0642	18.5°	29.4°	18.4°
0643	17.0°	27.88°	16.88°
0644	15°	24.76°	13.76°
0645	13.5°	24.31°	13.31°
0646	11.0°	22.98°	11.98°

4.3 Processing of the INDIA Data. In the INDIA exercise, the array is towed between two suspended broadband sources, in the geometry shown in Figure 22. Projector 1 in the figure is radiating broadband noise at a nominal source level of 160 dB re 1 μPa at 1 yard over the 17 to 500 Hz band, while projector number 2 ie operating at a source level of 120 dB. The stronger source range in nominally J Kyds, while the weaker source is a nominally 3 Kyds, so the projector 1 will appear nominally 36 dB stronger at the array. The geometry is such that projector 1 appears initially at 60^{o} forward of broadside and is at 48^{o} forward of broadside at the end of the exercise. Projector 2 starts at 32^{o} forward of broadside and finishes 14^{o} forward. The portion of the exercise processed by the adaptive tracking extends from 0035 to 0052.

The outputs of hydrophones 4 and 14 were applied to a broadband adaptive filter structure with 64 taps and with μ set at 2^{-10}. The adaptive filter weights vs time, plotted in Figure 23, show three primary peaks. The largest starts at about 60^{o} (or tap 45), with a smaller peak slightly to the right moving parallel to the large peak. Reference [7] notes that the peak associated with the strong source is often a doublet, and that a peak of unknown origin appears approximately 15^{o} to the right of the main peak, moving parallel to it. These are possibly surface reflections of projector 1. The third peak, considerably weaker than the main peak starts at about 28^{o}, or tap 39. This appears to be projector 2, based upon reconstruction from Figure 22 and the information provided [7].

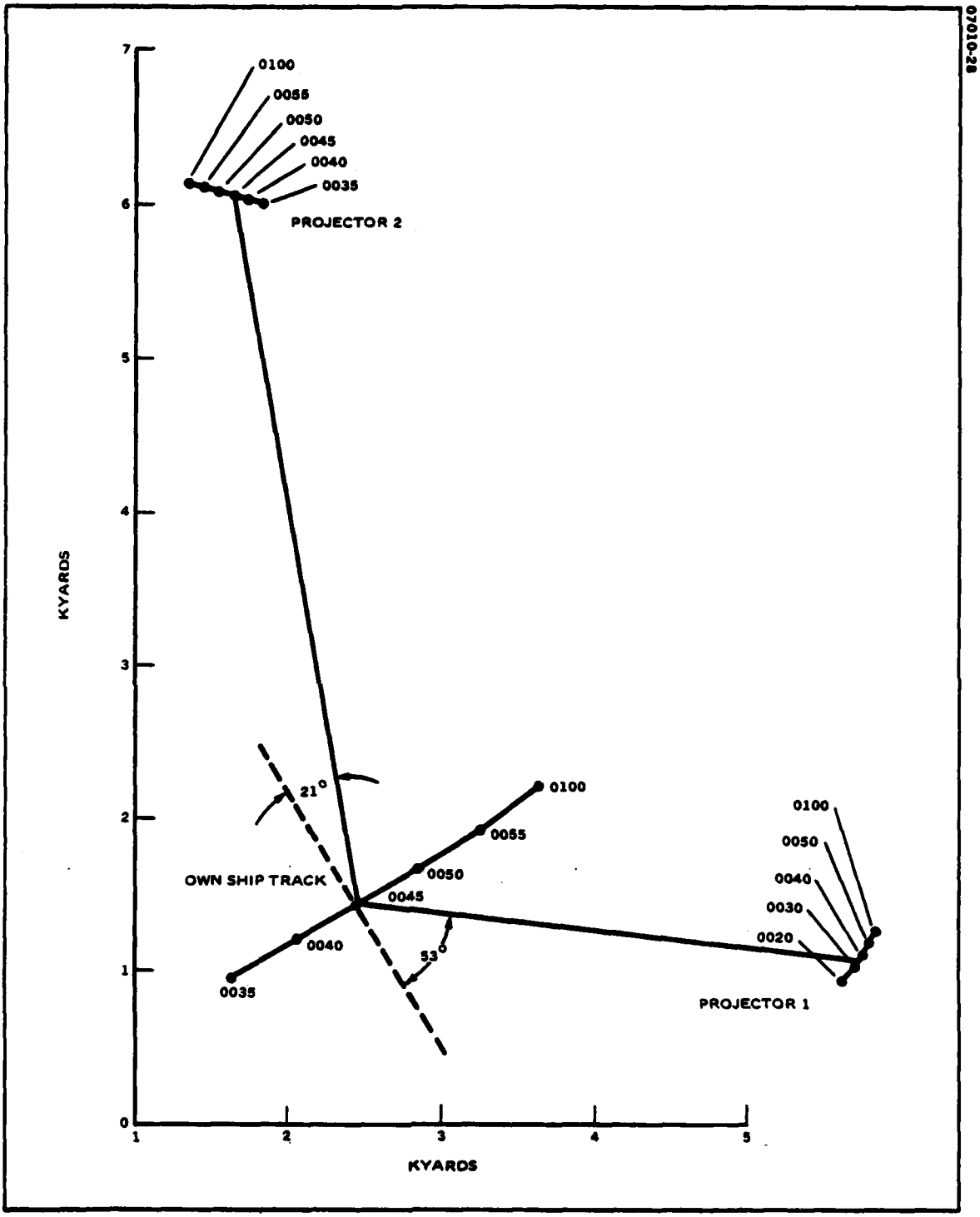

Figure 22. Array/Source Geometry for India Exercise

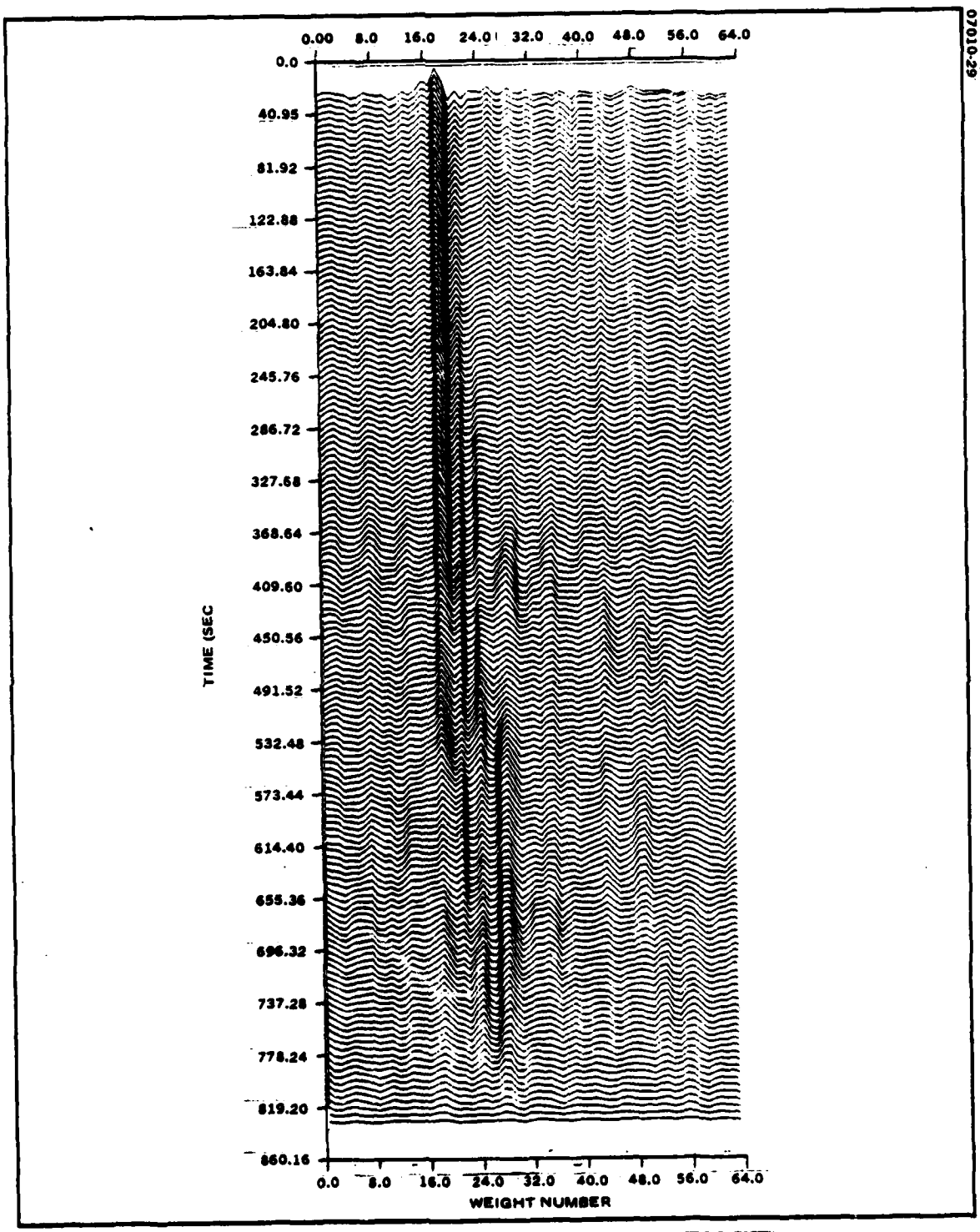

Figure 23. Adaptive Tracker Weights vs Time for INDIA Data

The adaptive tracker was assigned to the peaks at tap 45 and tap 39, using the windowing scheme described in Section 2.3. The window was selected to be 3 taps wide, centered on the tap nearest the previous delay estimate. However, the window center was not allowed to move more than one tap per iteration to prevent loss of track due to fluctuations. Figures 24 and 25 show the trades developed for the two sources projectors 1 and 2, respectively. Table 5 compares the estimates with the bearing reconstructed from the tracker of 22. The estimates for projector 1 tend to be high and relatively constant, although the reconstructed bearing is decreasing. The estimates are, however, consistent with the results of [7], in which the peak in the beamformer response due to projector 1 was constant at approximately 59^{o}. This indicates that some external phenomenon, such as array geometry, multipath, or interference between the two targets accounts for the shift in the estimates. Reference [7] notes that during this period a prominant surface reflection from the tow ship appears at 60^{o}, so it is assumed that this is the cause of the bias. The track for projector 2 shows excellent agreement with the reconstructed bearings.

As in section 4.2, the INDIA tapes were processed with additional computer generated random noise added to the hydrophone output. Since the signal-to-noise ratio on the tape was unknown, the power ratio, R_p given by (66) was varied from -10 dB to +10 dB in 10 dB steps. An R_p of X dB means that the total signal plus noise power on the tape was X dB above the added noise. Figures 26 and 27 show the tracks with R_p = 10 dB, Figures 28 and 29 with R_p = 0 dB, and Figures 30 and 31 with R_p = -10 dB. The tracks are maintained at R_p = 10 dB and 0 dB for both contacts. However, when R_p = -10 dB, the tracks are eventually lost, even though the contacts appear to be maintained initially.

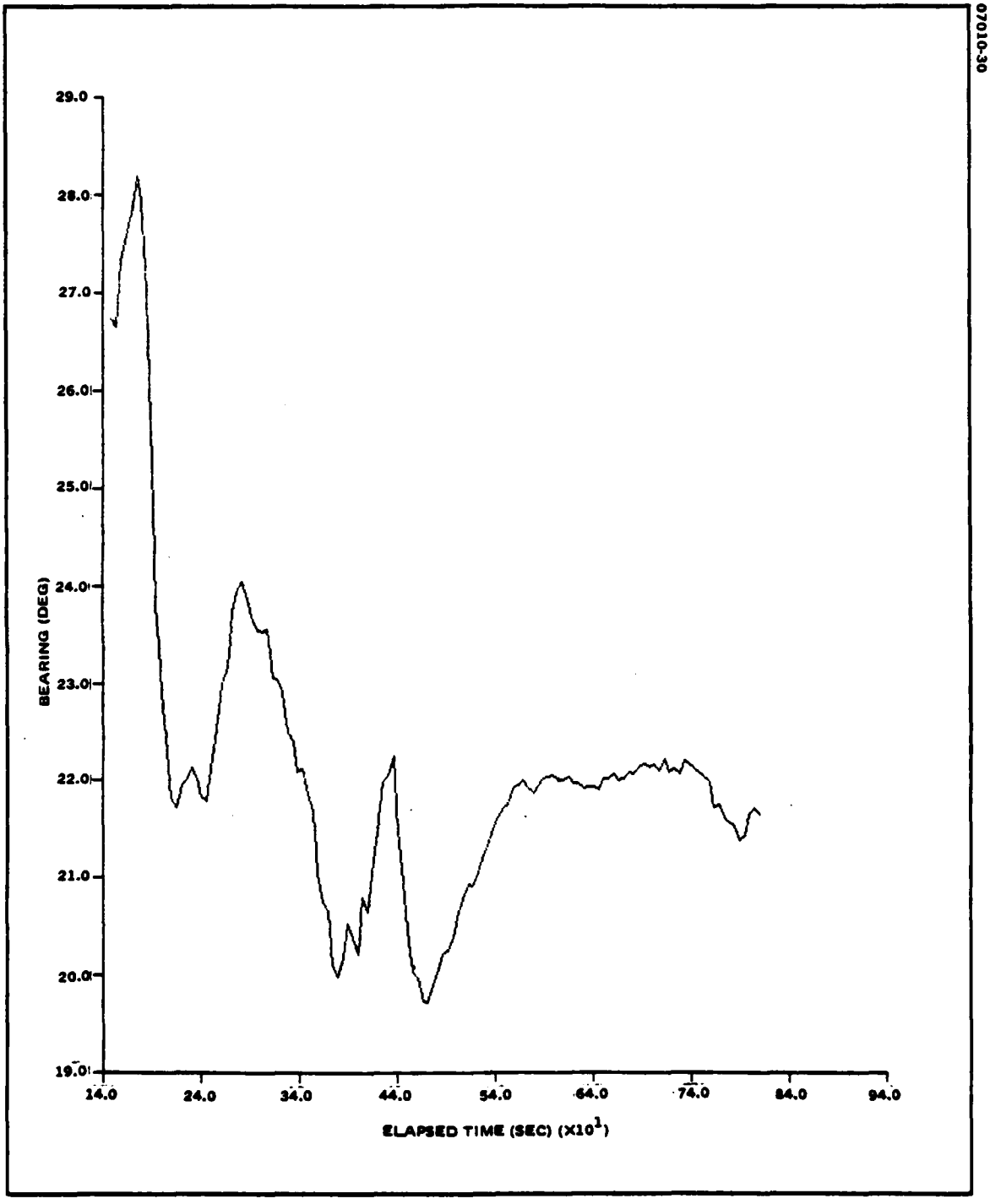

Figure 24. Track for Projector 1, India Data Start of Run = 0035, No Added Noise

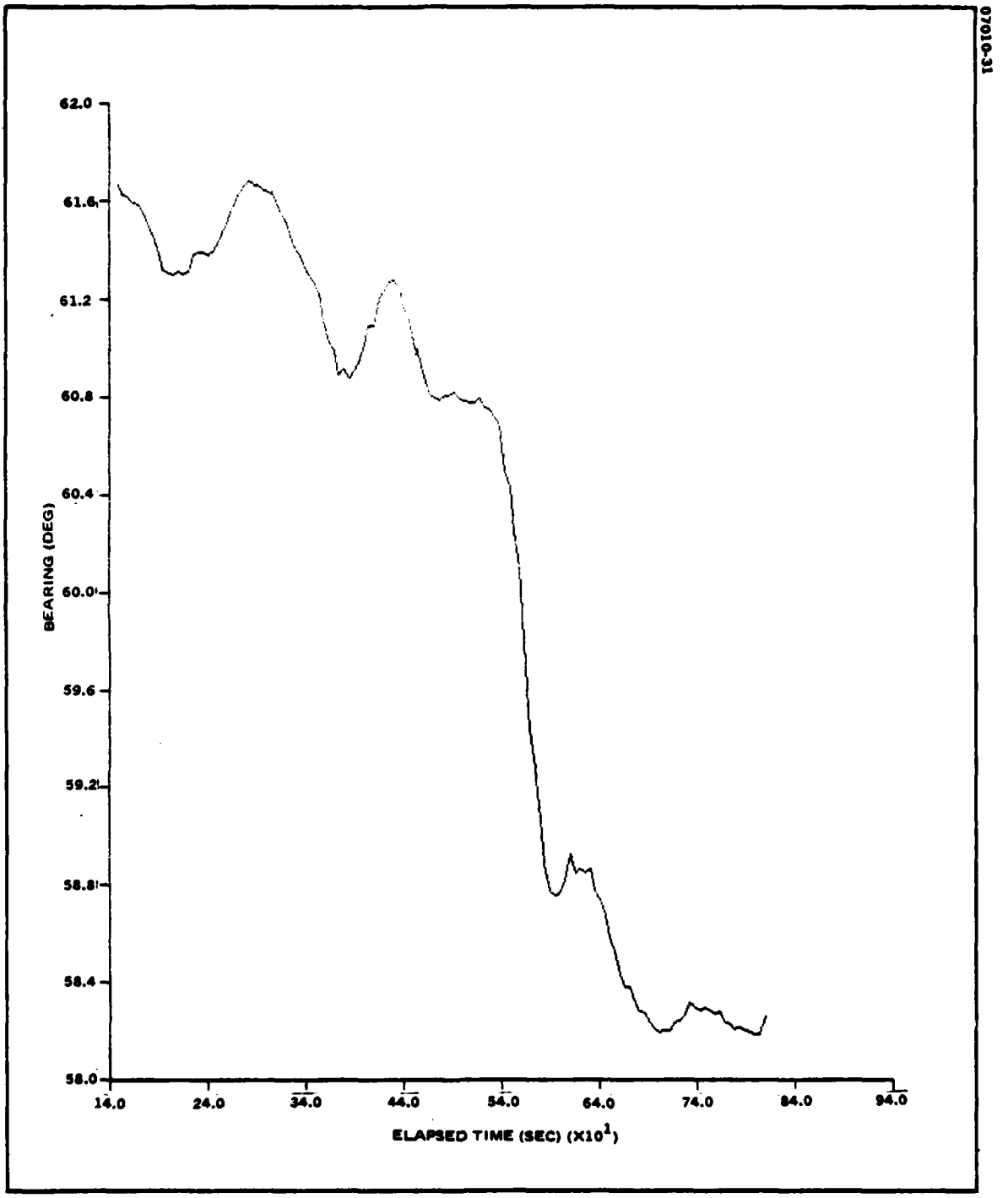

Figure 25. Track for Projector 2, India Data Start of Run = 0035, No Added Noise

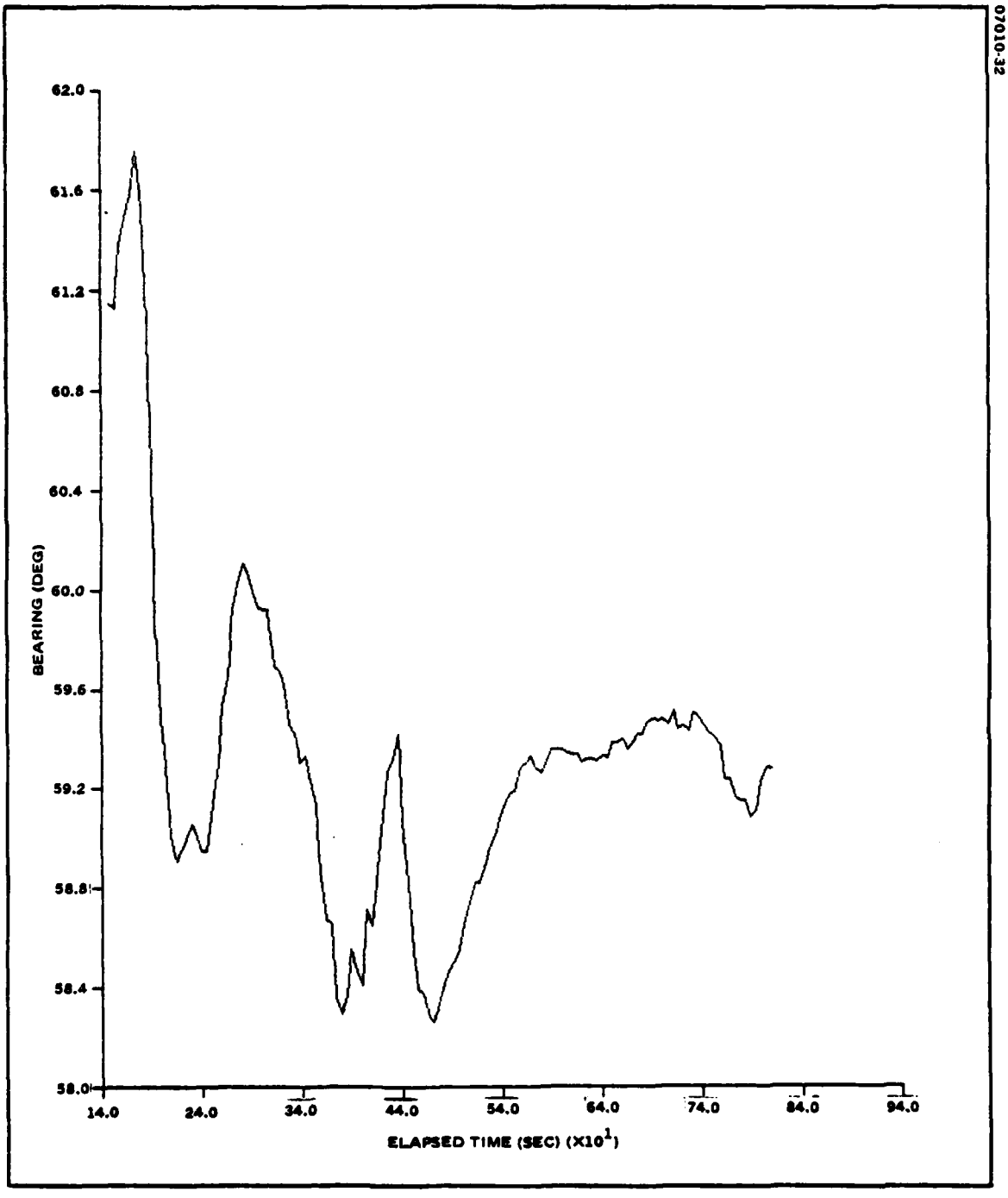

Figure 26. Track for Projector 1, India Data Start of Run = 0035, Computer Generator Noise Added, R_p = 10dB

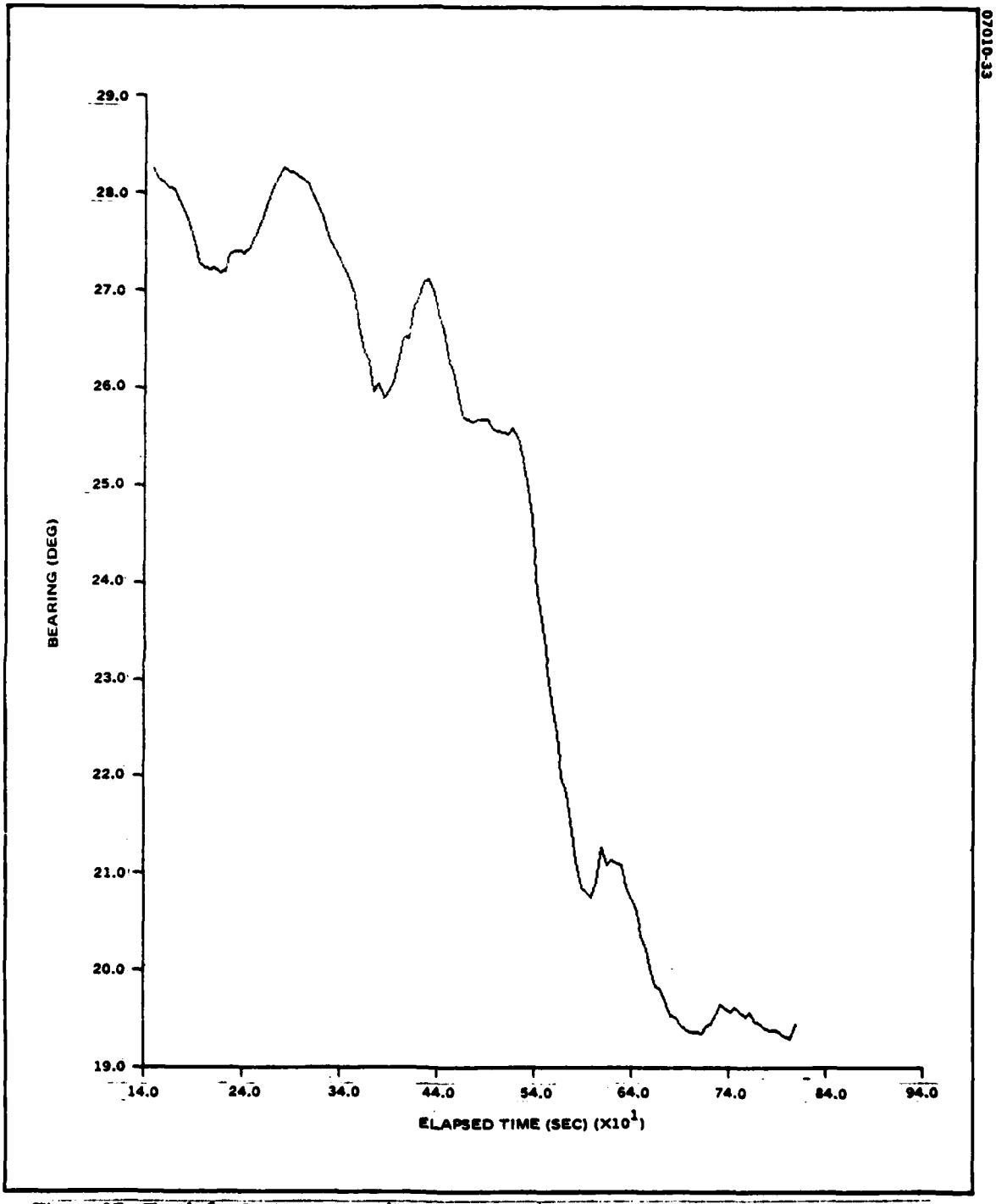

Figure 27. Track for Projector 2, India Data Start of Run = 0035 Computer Generated Noise Added Rp = 10 dB

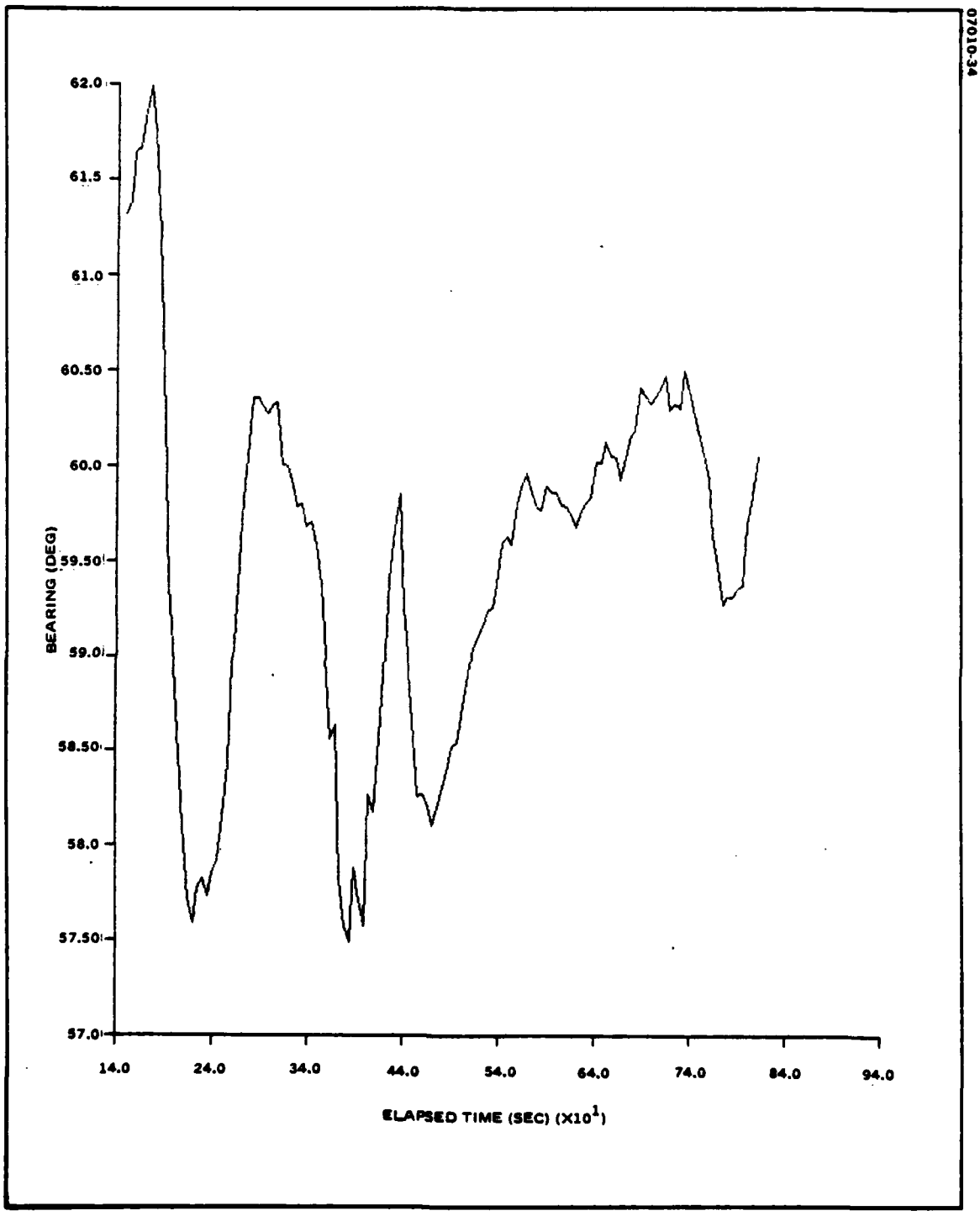

Figure 28. Track for Projector 1, India Data Start of Run = 0035, Computer Generated Noise Added, R_p = 0dB

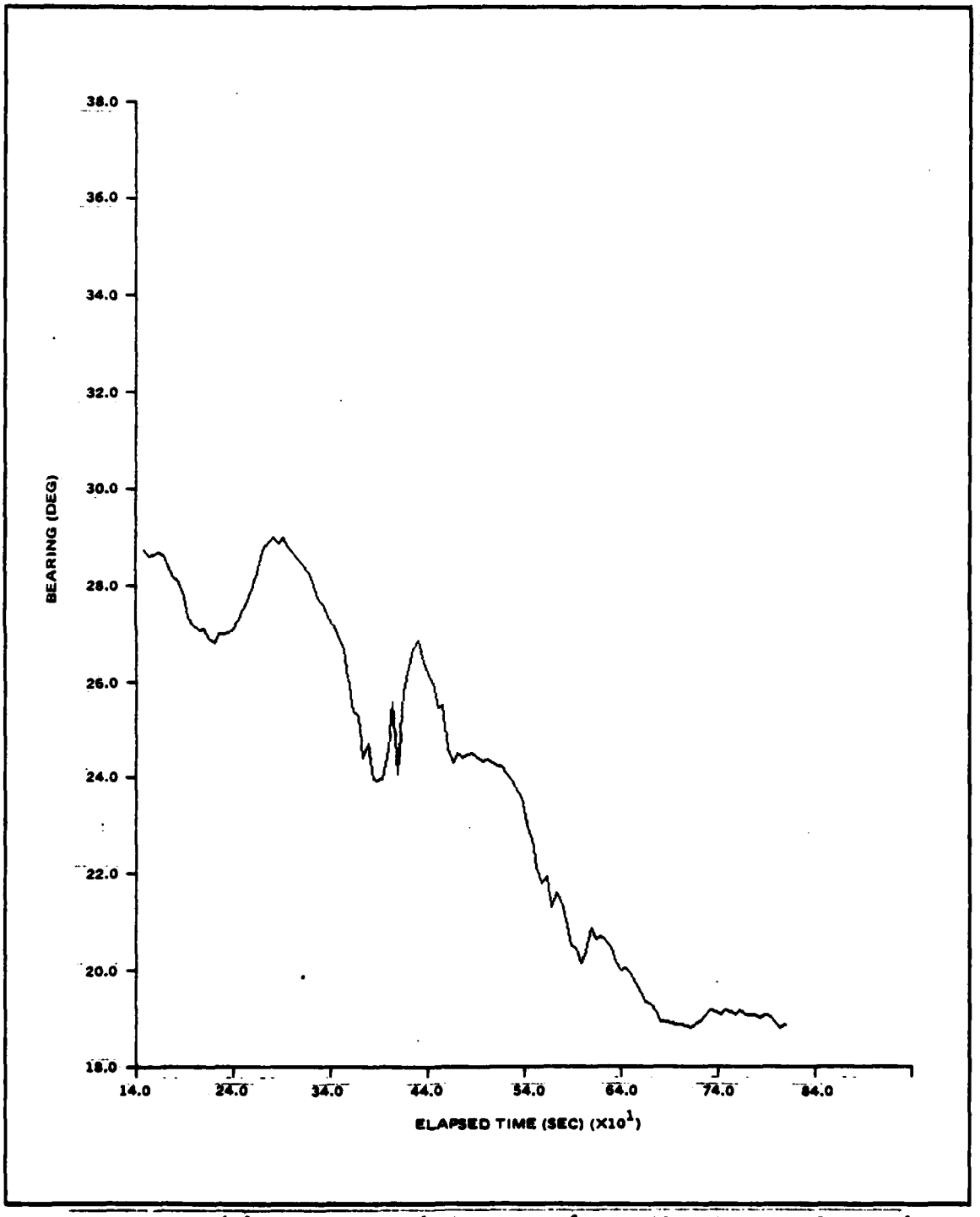

Figure 29. Track for Projector 2, India Data Start of Run = 0035, Computer Generated Noise Added, R_p = 0 dB

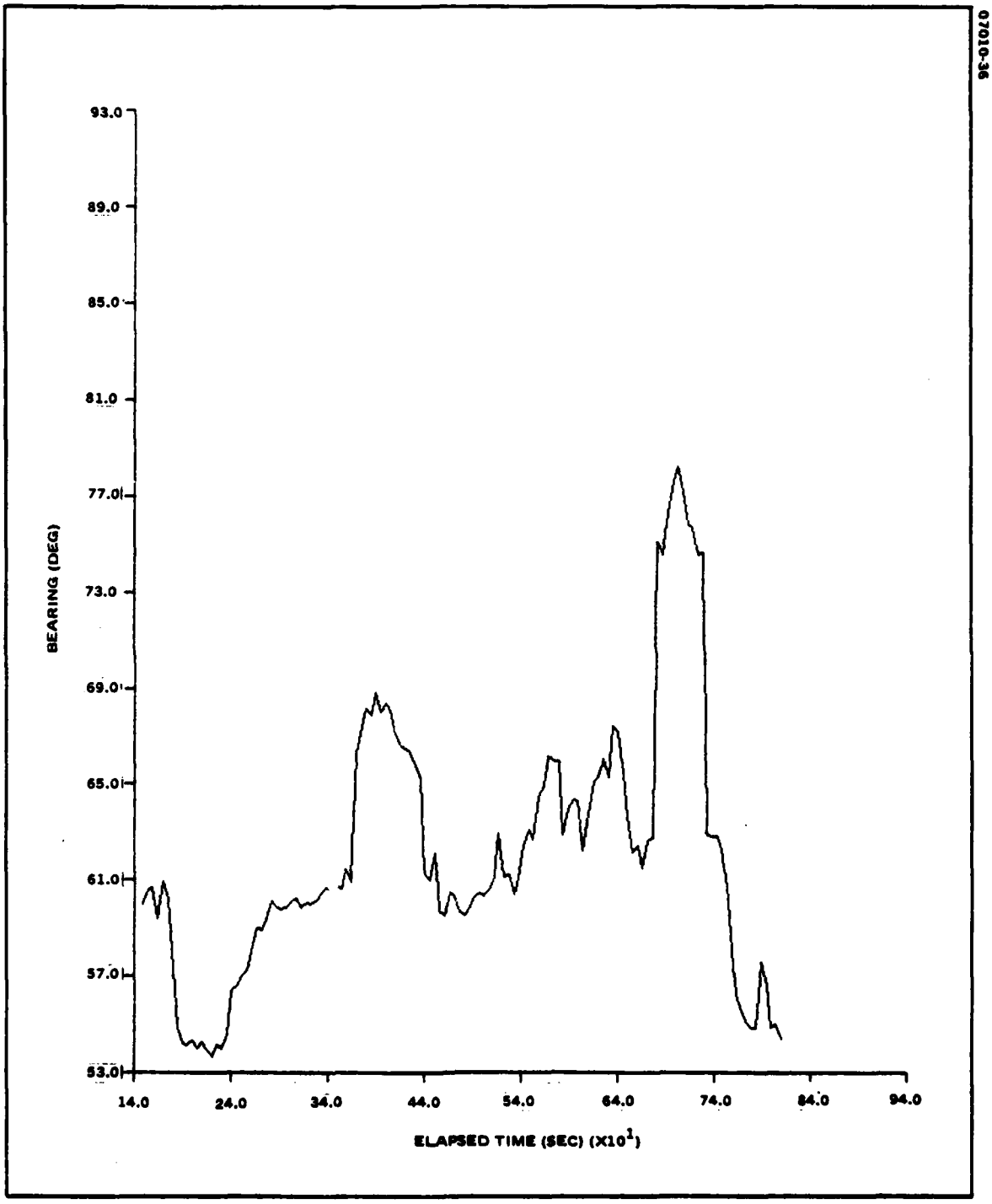

Figure 30. Track for Projector 1, India Data Start of Run = 0035, Computer Generated Noise Added, R_p = -10 dB

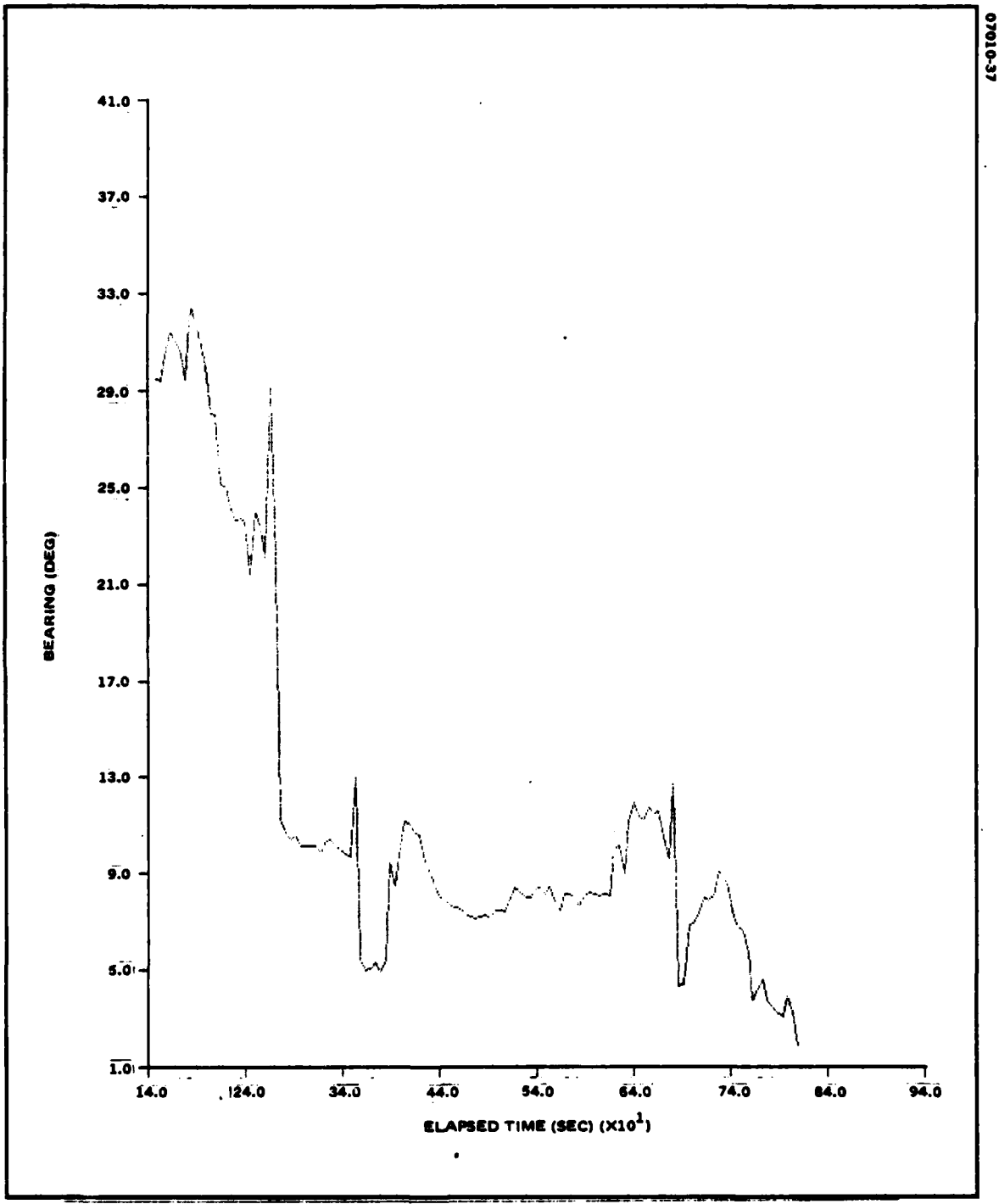

Figure 31. Track of Projector 2, India Data Start of Run = 0035, Computer Generated Noise Added, R_p = -10 dB

These results clearly indicate that multiple contacts can be tracked using a single adaptive tracker structure with the delay windowing discussed in Section 2.3. This tracking was possible in spite of the fact that the weaker source, projector 1, was not visible in the output of the conventional beamformer of reference [7]. Further, estimate standard deviations was obtained that are a small fraction of the array beamwidth at the frequencies involved.

TABLE 5. COMPARISON OF ADAPTIVE TRACKER ESTIMATES WITH RECONSTRUCTED BEARINGS FOR INDIA EXERCISE

Time	Projector 1		Projector 2	
	Reconstructed	Estimated	Reconstructed	Estimated
0037.5	58^{o}	61.4^{o}	30^{o}	28.1^{o}
0040	56^{o}	59.8^{o}	27^{o}	28^{o}
0042.5	55^{o}	58.4^{o}	24^{o}	26.5^{o}
0045	53^{o}	59.2^{o}	21^{o}	21.5^{o}
0047.5	52^{o}	59^{o}	19^{o}	19.75^{o}

SECTION 5.0

CONCLUSIONS

5.0 CONCLUSIONS – PHASES 1, 2 AND 3

A new split beam tracker structure has been presented, analyzed and simulated under a variety of single target, multiple target, broadband, narrowband, static and dynamic situations. Phase 1 demonstrated the theoretical feasibility of the device under idealistic input conditions, showing close agreement with lower bounds on the variance of the bearing estimate. In Phase 2, the performance in more realistic environments was analyzed and simulated. In particular, target dynamics and changing input spectra that differ from those used in the design of a conventional tracker were studied. The tracker responds much faster than the convergence time of the adaptive filter itself since the largest of the weights can be selected far before the weights have achieved steady-state. In the comparisons using changing input spectra, the adaptive filter tracker demonstrated the potential for dramatic improvements over a conventional tracker which is operated in an environment other than for which it was designed. This phase concluded that the adaptive filter tracker has all of the performance qualities one would associate with a tactical broadband or narrowband tracker, thus logically leading to the third phase.

Phase 3 addressed the systems considerations in the application of the adaptive tracker to sonar arrays. This included the simultaneous tracking of multiple targets, the effects of strong plane wave interference, the combining of both broadband and narrowband target data (rather than separating the data into a broadband tracker and a narrowband tracker), the effects of arrays on the inputs, and general operational system considerations. Again, the analytical results were verified with computer simulations. In addition, recorded sea-data from the elements of a towed array were employed as well.

In summary, there are some genuine advantages in performance and perhaps even in implementation offered by the adaptive filter tracker over conventional trackers. The performance benefits come when signal or noise statistics are not known to the designer of the front-end filters on a conventional system. Implementation benefits can occur when sampling rates at the beamformer outputs are much slower than the time resolution required to achieve a specified angular estimation accuracy. The adaptive tracker interpolates between tap values rather than having to sample at a higher rate. In terms of dynamic behavior, the adaptive filter tracker is understood, analysis predicting simulated tracking rates and the resulting possible lag. Windowing on the filter weights allows handling of multiple targets, and putting second-order dynamics on the track window functions enables a single adaptive filter tracker to follow more than one target, even if their tracks cross. Although the signal-to-noise ratio performance is comparable to that of nonadaptive trackers under ideal conditions, in practical unknown environments the adaptive filter tracker can realize the predicted performance via its capabilities to estimate statistics and adjust accordingly.

Thus, in the three phases of this study, the LMS adaptive filter configured as a bearing tracker has been carried from a concept, to a well understood design, to a stage ready for system application, test and evaluation.

REFERENCES

[1] P.L. Feintuch, F.A. Reed, and N.J. Bershad, "Final Report on Phase 1 of the Adaptive Tracking System Study," October 1978, Hughes Aircraft Company Final Report FR7B-11-1345, prepared for the Naval Sea Systems Command Code 06H1

[2] P.L. Feintuch, F.A. Reed, N.J. Bershad, and C.M. Flynn, "Final Report on Phase 2 of the Adaptive Tracking System Study," October 1979, Hughes Aircraft Company Final Report FR-11-1127, prepared for the Naval Sea Systems Command Code 63R

[3] F.A. Reed and P.L. Feintuch, "A Comparison of LMS Adaptive Cancellers Implemented in the Time Domain and Frequency Domain," submitted to IEEE Transactions on Acoustics, Speech, and Signal Processing

[4] V.H. MacDonald and P.M. Schultheiss, "Optimum Passive Bearing Estimation in a Spatially Incoherent Noise Environment," J. Acoustical Society of America, Vol. 46, No. 1, 1969

[5] B. Widrow, et al, "Adaptive Noise Cancelling: Principles and Applications," Proc. of the IEEE, Vol. 63, No. 12, Dec. 1975

[6] C.N. Pryor, "A Simplified Automatic Tracking Technique for Signal Correlation Systems," NOL Technical Report No. 67-152, 21 September 1967

[7] "An At-Sea Experiment to Evaluate Maximum Entropy Beamforming (S/NFD)," TI Final Report No. ALEX(03)-FR-77-02, 31 Oct. 1977

[8] "Evaluation of High Resolution Beamforming Techniques on At-Sea Data (S/NFD)," TI Final Report Number SUIT-FR-79-02, 18 May 1979

APPENDIX A

EFFECTS OF MULTIPATH

APPENDIX A

EFFECTS OF MULTIPATH

In the work during the first two phases of the adaptive tracking systems study [1,2], the signal has been assumed to arrive at the sonar array via a single plane wavefront. In most sonar environments, however, the signal arrives via multiple paths, for example, direct, surface reflection, and bottom bounce. This appendix considers the effects of the multipath propagation on the performance of the split beam adaptive tracker and, in particular, assesses the sensitivity of the adaptive tracker to multipath relative to conventional trackers.

A model for the outputs of the split array beamformers with N multipath arrivals of a single target is

$$x(t) = \sum_{n=1}^{N} a_n s(t-\gamma_n) + n_x(t) \tag{A-1}$$

and

$$d(t) = \sum_{n=1}^{N} b_n s(t-\lambda_n-\tau_n) + n_d(t) \tag{A-2}$$

Here, a_n and b_n are the attenuations of the signal along the nth path to the left half and right half arrays, respectively, γ_n and λ_n are the propagation delays along those paths, and τ_n is the inter-array delay associated with each path. The value of τ_n depends upon the angle, β_n, the wavefront makes with the axis of the phase centers,

$$\tau_n = \frac{d}{c} \sin\beta_n \tag{A-3}$$

where

$$\sin\beta_n = \cos\phi_n \sin\theta \tag{A-4}$$

with θ the target bearing for all paths and ϕ_n the arrival angle of the nth path in the vertical plane at angle θ.

This problem can be looked at in terms of linear system theory as

$$x(t) = h_x(t) \circledast s(t) + n_x(t) \tag{A-5}$$

and

$$d(t) = h_d(t) \circledast s(t) + n_d(t) \tag{A-6}$$

where $x \circledast y$ is the convolution of x and y and where h_x and h_d are impulse responses given by

$$h_x(\tau) = \sum_{n=1}^{N} a_n \delta(\tau - \gamma_n) \tag{A-7}$$

$$h_d(\tau) = \sum_{n=1}^{N} b_n \delta(\tau - \lambda_n - \tau_n) \tag{A-8}$$

Let $H_x(w)$ and $H_d(w)$ be the transfer functions corresponding to $h_x(\tau)$ and $h_d(t)$. Then the power-spectral density of x(t) is

$$S_{xx}(\omega) = \left|H_x(\omega)\right|^2 S_{ss}(\omega) + S_{nx}(\omega) \tag{A-9}$$

and the cross-spectrum between d and x is

$$S_{dx}^*(\omega) = H_d(\omega) H_x^*(\omega)\, S_{ss}(\omega) \tag{A-10}$$

with

$S_{ss}(\omega)$ = power spectrum of s(t)

$S_{nx}(\omega)$ = power spectrum of $n_x(t)$

The adaptive tracker weight will converge to the discrete Wiener filter for these inputs, which approximates the continuous Wiener filter if the filter is long enough and the sample rate is adequate. The continuous Wiener filter for this example is given by the ratio of (A-10) to (A-9)

$$W_f(\omega) = \frac{H_d(\omega)H_x^*(\omega)S_{ss}(\omega)}{|H_x(\omega)|^2 S_{ss}(\omega) + S_{nx}(\omega)} \tag{A-11}$$

From (A-7) and (A-8)

$$H_x(\omega) = \sum_{n=1}^{N} a_n e^{-j\omega\gamma_n} \tag{A-12}$$

and

$$H_d(\omega) = \sum_{n=1}^{N} b_n e^{-j\omega(\lambda_n+\tau_n)} \tag{A-13}$$

In most sonar encounters, the dimensions of the array are small in comparison to the range to the target, so that the target is in the far field (otherwise the plane wave assumption is invalid). It is therefore reasonable to assume that the array is a point receiver with respect to the target, so that the propagation delays along any path to the half arrays are the same, i.e., $\gamma_n=\lambda_n$. Consequently, $a_n=b_n$ and

$$H_x(\omega) = \sum_{n=1}^{N} a_n e^{-j\omega\gamma_n} \tag{A-14}$$

and

$$H_d(\omega) = \sum_{n=1}^{N} a_n e^{-j\omega(\gamma_n+\frac{d}{c}\cos\phi_n\sin\theta)} \tag{A-15}$$

One comparison of interest is between the adaptive tracker and a conventional split beam tracker which bases its delay estimate on the location of the peak of the correlation function of the split beam outputs (or, equivalently, on the zero crossing of its derivative)[4]. If $H_w(\omega)$ is the transfer function of the fixed spectral weighting filter of the conventional tracker, the cross-spectral density between the split array outputs is

$$C(\omega) = |H_w(\omega)|^2 \; H_d(\omega)H_x^*(\omega)S_{ss}(\omega) \tag{A-16}$$

From[4], the optimal choice of $|H_w(\omega)|^2$ is the generalized Eckart filter,

$$|H_w(\omega)|^2 = \frac{S_{ss}(\omega)}{S_n^2(\omega)+MS_{ss}(\omega)S_n(\omega)} \tag{A-17}$$

Here it has been assumed that the details of the multipath structure are unknown and the Eckart filter design must be based upon the signal and noise spectra only. At low signal-to-noise ratio (SNR), (A-11) reduces to

$$W_f(\omega) \approx \frac{1}{S_{nx}(\omega)} \; H_d(\omega)H_x^*(\omega)S_{ss}(\omega) \tag{A-18}$$

while (A-16) becomes

$$C(\omega) = \frac{S_{ss}(\omega)}{S_n^2(\omega)} H_d(\omega)H_x^*(\omega)S_{ss}(\omega) \tag{A-19}$$

Now, assume that the signal and noise both have the same spectral shape, i.e.,

$$S_s(\omega) = P_s S(\omega) \text{ and } S_n(\omega) = P_n S(\omega) \tag{A-20}$$

so

$$W_f(\omega) \approx \frac{P_s}{P_n} H_d(\omega)H_x^*(\omega) \tag{A-21}$$

AD-A096 167 HUGHES AIRCRAFT CO FULLERTON CA GROUND SYSTEMS GROUP F/G 17/1
ADAPTIVE TRACKING SYSTEM STUDY.(U)
OCT 80 P L FEINTUCH, F A REED, N J BERSHAD N00024-79-C-6405
UNCLASSIFIED HAC-FR81-11-70 NL

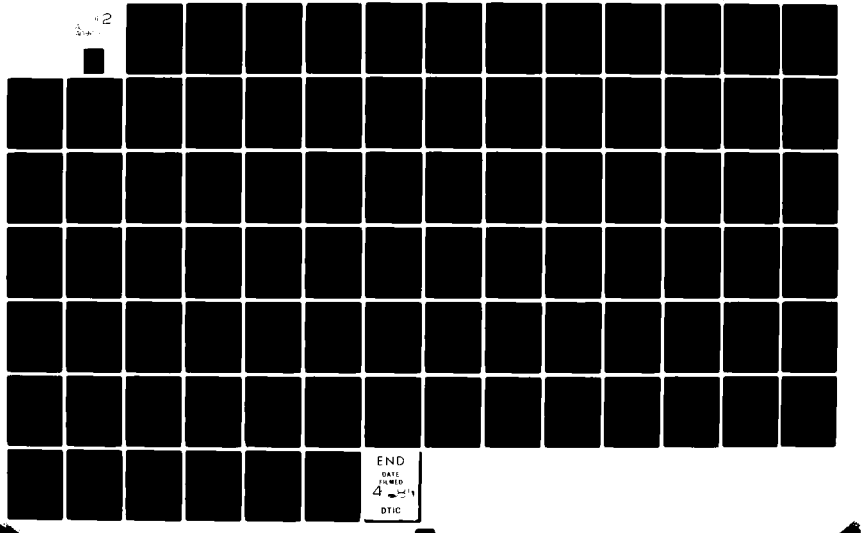

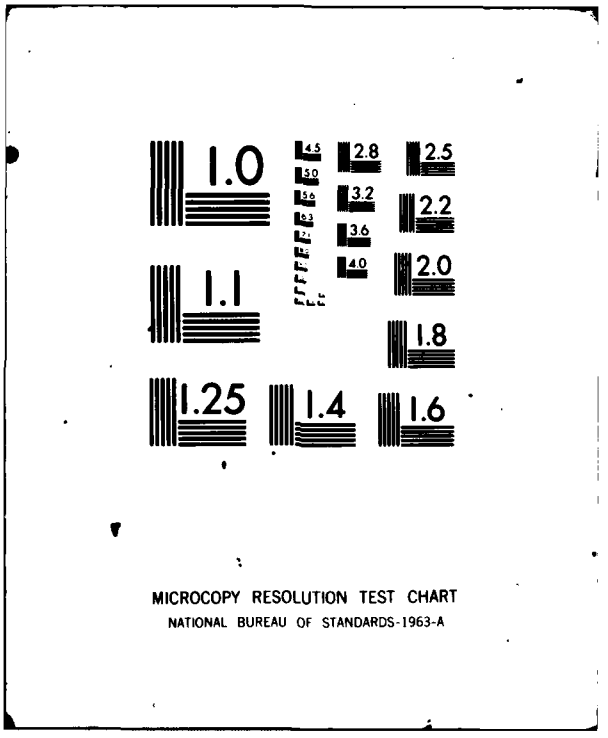
1.0
1.1
1.25
1.4
1.6
1.8
2.0
2.2
2.5
2.8
3.2
3.6
4.0
4.5
5.0
5.6
6.3
7.1
MICROCOPY RESOLUTION TEST CHART
NATIONAL BUREAU OF STANDARDS-1963-A

and

$$C(\omega) = \frac{P_s^2}{P_n^2} H_d(\omega) H_x^*(\omega) \tag{A-22}$$

Comparing (A-21) and (A-22), it can be seen that at low SNR, the adaptive filter weight vector and the cross-correlation function have the same form except for a scale factor. Therefore, the two trackers will exhibit the same sensitivities to multipath, at least in terms of mean behavior.

Similarly, a conventional narrowband estimate would be based upon the phase of the cross-spectrum at the signal frequency, ω_o, where high SNR is of interest for most broadband targets. From (A-11) and (A-16), it can be seen that the weight vector and cross-spectrum will have the same phase, so that the sensitivity of the two trackers to multipath will be the same.

In order to examine the sensitivity of the adaptive tracker to multipath in the broadband case (low SNR), let

$$G(\omega) = \frac{S_{ss}(\omega)}{S_{nx}(\omega)} \tag{A-23}$$

and let $g(\tau)$ be the inverse Fourier transform of $G(\omega)$. Also, let

$$k_N(\omega) = H_d(\omega) H_x^*(\omega) = \sum_{n=1}^{N} \sum_{m=1}^{N} a_n e_m e^{-j\omega\left[(\gamma_m - \gamma_n) + \tau_n\right]} \tag{A-24}$$

and its inverse transform be

$$k_N(\tau) = \sum_{n=1}^{N} \sum_{m=1}^{N} a_n a_m \delta(\tau - (\gamma_m - \gamma_n) - \tau_n) \tag{A-25}$$

Using (A-18), the adaptive filter weight vector is approximately given by the convolution of $g(\tau)$ and $k_N(\tau)$, which is a weighted sum of shifted versions of $g(\tau)$, i.e.,

$$W_f(\tau) = \sum_{n=1}^{N} \sum_{m=1}^{N} a_n a_m g(\tau - (\gamma_n - \gamma_m) - \tau_n) \qquad \text{(A-26)}$$

Now consider an environment with a direct path, n=1, with arrival angle near the horizontal, $a_1 > a_m$ for $m \neq 1$, and $\phi_1 \approx 0$. The arrival of the direct path near the horizontal allows the bearing to be estimated from τ_1 as

$$\hat{\theta} = \sin^{-1}\left[\frac{c}{d}\tau_1\right] \qquad \text{(A-27)}$$

Because $a_1 > a_m$, all $m \neq 1$, the n=m=1 term of (A-26) is the largest, given by $a_1^2 g(\tau - \tau_1)$. Note that this is exactly the peak that would occur if there were only a direct path.

The effect of the other terms of (A-26) will depend upon their proximity to the peak at τ_1. If $\gamma_n - \gamma_m + \tau_n \approx \tau_1$, then the term will tend to modify the peak at $\tau = \tau_1$, biasing it in the direction of $\tau = \gamma_n - \gamma_m + \tau_n$ and broadening it. Since there is no reason for the terms of (A-26) near $t = t_1$ to be symmetrical about t_1, then the multipath structure may bias the peak away from $\tau = \tau_1$. The broadening of the peak can be interpreted as a reduction in the effective bandwidth of the signal process. From [1], Appendix IV, the standard deviation of the bearing estimate is inversely proportional to bandwidth to the 3/2 power, while inversely proportional to signal-to-noise ratio. Thus, a given percentage decrease in the effective bandwidth due to multipath will degrade tracker performance more than an equivalent decrease in SNR.

Other terms of (A-26) that are peaked at values of τ not near τ_1 will produce additional signal related peaks in the mean weight vector. These peaks will, in turn, be biased and broadened by other multipath arrivals with a peak in the same vicinity. It would be possible, given an unfortunate multipath structure,

for one of these other peaks to be larger in amplitude due to the combination of several paths. However, by use of a windowing scheme as described in Section 2.3 for use with multiple targets, it will be possible to track on the peak at $\tau=\tau_1$ provided the window is narrow enough with respect to the separation of the various peaks.

It is difficult to further generalize the effects of multipath on the adaptive tracker structure, since the effects depend very much on the particular multipath structure present. Potential effects include biasing of the bearing estimate, increased estimation variance, and ambiguity in the weight vector as to the correct peak for tracking. However, these factors affect the adaptive tracker in very much the same way they do conventional trackers, and their sensitivities to multipath will be similar.

APPENDIX B

THE EFFECTS OF ARRAYS ON THE ADAPTIVE TRACKER WITH STATIC TARGETS

APPENDIX B

THE EFFECTS OF ARRAYS ON THE ADAPTIVE TRACKER WITH STATIC TARGETS

Throughout the first two phases of the adaptive tracker study [1,2], the inputs to the adaptive tracker have been modeled as:

$$x(t) = s(t) + n_x(t) \tag{B-1}$$

and

$$d(t) = s(t-\tau) + n_d(t) \tag{B-2}$$

where $s(t)$ is the plane wave signal, $n_x(t)$ and $n_d(t)$ are random noise, uncorrelated with each other, and τ is the delay in the signal due to the offset of the target from the steering angle. If the sensors consist of two omnidirectional hydrophones, each driving one of the tracker inputs, then

$$\tau = \frac{d}{c}\sin\theta \tag{B-3}$$

where d = distance between sensors

c = speed of sound

θ = angle between plane wavefront and line passing through the hydrophones

This model may also be applied to the more general situation of Figure B1, in which a half array, steered in the general vicinity of the target, drives each tracker input. In this case, d must be replaced by the distance between the phase centers of the half arrays. However, as the mis-steering angle deviates from zero (that is, the target bearing differs from the steering angle), the frequency response of the half array/beamformers change, modifying the signal spectrum. The model given in (B-1), (B-2), and (B-3) has therefore been used as a good

approximation when the mis-steering angle is small. The analysis that follows will show that the model used above applies for a very general class of arrays even when the mis-steering angle is not small, provided the spectrum of s(t) is appropriately modified.

Let each half array consist of K hydrophones arbitrarily arranged in space as shown in Figure B2, where $\underline{V}_m$ is a vector from the origin to the m^{th} hydrophone. If $\underline{U}_t$ is a unit vector in the direction of the target, and $\underline{U}_s$ is the steering angle of the array, then the output of the i^{th} hydrophone can be written as

$$Z_m(t) = s\left[t - \frac{1}{c}\underline{V}_m{}^{+}(\underline{U}_s - \underline{U}_t)\right] + n_i\left[t - \frac{1}{c}\underline{V}_m{}^{+}\underline{U}_s\right] \qquad \text{(B-4)}$$

where the $n_i(t)$ are uncorrelated with each other. Now, let m=1, 2, ... K be the left half array elements with shading coefficients a_m, and m=K+1, ... 2K be the right half elements. Then the outputs of the two half arrays are

$$x(t) = \sum_{m=1}^{K} a_i \left\{ s(t - \frac{1}{c}\underline{V}_m{}^{+}(\underline{U}_s - \underline{U}_t)) + n\,(t - \frac{1}{c}\underline{V}_m{}^{+}\underline{U}_s) \right\} \qquad \text{(B-5)}$$

$$d(t) = \sum_{m=K+1}^{2K} a_i \left\{ s(t - \frac{1}{c}\underline{V}_m{}^{+}(\underline{U}_s - \underline{U}_t)) + n\,(t - \frac{1}{c}\underline{V}_m{}^{+}\underline{U}_s) \right\} \qquad \text{(B-6)}$$

The mean weight vector of the M tap adaptive filter is the discrete Wiener filter, given by

$$E\left[\underline{W}\ (s.s)\right] = R_{xx}^{-1} R_{dx} \qquad \text{(B-7)}$$

where R_{xx} is an MxM matrix with the p, q element given by

$$(R_{xx})_{p,q} = E\left[x(t - qT_s)\ x\ (t - pT_s)\right] \qquad \text{(B-8)}$$

where T_s is the adaptive algorithm sample rate.

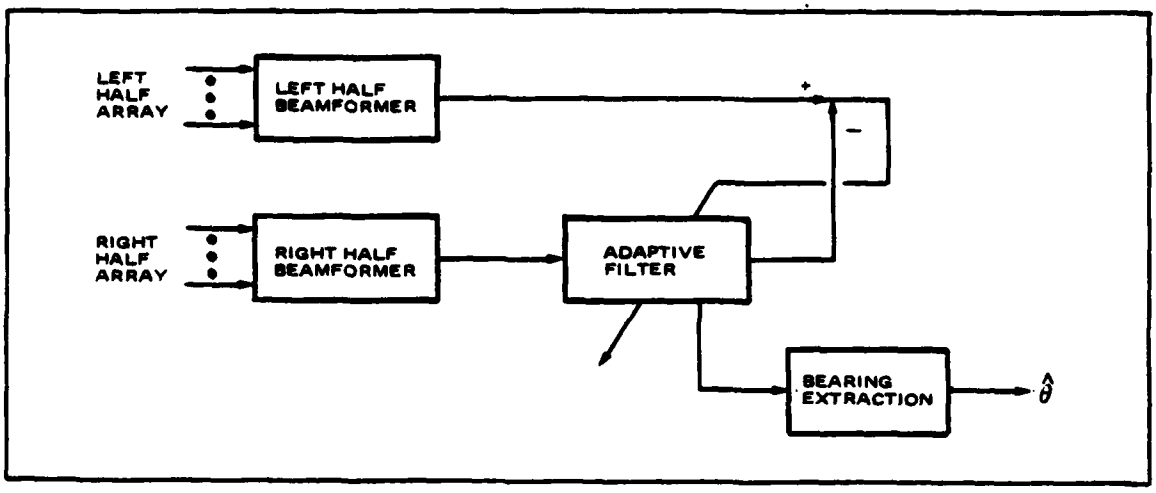

Figure B-1. Split Array Adaptive Tracker

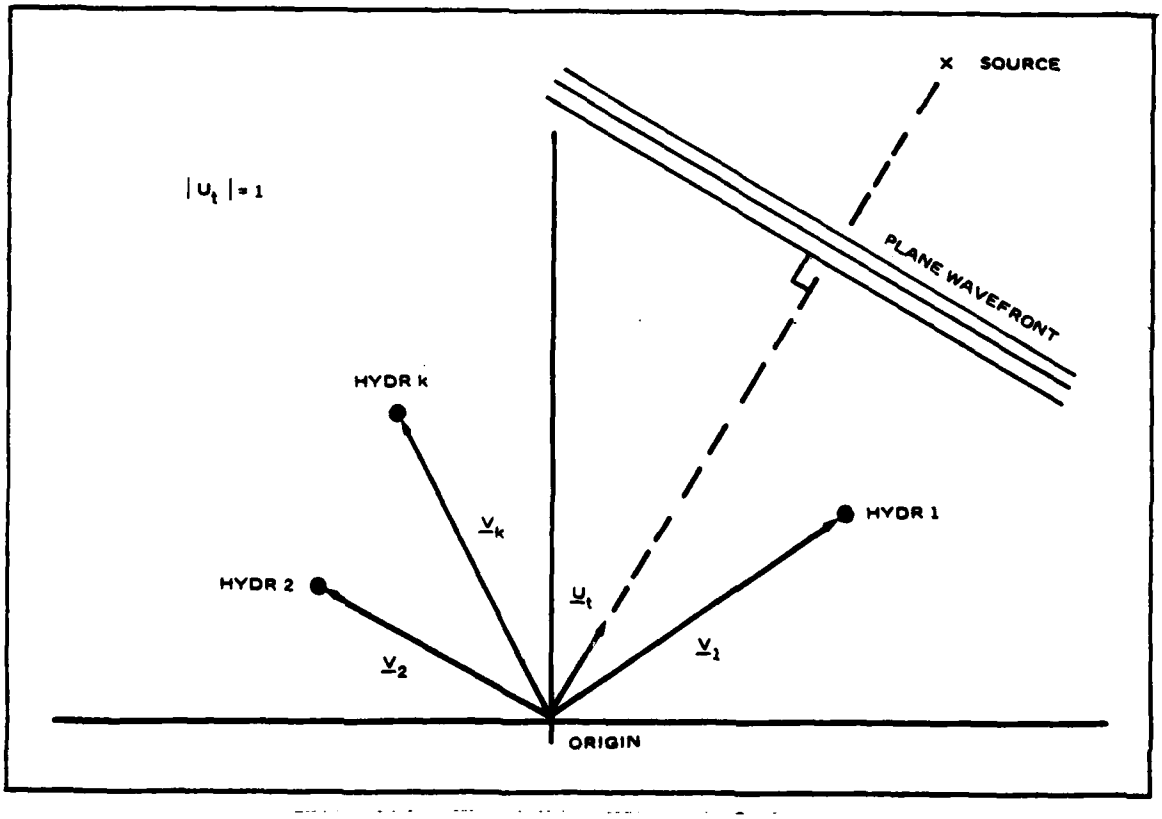

Figure B-2. Hydrophone and Wavefront Geometry

and R_{dx} is a K dimensional column vector with the q^{th} element given by

$$(R_{dx})_q = E[x(t-qT_s)\, d^*(t)] \tag{B-9}$$

Now, let $\rho_s(t)$ and $\rho_n(t)$ be the normalized covariance functions of the signal and noise (assumed wide sense stationary),

$$\rho_x(\tau) = \frac{1}{P_x} E\,[x(t)\, x^*(t+\tau)] \tag{B-10}$$

with P_x the power in x(t). Denote the power spectral density of the signal and noise respectively as $S_s(\omega)$ and $S_n(\omega)$. Then, using (B-5) and (B-6),

$$(R_{dx})_q = P_s \sum_{i=1}^{K} \sum_{k=K+1}^{2K} a_i a_k^* \rho_s \left[qT_s + \frac{1}{c}(\underline{V}_i - \underline{V}_k)^+ (\underline{U}_s - \underline{U}_t)\right] \tag{B-11}$$

Writing this in terms of the power spectral density of the signal, where

$$P_s\, \rho_s(\tau) = \frac{1}{2\pi} \int_{-\infty}^{\infty} S_s(\omega) e^{j\omega\cdot\tau} d\omega \tag{B-12}$$

gives

$$(R_{dx})_q = \sum_{i=1}^{K} \sum_{k=K+1}^{2K} a_i a_k^* \frac{1}{2\pi} \int_{-\infty}^{\infty} S_s(\omega) e^{j\omega} \left[qT_s + \frac{1}{c}(\underline{V}_i - \underline{V}_k) + (\underline{U}_s - \underline{U}_t)\right] d\omega$$

$$= \frac{1}{2\pi} \int_{-\infty}^{\infty} S_s(\omega) e^{j\omega q T_s} \left[\sum_{i=1}^{K} a_i e^{-j\frac{\omega}{c}\underline{V}_i^+ (\underline{U}_s - \underline{U}_t)}\right] \left[\sum_{k=K+1}^{2K} a_k e^{-j\frac{\omega}{c}\underline{V}_k^+ (\underline{U}_s - \underline{U}_t)}\right] d\omega$$

(B-13)

Similarly,

$$(R_{xx})_{p,q} = \frac{1}{2\pi} \int_{-\infty}^{\infty} S_s(\omega) e^{j\omega(p-q)T_s} \left[\sum_{i=1}^{K} a_i e^{j\frac{\omega}{c}\underline{V}_i^+(\underline{U}_s - \underline{U}_t)} \right] \left[\sum_{k=K+1}^{2K} a_k e^{-j\frac{\omega}{c}\underline{V}_k^+(\underline{U}_s - \underline{U}_t)} \right] d\omega$$

$$+ \frac{1}{2\pi} \int_{-\infty}^{\infty} S_n(\omega) e^{j\omega(p-q)T_s} \left[\sum_{i=1}^{M} \left| a_i \right|^2 \right] d\omega \qquad \text{(B-14)}$$

Equations (17) and (18) can be simplified by defining

$$H_d(\omega) = \sum_{k=1}^{K} a_k e^{j\frac{\omega}{c}\underline{V}_k^+(\underline{U}_s - \underline{U}_t)} \qquad \text{(B-15)}$$

and

$$H_x(\omega) = \sum_{k=K+1}^{2K} a_k e^{j\frac{\omega}{c}\underline{V}_k^+(\underline{U}_s - \underline{U}_t)} \qquad \text{(B-16)}$$

so that

$$(R_{dx})_q = \frac{1}{2\pi} \int_{-\infty}^{\infty} S_s(\omega) H_d(\omega) H_x^*(\omega) d\omega \qquad \text{(B-17)}$$

and

$$(R_{xx})_{p,q} = \frac{1}{2\pi} \int_{-\infty}^{\infty} S_s(\omega) \left| H_x(\omega) \right|^2 d\omega + \frac{1}{2\pi} \int_{-\infty}^{\infty} S_n(\omega) \sum_{i=1}^{K} a_i^2 \, d\omega \qquad \text{(B-18)}$$

Note that the model of (B-1), (B-2), and (B-3) with a single omnidirectional hydrophone, K=1, would give

$$\left| H_x(\omega) \right|^2 = 1 \tag{B-19}$$

and

$$H_d(\omega) H_x^*(\omega) = e^{-j\omega \frac{d}{c} \sin\theta} \tag{B-20}$$

The model can then be interpreted as replacing the half arrays and beamformers with the linear filters, $H_x(\omega)$ and $H_d(\omega)$, as shown in Figure B2.

Suppose that the array geometry is constrained so that

$$\underline{V}_{k+M} = \underline{V}_k + \underline{V}_o \qquad k = 1, 2, \ldots K \tag{B-21}$$

and that the shading coefficients satisfy

$$a_{k+M} = a_k \qquad k = 1, 2, \ldots, K \tag{B-22}$$

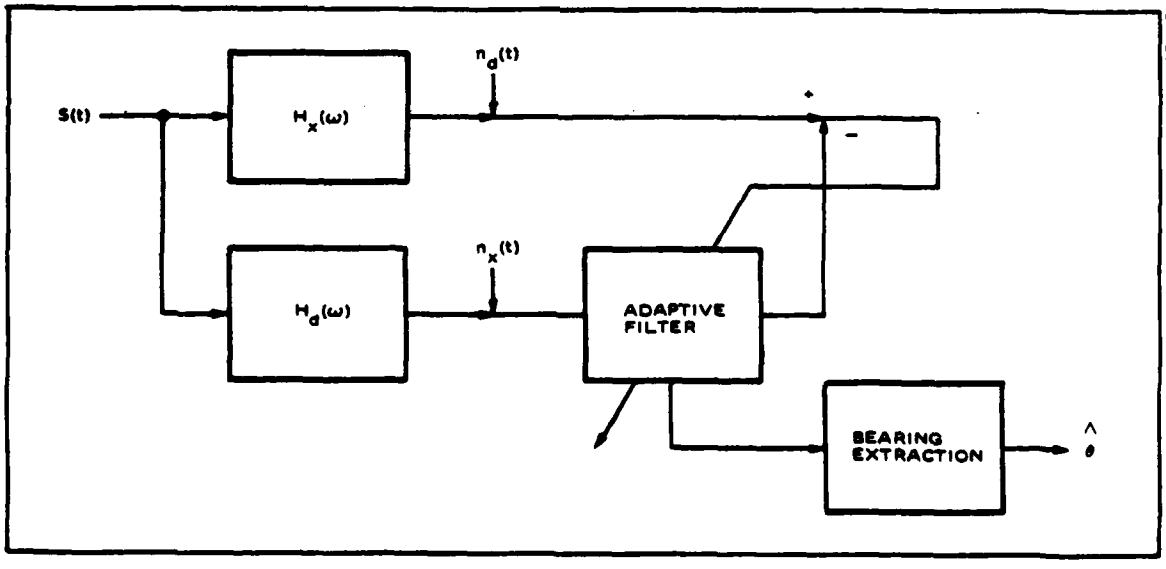

Figure B2. Equivalent Model for Split Array Tracker

Then (B-16) can be written

$$H_x(\omega) = \sum_{k=K+1}^{2K} a_k e^{j\frac{\omega}{c}\underline{V}_k^{+}(\underline{U}_s - \underline{U}_t)}$$

$$= \sum_{k=1}^{K} a_k e^{j\frac{\omega}{c}\underline{V}_k^{+}(\underline{U}_s - \underline{U}_t)} e^{j\frac{\omega}{c}\underline{V}_o^{+}(\underline{U}_s - \underline{U}_t)}$$

or

$$H_x(\omega) = H_d(\omega) e^{j\frac{\omega}{c}\underline{V}_o^{+}(\underline{U}_s - \underline{U}_t)} \tag{B-23}$$

In this case,

$$(R_{dx})_q = \frac{1}{2\pi}\int_{-\infty}^{\infty} S_s(\omega) \left|H_x(\omega)\right|^2 e^{j\frac{\omega}{c}\underline{V}_o^{+}(\underline{U}_s - \underline{U}_t)} d\omega \tag{B-24}$$

and

$$(R_{xx})_{p,q} = \frac{1}{2\pi}\int_{-\infty}^{\infty} S_s(\omega) \left|H_x(\omega)\right|^2 d\omega + \frac{1}{2\pi}\int_{-\infty}^{\infty} S_n(\omega) \sum_{i=1}^{K} \left|a_i\right|^2 \tag{B-25}$$

This is exactly the same form as the case with two omnidirectional hydrophones if the signal spectrum is replaced by $S_s(\omega) \left|H_x(\omega)\right|^2$ and the noise power scaled by

$$\sum_{i=1}^{K} \left|a_i\right|^2$$

In this equivalent model, the delay between the outputs of the two hydrophones is

$$\tau = \frac{\left|\underline{V}_o\right|}{c} \cos\psi \tag{B-26}$$

where ψ is the angle between $\underline{V}_o$ and $(\underline{U}_s - \underline{U}_t)$. This equivalent model is shown in Figure B3. Thus, the analyses of [1] and [2] can be applied when the array meets B-21) and (B-22).

A number of array configurations of interest meet these constraints. For example, let the full array consist of uniformly spaced, unshaded elements on a straight line, with spacing d_s. Then

$$H_d(\omega) = \frac{\sin(\frac{M}{2}\omega\alpha)}{\sin(\frac{1}{2}\omega\alpha)} e^{j\omega(\frac{1}{2}\frac{M-1}{M})\alpha} \tag{B-27}$$

and

$$\tau = \frac{Md_s}{c} \sin\psi \tag{B-28}$$

with ψ the angle between the array and the plane wavefront. Incorporation of non-uniform shading satisfying (B-22) will change $H_d(\omega)$, but not τ. More generally, any two identical arrays with identical shading and arbitrary relative position satisfy the constraints in (B-21) and (B-22), and can be modeled using the omnidirectional hydrophones.

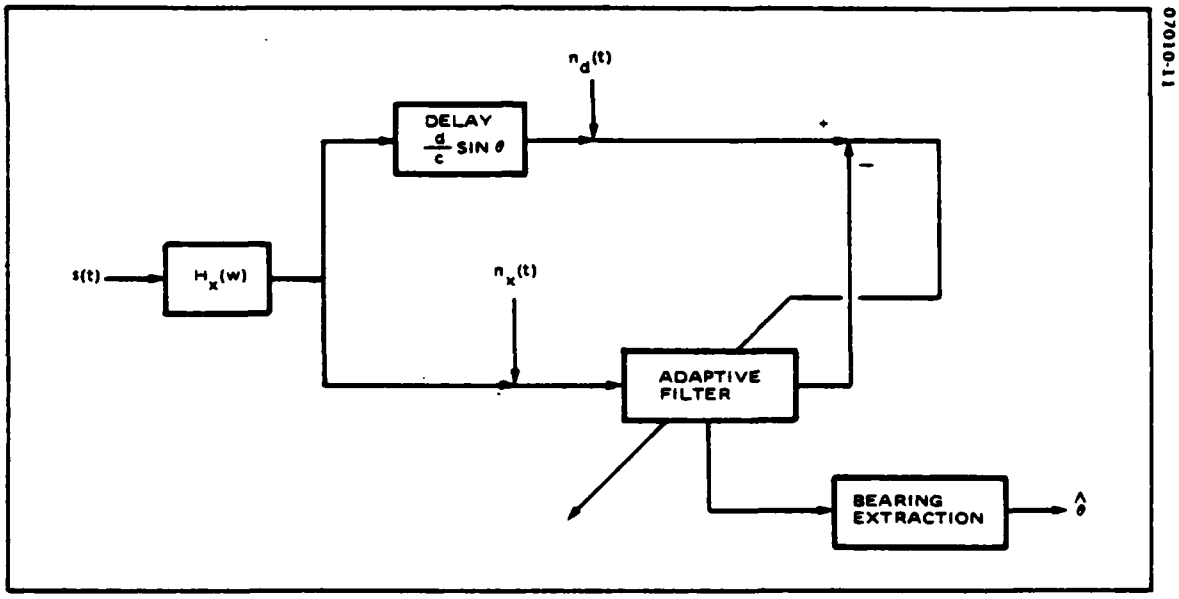

Figure B- 3. Equivalent Model for Split Array Tracker in Special Case

APPENDIX C

THE EFFECTS OF ARRAYS ON DYNAMIC TRACKING

APPENDIX C

EFFECTS OF ARRAYS ON DYNAMIC TRACKING

In the second phase of the Adaptive Tracker Study, [2] the performance of the adaptive tracker in the presence of dynamic targets was investigated when the tracker inputs were provided by two omnidirectional hydrophones. This was done under the assumption that the array effects could be introduced later by modifying the input spectra. Appendix B of this report showed that his assumption was true for static targets. This section considers the effects of split arrays in the dynamic case.

As in the omnidirectional hydrophone case, when the target is dynamic, the weight vector is continually changing with the peak of the time domain weight vector tracking the true delay. It would be expected that eventually, the peak would lag a linearly varying delay by a fixed amount, corresponding to the steady static lag of a first order system. This is complicated, however, by the fact that a linearly moving target will eventually leave the mainlobe of a beam, either requiring that the beam be steered or the tracking operation handed over to another beam (for a discussion of this process, see Section 2.4). In either case, this introduces a discontinuity in the position of the target relative to the maximum response axis (MRA) of the tracking beam. Further, if the weights are reinitialized to reflect the bearing estimate already computed, this introduces a discontinuity in the weight vector.

The goal of this analysis is to determine the main steady state weight vector of the adaptive tracker with split arrays and a broadband target with linearly varying time delay. However, since a target with linearly charging delay will eventually leave the mainlobe, the steady state mean weight vector for this

target is zero. This difficulty was avoided by introducing a periodicity into the time delay input as shown in Figure C-1. This periodic waveform allows the target to remain in the beam so that a steady state mean vector can be obtained at the point when the target is about to leave the mainlobe, as shown in Figure C-1. The periodicity is a mathematical artifice only, and does not represent any aspect of the physical problem. This periodicity is shown to produce a separate term in the expression for the lag in the time delay estimate, so that its effect can be removed by neglecting that term.

From reference [2], the mean weights of the adaptive filter are given by

$$E\left[W(n)\right] = \mu \sum_{k=0}^{n-1} \left[I - \mu R_{xx}(n-k-1)\right]^{n-k-1} R_{dx}(k) \qquad \text{(C-1)}$$

where

$W(n)$ = n^{th} time domain weight

μ = feedback coefficient

$R_{xx}(n)$ = covariance matrix of adaptive filter data vector on n^{th} iteration

$R_{dx}(k)$ = cross correlation between data vector and desired input

Consider the outputs of two split array beamformers operating on a uniformly spaced line array with a dynamic target. The signal propagates across the array with a time varying delay, $\alpha(t)$, between adjacent hydrophones. The beamformers apply a delay τ_s between adjacent hydrophones and a bulk delay,

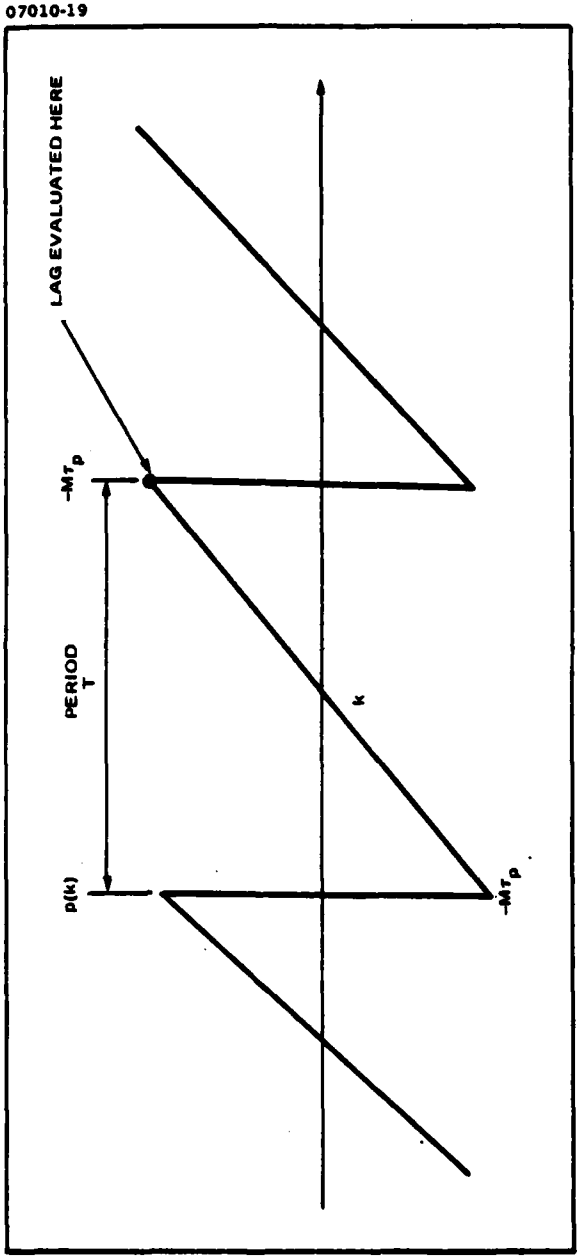

Figure C-1. Sawtooth Delay Model for Dynamic Analysis

M τ_s, where M is the number of hydrophones in a half array, between half array outputs.

If the split array beamformer outputs are to provide the inputs to the adaptive filter, than they can be modelled as

$$x(t) = \sum_{i=1}^{M} s(t-i\left[\alpha(t)-\tau_s\right]) + \sum_{i=1}^{M} n_i(t-i\tau_s) \qquad \text{(C-2)}$$

$$d(t) = \sum_{i=1}^{M} s(t-\left[M+i\right]\left[\alpha(t)-\tau_s\right]) + \sum_{i=1}^{M} n_{i+M}(t-i\tau_s) \qquad \text{(C-4)}$$

where s(t) is the signal and the $n_i(t)$ are zero mean noise with

$$E\left[n_i(t)n_j(t+\tau)\right] = \begin{cases} 0 & ,i\neq j \\ \sigma_n{}^2\delta(\tau)_{i=j} \end{cases} \qquad \text{(C-5)}$$

Also, assume that

$$E\left[s(t)s(t+\tau)\right] = \sigma_s{}^2\rho_s(\tau) \qquad \text{(C-6)}$$

and that the signal is independent of the noise.

Now let δ be the adaptive filter tap spacing in seconds, and write

$$d(t+q\delta) = \sum_{i=1}^{M} s(t+q\delta-\left[M+i\right]\left[\alpha(t+q\delta)-\tau_s\right]) + \sum_{i=1}^{M} n_{i+M}(t+q\delta+i\tau_s) \qquad \text{(C-7)}$$

Therefore, the q^{th} element of $R_{dx}(n)$ is

$$E\left[x(t)d(t+q\delta)\right] = \sum_{i=1}^{M}\sum_{j=1}^{M} \sigma_s^2 \rho_s \left\{-q\delta+\left[M+i\right]\left[\alpha(t+q\delta)-\tau_s\right] - j\left[\alpha(t)-\tau_s\right]\right\} \quad \text{(C-8)}$$

In order to use the triangular input given in Figure C1, let

$$p(t) = \alpha(t)-\tau_s = r(t-ST)-\tau_p \quad \text{(C-9)}$$

where

$$S\frac{T}{\delta} < k < (S+1)\frac{T}{\delta} \text{ and } r = \frac{2\tau_p}{T}$$

Here, T is the period of the sawtooth, $2\tau_p$ is the peak to peak amplitude of the sawtooth, and S is the index of the cycle of the sawtooth (i.e., S=2 indicates the second cycle).

Now, it is assumed that the signal to noise ratio is sufficiently low that

$$R_{xx}(t) = E\left[\underline{x}(t)\underline{x}^T(t)\right] \approx M\sigma_n^2 I \quad \text{(C-10)}$$

where $M\sigma_n^2$ is the noise power after beamforming. Then to evaluate (C-1), (C-8) and (C-10) are used with the substitution $t=k\delta$, so the q^{th} mean weight is

$$E\left[W_q(n)\right] = \mu \sum_{k=0}^{n-1} (1-\mu M\sigma_n^2)^{n-k-1} \sum_{i=1}^{M}\sum_{j=1}^{M} \sigma_s^2 \rho_s \left\{-q\delta+\left[M+i\right]\left[p(k\delta+q\delta)\right] - jp(k\delta)\right\} \quad \text{(C-11)}$$

Now

$$p(k\delta+q\delta) = r\delta\,(k+q\,\frac{ST}{\delta}) - M\tau_p = p(k\delta) + r\delta q \tag{C-12}$$

so letting $p(k\delta) = p(k)$,

$$E\left[W_q(n)\right] = \mu\sigma_s^2 \sum_{i=1}^{M}\sum_{j=1}^{M}\sum_{k=0}^{M} (1-\mu M\sigma_n^2)^{n-k-1}\ \rho_s\Big\{(M+i-j)p(k) - (M+i)rq\delta - q\delta\Big\} \tag{C-13}$$

It is now assumed that the signal has an exponential correlation function,

$$\rho_s(\tau) = \rho^{|\tau|}\quad,\ \rho\in(0,1) \tag{C-14}$$

so

$$E\left[W_q(n)\right] = \mu\sigma_s^2 \sum_{i=1}^{M}\sum_{j=1}^{M}\sum_{k=0}^{n-1} (1-\mu M\sigma_n^2)^{n-k-1}\ \rho^{\delta\left|(M+i-j)\frac{p(k)}{\delta} - (M+i)rq - q\right|} \tag{C-15}$$

Now suppose that $(M+i)r << 1$, so that $(M+i)rq$ can be neglected with respect with to q. Therefore, (C-15) can be approximated as

$$E\left[W_q(n)\right] \approx \mu\sigma_s^2 \sum_{i=1}^{M}\sum_{j=1}^{M}\sum_{k=0}^{n-1} (1-\mu M\sigma_n^2)^{n-k-1}\ \rho^{\delta\left|(M+i-j)\frac{p(k)}{\delta} - q\right|} \tag{C-16}$$

Further, using $r=2\tau_p/T$ requires $\tau_p = \frac{rT}{2\tau}$, so that

$$p(k) = r\delta\left[k-(S+\tfrac{1}{2})\frac{T}{\delta}\right] \tag{C-17}$$

Using this, it is possible to evaluate the inner summation in (C-16) by taking advantage of the periodic nature of p(k). Assume that the period of the input is an integer number of iterations, i.e., T/S is an integer, so that (C-16) can be written

$$E\left[W_q(n)\right] \approx \mu\sigma_s^2 \sum_{i=1}^{M}\sum_{j=1}^{M}\left[\sum_{s=0}^{(n-1)\frac{\delta}{T}}\sum_{k=\frac{sT}{\delta}}^{(s+1)\frac{T}{\delta}}(1-\mu M\sigma_n^2)^{n-k-1}\right.$$
$$\left.\rho\delta\left|(M+i-j)r\left[k-(s+\tfrac{1}{2})\tfrac{T}{\delta}\right]-q\right|\right] \qquad \text{(C-18)}$$

Letting $v=k-(S+\frac{1}{2})\frac{T}{\delta}$ in (C-18) gives

$$E\left[W_q(n)\right] \approx \mu\sigma_s^2 \sum_{i=j}^{M}\sum_{j=1}^{M}\left[\sum_{s=0}^{(n-1)\frac{\delta}{T}}(1-\mu M\sigma_n^2)^{n-1-(S+\frac{1}{2})\frac{T}{\delta}}\sum_{v=-\frac{T}{2\delta}}^{T/2\delta}(1-\mu M\sigma_n^2)^{-v}\right.$$
$$\left.\rho\,\delta\left|(M+i-j)\,rv-q\right|\right] \qquad \text{(C-19)}$$

These two sums can be calculated separately.

For the first sum,

$$\sum_{s=0}^{(n-1)\frac{\delta}{T}}(1-\mu M\sigma_n^2)^{n-1-(s+\frac{1}{2})\frac{T}{\delta}} = (1-\mu M\sigma_n^2)^{n-1-\frac{T}{2\delta}}\left[\frac{1-(1-\mu M\sigma_n^2)^{-(n-1)-\frac{T}{\delta}}}{1-(1-\mu M\sigma_n^2)^{-\frac{T}{\delta}}}\right] \qquad \text{(C-20)}$$

As $n\longrightarrow\infty$, the first sum goes to

$$\lim_{n\to\infty}\sum_{s=0}^{(n-1)\frac{\delta}{T}}(1-\mu M\sigma_n^2)^{n-1-(s+\frac{1}{2})\frac{T}{\delta}} = \frac{(1-\mu M\sigma_n^2)^{-T/2\delta}}{1-(1-\mu M\sigma_n^2)^{T/\delta}} \qquad \text{(C-21)}$$

This assumes that $\left|1-\mu M\sigma_n^2\right| < 1$, which is the usual condition for stability at low SNR. Note that this sum is not a function of q, so that it affects all weights equally, and does not affect the location of the peak. It represents a loss due to the finite response time of the algorithm.

The remaining sum in equation (C-19) is dependent on q, i, and j. In order to account for the absolute value in the exponent, assume that for each i and j there is a v such that

$$v = \frac{q}{r(M+1-j)} \tag{C-22}$$

so that the sum can be written as

$$\sum_{v=-\frac{T}{2\delta}}^{T/2\delta} (1-\mu\sigma_n^2)^{-v}\,\rho^{\delta\left|(M+1-j)rv-q\right|} = \sum_{v=-T/2\delta}^{\frac{q}{r(M+1-j)}-1} (1-\mu M\sigma_n^2)^{-v}\,\rho^{q-(M+1-j)rv} + \sum_{v=\frac{q}{r(M+1-j)}}^{T/2\delta} (1-\mu M\sigma_n^2)^{-v}\,\rho^{(M+1-j)rv} \tag{C-23}$$

$$= \rho^{\delta q}\left\{\frac{\left[(1-\mu M\sigma_n^2)\rho^{(M+1-j)\delta r}\right]^{T/2\delta} - \left[(1-\mu M\sigma_n^2)\rho^{(M+1-j)r\delta}\right]^{-\frac{q}{r(M+1-j)}}}{1-\left[\rho^{(M+1-j)\delta c}(1-\mu M\sigma_n^2)\right]^{-1}}\right\}$$

$$+\rho^{-\delta q}\left\{\frac{\left[\frac{\rho^{(M+1-j)\delta r}}{1-\mu M\sigma_n^2}\right]^{\frac{q}{r(M+1-j)}} - \left[\frac{\rho^{(M+1-j)\delta r}}{1-\mu M\sigma_n^2}\right]^{\frac{T}{2\delta}+1}}{1-\frac{\rho^{(M+1-j)\delta r}}{1-\mu M\sigma_n^2}}\right\} \tag{C-24}$$

This must now be summed on i and j as in equation (C-19). To do this, let i=j in the denominator, so

$$\rho^{(M+i-j)\delta r} \approx \rho^{M\delta r}$$

which is approximately true if $Mbr\delta << 1$. Then (C-24) reduces to

$$\frac{\rho^{\delta q}(1-\mu M\sigma_n^2)^{T/2\delta}\,\rho^{(M+i-j)\frac{Tr}{2}}}{1-\rho^{-Mr\delta}(1-\mu M\sigma_n^2)^{-1}} - \frac{(1-\mu M\sigma_n^2)^{-\frac{q}{r(M+i-j)}}}{1-\rho^{-Mr\delta}(1-\mu M\sigma_n^2)^{-1}}$$

$$+\frac{(1-\mu M\sigma_n^2)^{\frac{q}{r(M+i-j)}}}{1-\rho^{Mr\delta}(1-\mu M\sigma_n^2)^{-1}} - \frac{(1-\mu M\sigma_n^2)^{-\frac{T}{2\delta}-1}\,\rho^{(M+i-j)(\frac{Tc}{2}+\delta r)-\delta r}}{1-\rho^{Mr\delta}(1-\mu M\sigma_n^2)^{-1}} \qquad \text{(C-25)}$$

Now, approximating the sum, (C-19), by letting i=j in the second and third terms of (C-25) gives

$$E\left[W_q(n)\right] = \mu\sigma_s^2\left[K_1'(1-\mu M\sigma_n^2)^{-q/Mr} - K_2'\rho^{\delta q} - K_3'\rho^{-\delta q}\right] \qquad \text{(C-26)}$$

where

$$K_1' = M^2\left[\frac{\rho^{Mr\delta}}{(1-\mu M\sigma_n^2)^{-1}-\rho^{Mr\delta}} + \frac{1}{1-(1-\mu M\sigma_n^2)^{-1}\rho^{Mr\delta}}\right]$$

$$K_2' = \rho^{\delta Mr}\left[(1-\mu M\sigma_n^2)\rho^{r\delta}\right]^{T/2\delta}\frac{(1-\rho^{MrT/2})^2}{(1-\rho^{rT/2})^2(1-\mu M\sigma_n^2)} \qquad \text{(C-27)}$$

and

$$K_3' = \frac{\left[\frac{\rho^{r\delta}}{1-\mu\sigma_n^2}\right]^{1+\frac{T}{2\delta}}}{1-(1-\mu M\sigma_n^2)^{-1}\rho^{Mr\delta}} \quad \frac{\left[1-\rho^{\delta Mr(1+\frac{T}{2\delta})}\right]^2}{\left[1-\rho^{\delta r(1+\frac{T}{2\delta})}\right]^2} \tag{C-28}$$

The time delay estimate will correspond to the peak of the mean weight function, so assume that q is a continuous parameter as in Appendix G of [2]. In order to obtain the peak relative to the true delay (i.e., the lag) let

$$q = \frac{MrT}{2} - p \quad , \quad p \geq 0 \tag{C-29}$$

Then (C-26) can be written

$$E[W_q(n)] = \mu\sigma_s^2\left[K_1(1-\mu M\sigma_n^2)^{\frac{p}{Mr}} - K_2\rho^{-\delta p} - K_3\rho^{\delta p}\right] \tag{C-30}$$

with

$$K_1 = (1-\mu M\sigma_n^2)^{-\frac{T}{2\delta}} K_1'$$

$$K_2 = \rho^{MrT/2} K_2' \tag{C-31}$$

$$K_3 = \rho^{-MrT/2} K_3'$$

Noting that

$$\frac{K_2}{K_3} \approx \rho^{(M-1)r\delta}(1-\mu M\sigma_n^2)\left[(1-\mu M\sigma_n^2)\rho^{Mr\delta}\right]^{T/\delta} << 1 \tag{C-32}$$

the mean weight can be further approximated as

$$E\left[W_q(n)\right] \approx \mu\sigma_s^2\left[K_1(1-\mu M\sigma_n^2)^{p/Mr} - K_3\rho^{\delta p}\right] \qquad \text{(C-33)}$$

To determine the peak of this function, differentiate with respect to p and set to zero, yielding

$$p = Mr\,\frac{\ell n\,\frac{K_3}{K_1}\,\frac{\ell n\,\rho^{Mr\delta}}{\ell n\,(1-\mu M\sigma_n^2)}}{\ell n\,(1-\mu M\sigma_n^2) - \ell n\,\rho^{Mr\delta}} \qquad \text{(C-34)}$$

as the lag in taps in the peak of the mean weights in comparison to the true delay. If $\mu M\sigma_n^2 \ll 1$ and for an exponential correlation,

$$\rho = e^{-b}$$

with $\rho^{Mr\delta} \approx 1-Mrb\delta$, then the lag reduces to

$$\text{Lag} \approx \frac{Mr}{\mu M\sigma_n^2 - bMc\delta}\left\{.69 + 2\,\ell n\left[\frac{M(1-e^{-br\delta\,(1+T/2\delta)})}{(1-e^{-b\delta Mr(1+T/2\delta)})}\right] - br\delta\left[(M-1)\frac{T}{2\delta} - 1\right]\right\} \qquad \text{(C-35)}$$

This can be compared to the analogous results without the array present given in Appendix G of [2] it it is noted that Mr, the rate between array centers, corresponds to c in the reference. The first term is identical to the result obtained without the use of arrays, that is, with a pair of omnidirectional sensors. The second term represents the additional lag introduced by the array. It appears that the third term is a reduction in the lag due to the periodicity of the

input, and is therefore a product of the mathematical artifice introduced to solve the problem, not of the device itself. The lag in taps can therefore be approximated as

$$\text{Lag} \approx \frac{Mr}{\mu M\sigma_n^2 - bMr\delta} \left\{ .69 + 2\,\ell n \left[\frac{M(1-\rho^{-br\delta(1+T/2\delta)})}{1-e^{-b\delta Mr(1+T/2\delta)}} \right] \right\} \qquad \text{(C-36)}$$

Note that this reduces to previous results for M=1. This can be written

$$\text{Lag} \approx \frac{Mr}{\mu M\sigma_n^2 - bMr\delta} \left\{ .69 + 2\ell n\, M + 2\,\ell n \left[\frac{1-e^{-br\delta(1+T/2\delta)}}{1-e^{-brM\delta(1+T/2\delta)}} \right] \right\} \text{(C-37)}$$

Now, from (C-9),

$$r = \frac{2\tau_p}{T} \tag{C-38}$$

where $2\tau_p$ is the peak to peak amplitude of the sawtooth. Taking τ_p to be the delay associated with the target at the edge of the mainlobe, i.e., when the deviation from the MRA equals the beamwidth, assuming a distance Md between phase centers, gives

$$\tau_p = \frac{2\tau_p}{r} \sin B_w \tag{C-39}$$

with B_w the beamwidth. Then

$$T = \frac{2\tau_p}{r} = \frac{2Md}{rc} \sin B_w \tag{C-40}$$

and

$$br\delta(1 + T/2\delta) = b(r\delta + \frac{Md}{c} \sin B_w) \tag{C-41}$$

Note that $r\delta$ is the change in delay of the target in one algorithm iteration while $d/c \sin B_w$ is the time delay associated with a target at $\theta = B_w$. In practical applications $r\delta << d/c \sin B_w$, so

$$\text{Lag} \approx \frac{Mr}{|\mu M\delta_n^2 - Mc\delta|} \left\{ .69 + 2 \ln M + 2 \ln \left[\frac{1 - e^{-b\frac{Md}{d} \sin B_w}}{1 - e^{-b\frac{d}{2} M^2 \sin B_w}} \right] \right\} \tag{C-42}$$

The third term in the bracket will be neglible in most cases, which can be shown as follows. Assume that the array design frequency (the frequency at which the hydrophones are one-half wavelength apart) is b, so that the array is designed for the highest frequency in the band. Then

$$d = \frac{c}{2b}$$

and

$$b\frac{Md}{c} \sin B_w = \frac{M}{2} \sin B_w \qquad \text{(C-43)}$$

if the beamwidth is less than 30°, then $\sin B_w \approx B_w$, and

$$\frac{M}{2} \sin B_w \approx \frac{MB_w}{2} \qquad \text{(C-44)}$$

Clearly M and B_w are inversely proportional. A reasonable approximation, based upon the beamwidth of a line array, is that

$$B_w \approx \frac{50}{L/\lambda} \qquad \text{(C-45)}$$

with L the array length. The half array beamwidth chosen above is $(M-1)\, c/2b$, where $\lambda = c/b$. Then

$$\frac{MB_w}{2} = \frac{M}{2} \frac{50}{(M-1)/2} = \frac{M}{M-1}\ 50 \qquad \text{(C-46)}$$

The third term in the bracket is then

$$\frac{1 - e^{-b\frac{Md}{c}\sin B_w}}{1 - e^{-b\frac{M^2 d}{c}\sin B_w}} \quad \frac{1 - e^{-\frac{50}{M-1}\,50}}{1 - e^{-\frac{M^2}{M-1}\,50}} \qquad \text{(C-47)}$$

which is virtually unity for all values of M > 1. Therefore, the lag is taps is

$$\text{Lag} \approx \frac{Mr}{|\mu M\sigma_n^2 - bMr\delta|} \left\{ .69 + 2 \ln M \right\} \qquad \text{(C-48)}$$

In order to interpret this as a bearing lag, assure that the bearing angle is near enough to broadside so that the bearing θ, is related to delay, τ, by

$$\theta = \sin^{-1}\left(\frac{\tau c}{D}\right) \approx \frac{c}{D}\tau$$

where c is the speed of sound and D the distance between array phase centers. For the array considered here,

$$D = Md$$

and the lag in seconds is (Lag) δ. Therefore, the lag in bearing is

$$\theta_{\underline{\text{LAG}}} \approx \frac{rc\delta}{d\,\mu\sigma_n^2 - b\,r\delta} \left\{ \frac{.69 + 2/nM}{M} \right\} \qquad \text{(C-49)}$$

APPENDIX D

ESTIMATOR STRUCTURES FOR SIGNALS WITH BOTH BROADBAND AND NARROWBAND COMPONENTS

APPENDIX D

ESTIMATOR STRUCTURES FOR SIGNALS WITH BOTH BROADBAND AND NARROWBAND COMPONENTS

As pointed out in the introduction, one of the motivations for use of an adaptive tracker is that is has the potential to track signals using both broadband and narrowband energy simultaneously. Reference [1] developed estimator structures for use when either broadband or narrowband energy only were present in the radiated noise of the target. References [1] and [2] then analyzed the performance of these two estimators in the presence of targets that are broadband, narrowband, or a combination of the two. However, a means of combining the two estimates, or performing a different estimate when the target has both broadband and narrowband components was not considered.

In this section, estimator structures that are tailored to targets with both broadband and narrowband energy are developed. Two of the structures are based upon a maximum likelihood estimate of the target bearing given certain assumptions on the weight vector statistics. However, several of these assumptions have not been proven rigorously, and are made primarily for analytical tractability. Therefore the resulting structure cannot rightfully be called the maximum likelihood estimator. The estimator does combine the elements of the broadband and narrowband trackers described in reference [1].

In the adaptive tracker, the bearing estimate is extracted from the weight vector. Assume that the weight vector is a complex, gaussian random vector,

$$\underline{W} = [W(0), W(1), \ldots W(M-1)]^T \qquad \text{(D-1)}$$

with mean

$$M_w(k) = E\left[W(k)\right] = a e^{-j\omega_o (k\tau_s - \frac{d}{c}\sin\theta)} + b\rho(k\tau_s - \frac{d}{c}\sin\theta) \quad \text{(D-2)}$$

The function, $\rho(\tau)$, is an arbitrarily normalized function, corresponding to the shape of the weights due to the broadband component. Also,

ω_o = radian frequency of narrowband component

T_s = algorithm sample rate

d = distance between split array phase centers

c = speed of sound

θ = bearing of target.

The gaussian property of the weights can be argued based upon the large number of iterations of the weight update algorithm, while the structure of the mean weight is from references [1] and [2]. Now, assume that the weight vector has arbitary covariance matrix, R_w, which is independent of target bearing. In [2], the variance of the frequency domain weights are shown to be independent of target bearing, so it seems reasonable that this property should hold for R_w.

Given these assumptions, the log-likelihood function of the weight vector can be written as

$$\ell(\underline{W}|\theta, a, b) = C_1 + 1/2\ (\underline{W} - \underline{m}_w)^+ R_w^{-1} (\underline{W} - \underline{m}_w) \quad \text{(D-3)}$$

where C_1 is a constant independent of θ and the superscript + denotes conjugate-transponse. The maximum likelihood estimate of θ is that value of θ which maximizes the second term of (D-3). Expanding (D-3) gives

$$\ell(\underline{W}|\theta, a, b) = C_1 + 1/2\ \underline{W}^+ R_w^{-1} \underline{W} + 1/2\ \underline{m}_w^+ R_w^{-1} \underline{m}_w - \mathrm{Re}\left[\underline{m}_w^+ R_w^{-1} \underline{W}\right] \quad \text{(D-4)}$$

The first term of (D-4) does not depend upon the variables to be estimated, so it need not be considered.

In order to proceed further, it is assumed that the weights have equal variance and are uncorrelated, that is,

$$R_w = \sigma_W^2 I$$

The assumption of equal variance has been demonstrated, at least for narrowband plus white broadband signals in [1] and [2]. However, the weights are probably not uncorrelated when the sample rate is several times the Nyquist rate, as will be the case in practice. However, the assumption does yield a physically satisfying result, even though it is not truly the maximum likelihood estimator.

With the assumption, the second term of (D-4) can be written

$$\frac{1}{2}(\underline{m}_w^+ R_w^{-1} \underline{m}_w) = \frac{1}{2\sigma_w^2} \sum_{k=0}^{M-1} \left\{ a^2 + b^2 \rho^2 (kT_s - \frac{d}{c} \sin\theta) + 2ab\, \rho(kTs - \frac{d}{c} \sin\theta) \cos\left[\omega_o (kTs - \frac{d}{c} \sin\theta)\right] \right\} \quad \text{(D-5)}$$

If the length of the adaptive filter is long in comparison to the period of the sinusoid and the correlation time of the narrowband component and the delay is not near either end of the tapped delay line (that is $d/c \sin\theta$ is not close to zero or $(M-1)T_s$), this is essentially independent of θ. The third term of (D-4) is

$$\mathrm{Re}\left[\underline{M}_w^+ R_w^{-1} \underline{W}\right] = \frac{1}{\sigma_w^2} \mathrm{Re}\left[\sum_{k=0}^{M-1} W(k) \left\{ a e^{-j\omega_o (kTs - \frac{d}{c} \sin\theta)} + b\rho(kTs - \frac{d}{c} \sin\theta) \right\} \right] \quad \text{(D-6)}$$

Then the joint estimate of θ, a, and b is that (θ,a,b) which minimizes

$$J(\theta,a,b) = \frac{1}{2\sigma_w^2}\sum_{k=0}^{M-1}\Bigg\{ - \Big[a^2 + b^2\,\rho^2(kTs - \frac{d}{c}\sin\theta) + 2ab\rho\,(kTs - \frac{d}{c}\sin\theta)\cos\Big[\omega_o(kTs - \frac{d}{c}\sin\theta)\Big] + \mathrm{Re}\Big[2W(k)b\rho(kTs - \frac{d}{c}\sin\theta) + 2\,aW(k)_e^{-j\omega_o(kTs - \frac{d}{c}\sin\theta)}\Big]\Bigg\} \qquad \text{(D-7)}$$

Now, let $W_f(m)$ be the FFT of the weight vector,

$$W_f(m) = \sum_{k=0}^{M-1} W(k)_e^{-j\frac{2\pi}{M}mK} \qquad \text{(D-8)}$$

and let $W_f(max)$ be the frequency domain weight with the largest magnitude (containing the signal). If the FFT resolution is sufficiently fine that the center frequency of the largest bin is a good approximation to ω_o, than (D-7) can be well approximated as

$$J(\theta,a,b) = \frac{1}{2\sigma_w^2}\Big\{-Ma^2 - C_1 b^2 - 2C_2 ab + 2a\,|W_f(max)|\cos(\phi_w - \omega_o\frac{d}{c}\sin\theta) + 2b\sum_{k=0}^{M-1}W(k)\rho(kTs - \frac{d}{c}\sin\theta) \qquad \text{(D-9)}$$

where

$$C_1 = \sum_{k=0}^{M-1}\rho^2(kTs - \frac{d}{c}\sin\theta)$$

$$C_2 = \sum_{k=0}^{M-1}\rho(kTs - \frac{d}{c}\sin\theta)\cos\Big[\omega_o(kTs - \frac{d}{c}\sin\theta\Big] \qquad \text{(D-10)}$$

Under the assumptions made following equation (D-5), C_1 and C_2 are essentially independent of θ.

Now,

$$\frac{\partial J}{\partial a} = \frac{1}{2\sigma_w^2}\left\{-2M_a - 2C_2 b + 2\left|W\ (\max)\right|\cos\left(\phi_\omega - \omega_o \frac{d}{c}\sin\theta\right)\right\} \tag{D-11}$$

and

$$\frac{\partial J}{\partial b} = \frac{1}{2\sigma_w^2}\left\{-2C_1 b - 2C_2 a + 2\sum_{k=o}^{M-1} W(k)\rho(kTs - \omega_o \frac{d}{c}\sin\theta)\right\} \tag{D-12}$$

Setting these to zero yields the maximum likelihood estimate of a and b provided θ also minimizes (D-9). Then

$$\hat{a} = \frac{C_1}{MC_1 - C_2^2}\left\{\frac{1}{M}\left|W_f(\max)\right|\cos\left(\phi_\omega - \omega_o \frac{d}{c}\sin\theta\right)\right.$$

$$\left. - \frac{C_2}{C_1}\sum_{k=o}^{M-1} W(k)\rho(kT_s - \frac{d}{c}\sin\theta)\right\} \tag{D-13}$$

and

$$\hat{b} = \frac{M}{MC_1 - C_2^2}\left\{\frac{1}{C_1}\sum_{k=o}^{M-1} W(k)\rho(kT_s - \frac{d}{c}\sin\theta)\right.$$

$$\left. - \frac{C_2}{M}\left|W_f(\max)\right|\cos\left(\phi_\omega - \omega_o \frac{d}{c}\sin\theta\right)\right\} \tag{D-14}$$

The minimization over θ cannot be carried out explicitly, and must be done numerically using (D-13), (D-14), and (D-9). This could be done by the following procedure:

(a) Select an initial bearing estimate, $\hat{\theta}_o$

(b) Extract the magnitude of the largest FFT bin, $|W_p(\max)|$, the phase, ϕ_ω, and its frequency, ω_o.

(c) Numerically minimize

$$J(\hat{\theta}_i, \hat{a}_i, \hat{b}_i) = \left\{ M\hat{a}_i^2 + C_1\hat{b}_i^2 + 2C_2\hat{a}_i\hat{b}_i - 2\hat{a}_i \left| W_f(\max) \right| \cos\left(\phi_\omega - \hat{\omega}_o \frac{d}{c} \sin\hat{\theta}_i\right) \right.$$
$$\left. - 2\hat{b}_i \sum_{k=0}^{M-1} W(k)\rho(kT_s - \frac{d}{c}\sin\hat{\theta}_i) \right\} \qquad \text{(D-15)}$$

where

$$\hat{a}_i = \frac{C_1}{MC_1 - C_2^2} \left\{ \frac{1}{M} \left| W_f(\max) \right| \cos\left(\phi_w - \omega_o \frac{d}{c}\sin\hat{\theta}_i\right) \right.$$
$$\left. - \frac{C_2}{C_1} \sum_{k=0}^{M-1} W(k)\rho(kT_s - \frac{d}{c}\sin\hat{\theta}_i) \right\} \qquad \text{(D-16)}$$

and

$$\hat{b}_i = \frac{M}{C_1 M - C_2^2} \left\{ \frac{1}{C_1} \sum_{k=o}^{M-1} W(k)\rho(kT_s - \frac{d}{c}\sin\hat{\theta}_i) \right.$$
$$\left. - \frac{C_2}{M} \left| W_f(\max) \right| \cos(\phi_\omega - \omega_o \frac{d}{c}\sin\hat{\theta}_i) \right\} \qquad \text{(D-17)}$$

Here, C_1 and C_2 are constants, essentially independent of $\hat{\theta}_1$ given by (D-10), and $\hat{\theta}_i$ is the value of the estimate on the i^{th} iteration of the minimization procedure. Note that the data extracted from the weights remains the same during the iterations on i.

This structure can be simplified by noting that by substituting (D-16) and (D-17) in (D-15) J can be written in the form

$$J(\hat{\theta}_i) = Q_1 f_1^2(\hat{\theta}_i) + Q_2 f_2^2(\hat{\theta}_i) + 2Q_3 f_1(\hat{\theta}_i) f_2(\hat{\theta}_i) \tag{D-18}$$

where

$$f_1(\hat{\theta}_i) = |W_f(\max)| \cos(\phi_w - \hat{\omega}_o \frac{d}{c} \sin\hat{\theta}_i) \tag{D-19}$$

$$f_2(\hat{\theta}_i) = \sum_{k=o}^{M-1} W(k)\rho(kT_s - \frac{d}{c}\sin\hat{\theta}_i) \tag{D-20}$$

and

$$Q_1 = \frac{C_1}{M}\left[1 + 2C_1 - (1+2M)C_2^2\right] \tag{D-21}$$

$$Q_2 = \frac{M}{C_1}\left[C_2^2\left(1-2M+\frac{C_1^2}{M}\right) - C_2 + 2C_1\right] \tag{D-22}$$

$$Q_3 = C_2^3 (M+1) - C_2(2C_1+1) \tag{D-23}$$

so that Q_1, Q_2, and Q_3 are constants essentially independent of $\hat{\theta}_i$. Then step (c) in the numerical procedure becomes

(c1) Numerically minimize

$$J(\hat{\theta}_1) = Q_1 f_1^2(\hat{\theta}_i) + Q_2 f_2^2(\hat{\theta}_i) + 2Q_3 f_1(\hat{\theta}_i) f_2(\hat{\theta}_i) \tag{D-24}$$

where $\hat{\theta}_i$ is the value of the estimate on the i^{th} iteration of the numerical procedure. This leads to the simpler structure shown in Figure D1.

An alternate approach is possible if the broadband signal-to-noise ratio (BSNR) and narrowband signal to noise ratio (NSNR) are known a priori or are available from the sonar.

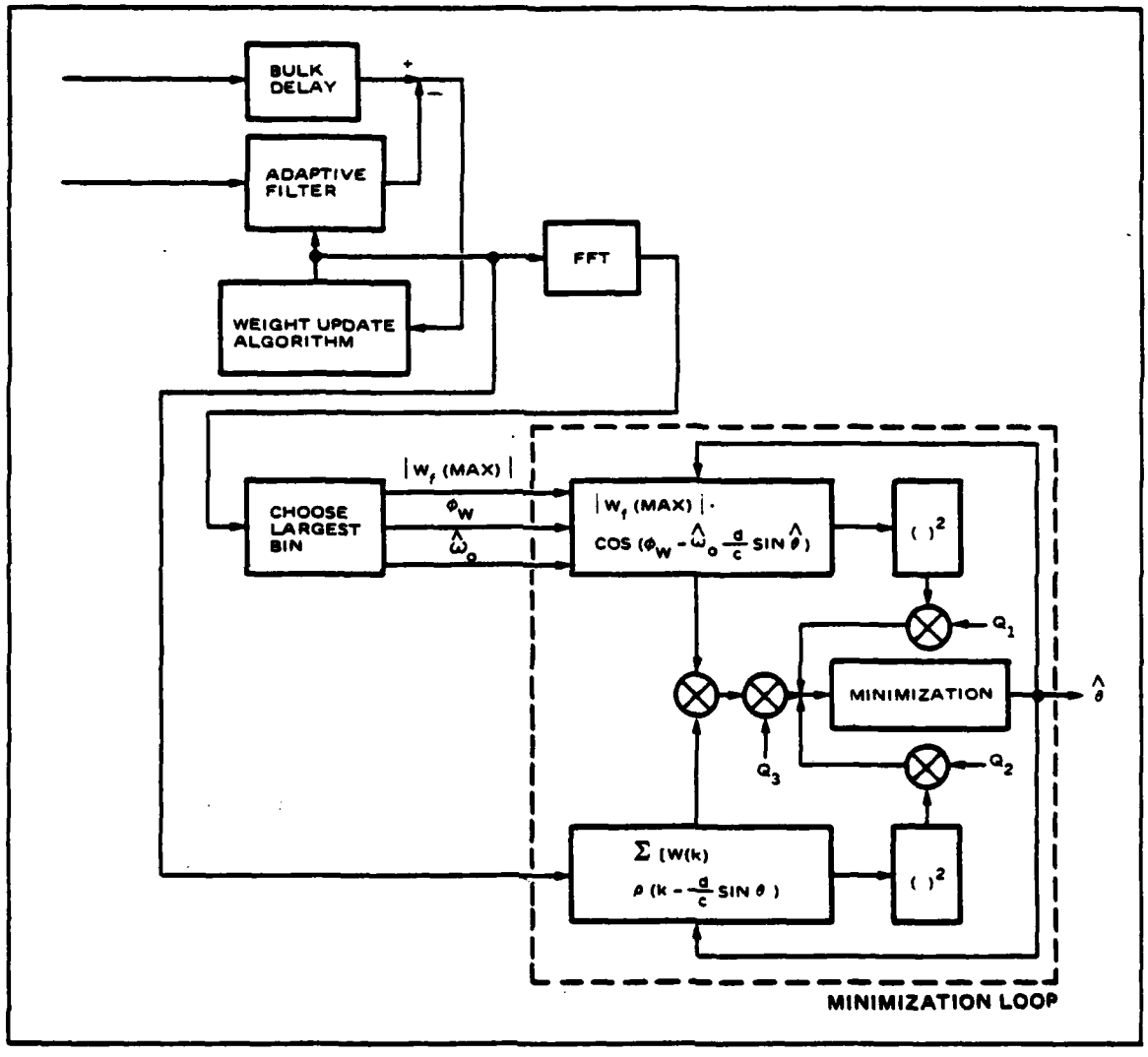

Figure D1. Combined Adaptive Tracking System with Unknown SNRs

From [2], the k^{th} element of frequency domain weight vector in steady state for a signal consisting of a white broadband source with a single line component is, neglecting FFT windowing effects

$$E[F_k(\infty)] = \frac{1}{|G(k,\omega_o)|^2 \sigma_{NB}^2 + M\sigma_{BB}^2 + M\sigma_N^2} \left[|G(k,\omega_o)|^2 \sigma_{NB}^2 e^{-j\omega_o \Delta T_s} + M\sigma_{BB}^2 e^{-j\frac{2\pi}{M}\Delta k} \right] \quad \text{(D-25)}$$

where

$$|G(k,\omega_o)|^2 = \frac{\sin^2\left[\frac{M}{2}\left(\frac{2\pi}{M}k - \omega_o T_s\right)\right]}{\sin^2\left[\frac{1}{2}\left(\frac{2\pi}{M}k - \omega_o T_s\right)\right]} \quad \text{(D-26)}$$

M = number of adaptive filter taps = FFT size

σ_{NB}^2 = narrowband signal power

σ_{BB}^2 = broadband signal power

σ_N^2 = noise power

ω_o = frequency of narrowband component

T_s = sample interval

Δ = signal delay between phase centers in sample intervals (assumed to be an integer)

Now, if the narrowband signal is bin centered, or approximately so, then

$$|G(k,\omega_o)|^2 \approx M^2 \delta_{kJ} \tag{D-27}$$

where δ_{kJ} is the Kronecker delta and J is the index of the bin containing the narrowband component. If windowing effects are negligible, as they will be in a well-designed tracker, then the time domain weight vector can be obtained by inverse transforming (D-25). If (D-27) is valid, then the n^{th} time domain weight is approximately given by

$$\begin{aligned}
E[W_n(\infty)] &= \frac{M\sigma_{NB}^2}{M^2\sigma_{NB}^2 + M\sigma_{BB}^2 + M\sigma_N^2} e^{+j\frac{2\pi}{M}Jn} e^{-j\frac{2\pi}{M}J\Delta} \\
&+ \left(\frac{\sigma_{BB}^2}{M^2\sigma_{NB}^2 + M\sigma_{BB}^2 + M\sigma_N^2} - \frac{\sigma_{BB}^2}{M\sigma_{BB}^2 + M\sigma_N^2} \right) e^{+j\frac{2\pi}{M}Jn} e^{-j\frac{2\pi}{M}J\Delta} \\
&+ \frac{M\sigma_{BB}^2}{M\sigma_{BB}^2 + M\sigma_N^2} \frac{1}{M} \sum_{k=0}^{M-1} e^{-j\frac{2\pi}{M}\Delta k} e^{j\frac{2\pi}{M}nk} \\
&= \frac{\sigma_{NB}^2}{M\sigma_{NB}^2 + \sigma_{BB}^2 + \sigma_N^2} e^{-j\frac{2\pi}{M}J(n-\Delta)} + \frac{\sigma_{BB}^2}{\sigma_{BD}^2 + \sigma N^2} \delta(n-\Delta) \\
&- \frac{\sigma_{NB}^2 \sigma_{BB}^2}{\left(M\sigma_{NB}^2 + \sigma_{BB}^2 + \sigma_N^2\right)\left(\sigma_{BB}^2 + \sigma_N^2\right)} e^{-j\frac{2\pi}{M}J(n-\Delta)} \\
&= \frac{\sigma_{NB}^2 \sigma_{BB}^2}{\left(M\sigma_{NB}^2 + \sigma_{BB}^2 + \sigma_N^2\right)\left(\sigma_{BB}^2 + \sigma_N^2\right)} e^{-j\frac{2\pi}{M}J(n-\Delta)} \\
&+ \frac{\sigma_{BB}^2}{\sigma_{BB}^2 + \sigma_N^2} \delta(n-\Delta)
\end{aligned} \tag{D-28}$$

This result indicates that the mean weight used in the derivation of the combined estimator is

$$M_w(k) = \frac{\sigma_{NB}^2 \sigma_N^2}{\left(M\sigma_{NB}^2 + \sigma_{BB}^2 + \sigma_N^2\right)\left(\sigma_{BB}^2 + \sigma_N^2\right)} e^{-j\omega_o(kT_s - \frac{d}{c}\sin\theta)}$$

$$+ \frac{\sigma_{BB}^2}{\sigma_{BB}^2 + \sigma_N^2} \rho(kTs - \frac{d}{c}\sin\theta) \qquad \text{(D-29)}$$

When these coefficients replace a and b in the derivations, the combined estimator must minimize the functional

$$J_1(\hat{\theta}) = \frac{\gamma_{NB}}{(M\gamma_{NB} + \gamma_{BB} + 1)(\gamma_{BB} + 1)} \left|W_f(max)\right| \cos(\phi_w - \hat{\omega}_o \frac{d}{c}\sin\hat{\theta})$$

$$+ \frac{\gamma_{BB}}{(\gamma_{BB} + 1)} \sum_{k=0}^{N-1} W(k)\,\rho(kT_s - \frac{d}{c}\sin\hat{\theta}) \qquad \text{(D-30)}$$

where $\gamma_{NB} = \sigma_{NB}^2/\sigma_N^2$ and $\gamma_{BB} = \sigma_{BB}^2/\sigma_N^2$. Hence, given a priori or external knowledge of γ_{NB} and γ_{BB}, step (c) in the minimization procedure becomes

(c2) Numerically minimize

$$J_1(\hat{\theta}_i) = \frac{\gamma_{NB}}{(M\gamma_{NB} + \gamma_{BB} + 1)(\gamma_{BB} + 1)} \left|W_f(max)\right| \cos(\phi_w - \hat{\omega}_o \frac{d}{c}\sin\hat{\theta}_i)$$

$$+ \frac{\gamma_{BB}}{\gamma_{BB} + 1} \sum_{k=0}^{N-1} W(k)\rho(kT_s - \frac{d}{c}\sin\hat{\theta}_i) \qquad \text{(D-31)}$$

This estimator structure is shown schematically in Figure D2.

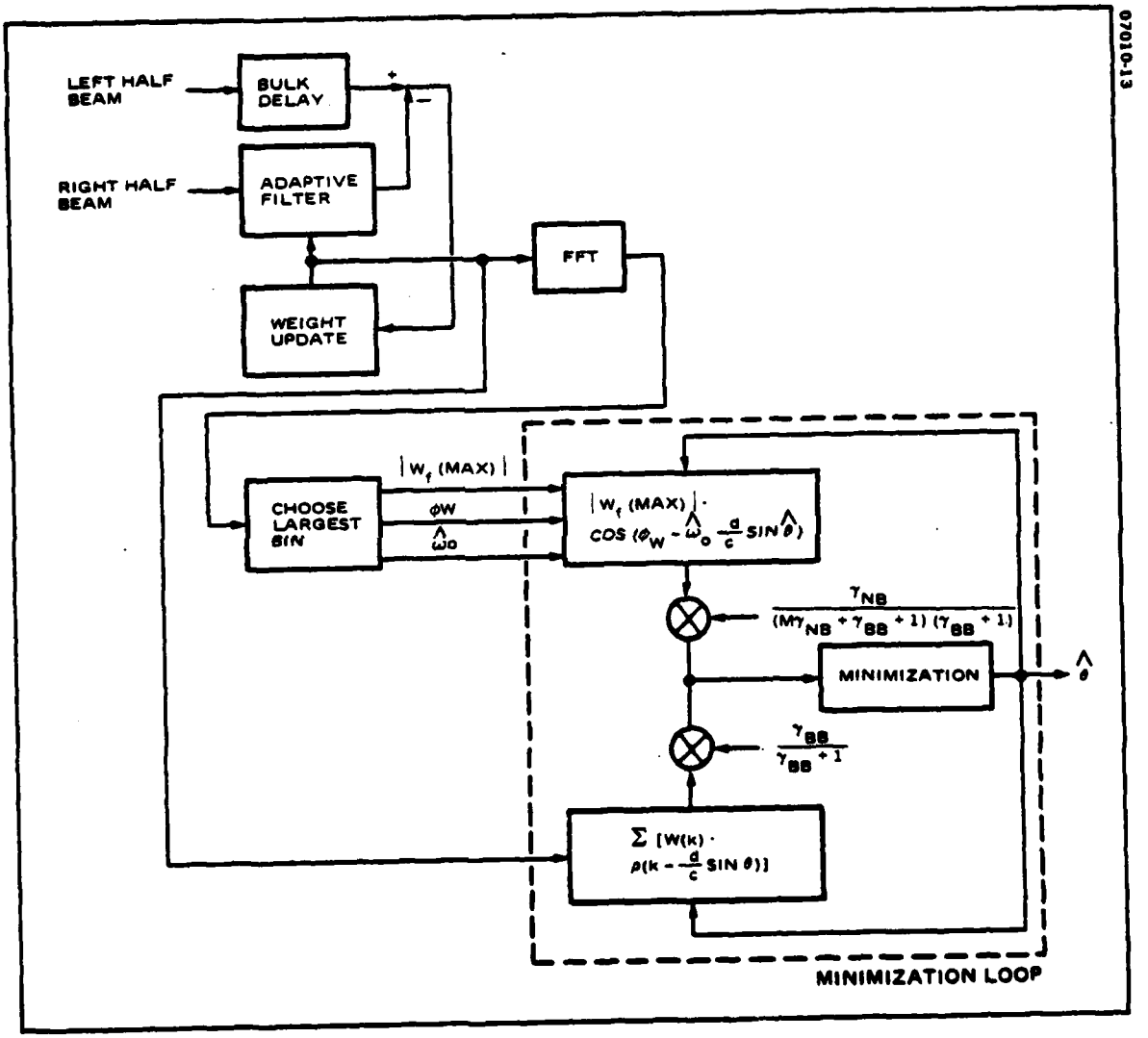

Figure D2. Combined Estimator with Known SNRs

This reduces to the broadband or narrowband estimator when the signal is purely narrowband or purely broadband. When $\sigma_{BB}^2 = 0$, then $\gamma_{BB} = 0$ and

$$J_1(\hat{\theta}) = \frac{\gamma_{NB}}{M\gamma_{NB} + 1} \left|W_f(\max)\right| \cos\left(\phi_w - \hat{\omega}\frac{d}{c}\sin\hat{\theta}\right) \tag{D-32}$$

which is minimized by choosing

$$\hat{\theta} = \arcsin\left[\frac{c}{d\hat{\omega}_o}\phi w\right]$$

which is exactly the procedure used for narrowband signals. If $\gamma_{NB} = 0$, then the procedure reduces to the minimization of

$$J_1(\hat{\theta}) = \sum_{k=1}^{M-1} W(k)\rho(kT_s - \frac{d}{c}\sin\hat{\theta}) \tag{D-33}$$

This is just a minimization of the interpolated time domain weights using the interpolation function $\rho(t)$. This is the broadband estimator if $\rho(T)$ is taken to be the $\sin(x)/x$ function. This result is a strong justification of the narrowband and broadband estimators originally described in [1].

One drawback of these estimator structures is that they are highly parametric. They not only require knowledge of (or estimation of) the signal powers, but assume a priori that the signal consists of a broadband component and a single line component in a non-directional background. They may, therefore, be very sensitive to deviations of the actual environment from the assumptions, i.e., multiple target lines, interferences, etc.

A completely different philosophy of providing estimates for targets with broadband and narrowband components is to combine the outputs of the broadband and narrowband estimates according to some weighting scheme. The weights are chosen according to a criterion, such as minimum variance of the combined estimate. Suppose initially that the two estimates, $\hat{\theta}_{NB}$ and $\hat{\theta}_{BB}$, were uncorrelated estimates of the bearing of a single target from the narrowband and broadband estimators, respectively. It can be shown that the linear combination, $\hat{\theta}_c$, of the two that yields the same mean and minimum variance among all linear combinations is given by

$$\hat{\theta}_c = \frac{\sigma_{\hat{\theta}_{NB}}^2}{\sigma_{\hat{\theta}_{NB}}^2 + \sigma_{\hat{\theta}_{BB}}^2} \hat{\theta}_{BB} + \frac{\sigma_{\hat{\theta}_{BB}}^2}{\sigma_{\hat{\theta}_{NB}}^2 + \sigma_{\hat{\theta}_{BB}}^2} \hat{\theta}_{NB} \tag{D-34}$$

where

$\sigma_{\hat{\theta}_{NB}}^2$ = variance of $\hat{\theta}_{NB}$

$\sigma_{\hat{\theta}_{BB}}^2$ = variance of $\hat{\theta}_{BB}$

If $\hat{\theta}_c^2$ is the variance of the combined estimate, then it can be shown that

$$\sigma_{\hat{\theta}_c}^2 \leq \sigma_{\hat{\theta}_{NB}}^2, \sigma_{\hat{\theta}_{BB}}^2 \tag{D-35}$$

The approach is easily extended to combining more than two estimates. Therefore, if the target had multiple lines, a narrowband estimate could be extracted from each and combined in this way.

It has been assumed that the estimates come from a single target, while, in fact, multiple targets and interferences may be present. A reasonable assumption is that if two estimates, or the mean of two estimates, are close together, then they come from the same target and can be combined in this way. The combiner may therefore be implemented (for a single broadband and a single narrowband estimate) as follows.

a. Compute a running sample mean, $M_{\hat{\theta}_{NB}}$ and $M_{\hat{\theta}_{BB}}$, and a running sample variance, $V_{\hat{\theta}_{NB}}$ and $V_{\hat{\theta}_{BB}}$, for the narrowband and broadband estimates, $\hat{\theta}_{NB}$ and $\hat{\theta}_{BB}$

b. If $\left|M_{\hat{\theta}_{NB}} - M_{\hat{\theta}_{BB}}\right| \leq \varepsilon$, where ε is a threshold, then combine $\hat{\theta}_{NB}$ and $\hat{\theta}_{BB}$ to get $\hat{\theta}_c$ as follows:

c. Compute

$$\hat{\theta}_c = \frac{V_{\hat{\theta}_{NB}}}{V_{\hat{\theta}_{NB}} + V_{\hat{\theta}_{BB}}} \hat{\theta}_{BB} + \frac{V_{\hat{\theta}_{BB}}}{V_{\hat{\theta}_{NB}} + V_{\hat{\theta}_{NB}}} \hat{\theta}_{NB} \qquad \text{(D-36)}$$

It should be clear that the sample variances in (D-36) are random variables, and that their fluctuations can increase the variance of $\hat{\theta}_c$ to the point where (D-35) is no longer true.

To this point, it has been assumed that $\hat{\theta}_{NB}$ and $\hat{\theta}_{BB}$ are uncorrelated. However, since they are extracted from the same data, the weight vector, this is unlikely. Of course, it is still possible to use the above combiner because of its simplicity, but the variance of $\hat{\theta}_c$ will be

$$\sigma_{\hat{\theta}_c}^2 = \frac{\sigma_{\hat{\theta}_{NB}}^2 + 2\rho\sigma_{\hat{\theta}_{BB}}\sigma_{\hat{\theta}_{NB}} + \sigma_{\hat{\theta}_{BB}}^2}{\left(\sigma_{\hat{\theta}_{NB}}^2 + \sigma_{\hat{\theta}_{BB}}^2\right)^2} \sigma_{\hat{\theta}_{NB}}^2 \sigma_{\hat{\theta}_{BB}}^2 \qquad \text{(D-37)}$$

where

$$\rho\sigma_{\hat{\theta}_{NB}}\sigma_{\hat{\theta}_{BB}} = E\left[\left(\sigma_{\hat{\theta}_{NB}} - E(\hat{\theta}_{NB})\right)\left(\hat{\theta}_{BB} - E(\hat{\theta}_{BB})\right)\right]$$

That is, ρ is the correlation coefficient between $\hat{\theta}_{NB}$ and $\hat{\theta}_{BB}$. Note that increasing correlation always increases the variance of $\hat{\theta}_c$. This can be written

$$\sigma_{\hat{\theta}_c}^2 = \left[\frac{\sigma_{\hat{\theta}_{NB}}^4 + 2\rho\sigma_{\hat{\theta}_{BB}}\sigma_{\hat{\theta}_{NB}}^3 + \sigma_{\hat{\theta}_{BB}}^2\sigma_{\hat{\theta}_{NB}}^2}{\sigma_{\hat{\theta}_{NB}}^4 + 2\sigma_{\hat{\theta}_{NB}}^2\sigma_{\hat{\theta}_{NB}}^2 + \sigma_{\hat{\theta}_{BB}}^2}\right]\sigma_{\hat{\theta}_{BB}}^2 \qquad \text{(D-38)}$$

or

$$\sigma_{\hat{\theta}_c}^2 = \left[\frac{\sigma_{\hat{\theta}_{NB}}^2\sigma_{\hat{\theta}_{BB}}^2 + 2\rho\sigma_{\hat{\theta}_{BB}}^3\sigma_{\hat{\theta}_{NB}} + \sigma_{\hat{\theta}_{BB}}^2}{\sigma_{\hat{\theta}_{NB}}^4 + 2\sigma_{\hat{\theta}_{NB}}^2\sigma_{\hat{\theta}_{BB}}^2 + \sigma_{\hat{\theta}_{BB}}^4}\right]\sigma_{\hat{\theta}_{NB}}^2 \qquad \text{(D-39)}$$

Therefore

$$\sigma_{\hat{\theta}_c}^2 \geq \sigma_{\hat{\theta}_{BB}}^2 \quad \text{if} \quad \rho \geq \frac{1}{2}\frac{\sigma_{\hat{\theta}_{BB}}}{\sigma_{\hat{\theta}_{NB}}}\left(1 + \frac{\sigma_{\hat{\theta}_{BB}}^2}{\sigma_{\hat{\theta}_{NB}}^2}\right) = T_1 \qquad \text{(D-40)}$$

$$\sigma_{\hat{\theta}_c}^2 \geq \sigma_{\hat{\theta}_{NB}}^2 \quad \text{if} \quad \geq \frac{1}{2}\frac{\sigma_{\hat{\theta}_{NB}}}{\sigma_{\hat{\theta}_{BB}}}\left(1 + \frac{\sigma_{\hat{\theta}_{NB}}^2}{\sigma_{\hat{\theta}_{BB}}^2}\right) = T_2 \qquad \text{(D-41)}$$

Consequently, if either (D-40) or (D-41) are true, the combiner cannot reduce the variance beyond that of the individual estimates. Figure D3 shows T_1 and T_2 plotted as a function of $(\sigma_{\hat{\theta}_{BB}}/\sigma_{\hat{\theta}_{NB}})$, which can be useful in determining the applicability of the combiner developed above. For example, if $\hat{\theta}_{NB}$ and $\hat{\theta}_{BB}$

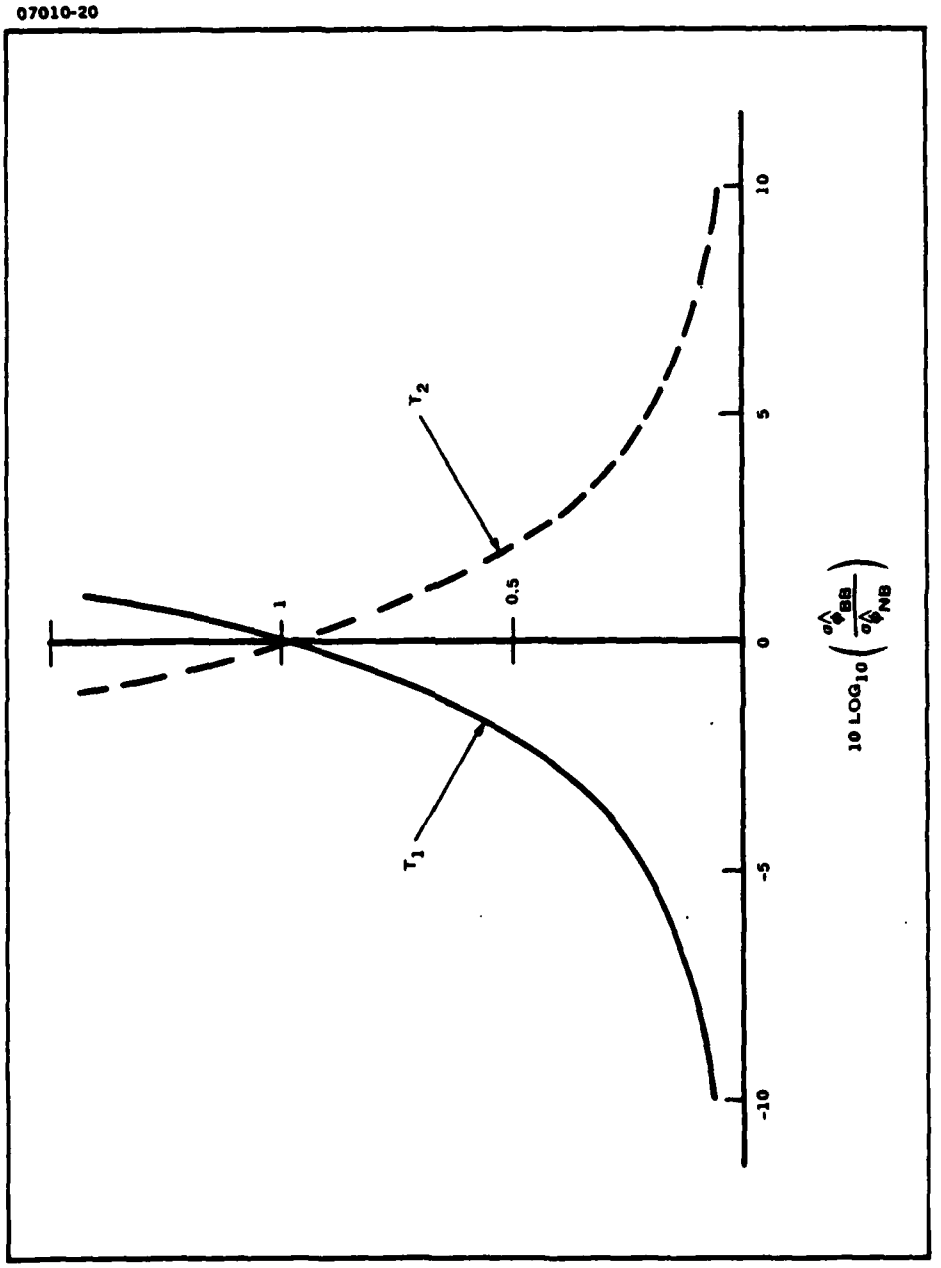

Figure D-3. Sensitivity of Combiner to Correlation of Estimates

are expected to have $\rho < .2$, then as long as $10 \log \sigma_{\hat{\theta}_{BB}} / \sigma_{\hat{\theta}_{NB}}$ is between -5 and +5. On the other hand, if higher correlations, say $\rho = .8$ are expected, then the combiner will be useful only when the two estimates have virtually the same variance (and even then, the improvement will be small).

APPENDIX E

COMPARISON OF A SIN(X)/(X) AND A QUADRATIC INTERPOLATOR

APPENDIX E

COMPARISON OF A SIN(X)/X AND QUADRATIC INTERPOLATOR

The first phase of the tracker study[1] developed and analyzed an interpolator for extracting a delay estimate from the adaptive filter weights when the inter-array delay falls between the discrete adaptive filter taps. This was done by forming a continuous interpolated weight function,

$$h_I(t) = \sum_{m=0}^{M-1} W(m)\, f(t-mT_s) \qquad \text{(E-1)}$$

where W(m) is the m^{th} adaptive filter weight, T_s is the sample interval, and f is an interpolation function. In [1], the function used was

$$f(t) = \frac{\sin 2\pi Bt}{2\pi Bt} \qquad \text{(E-2)}$$

The delay estimate was determined by locating the peak of the interpolated function (E-1). The analysis of the performance of this interpolator followed reference [4] in mapping the fluctuations in the weight vector, $\underline{W}$, into fluctuations in the determination of the peak location.

In practice, it would be desirable to reduce the number of computations required for interpolation relative to this sin x/x interpolator. This is particularly true in light of the three primary drawbacks of the sin x/x approach:

(1) for optimality, the input processes should be ideal band-limited random processes

(2) every weight value is used in the interpolation, even though some may be dominated by fluctuations

(3) an iterative search routine is required in order to estimate the zero crossing of the interpolated derivative of the weights

A quadratic interpolator overcomes these problems. The quadratic interpolator simply selects the largest weight and the two adjacent weights, and makes a quadratic fit to the data to find the peak. A performance analysis follows, along with a comparison of the two interpolation approaches based upon numerical evaluation of the expressions developed.

Suppose on a particular iteration, weight W_J is the largest of the weights of the adaptive filter, and W_{J-1} and W_{J+1} are the two weights adjacent to W_J. The quadratic interpolator will fit a curve

$$f(Z) = a_0 + a_1 Z + a_2 Z^2 \qquad \text{(E-3)}$$

such that it passes through the points $Z = W_{J-1}$, $Z = W_J$, and $Z = W_{J+1}$. For such a curve, the coefficients of (E-3) are given by

$$a_0 = W_J \qquad \text{(E-4)}$$

$$a_1 = \frac{W_{J+1} - W_{J-1}}{2T_s} - \frac{J}{T_s}\left[W_{J+1} + W_{J-1} - 2W_J\right] \qquad \text{(E-5)}$$

and

$$a_2 = \frac{W_{J-1} + W_{J+1} - 2W_J}{2T_s^2} \qquad \text{(E-6)}$$

where T_s is the algorithm sample rate. Then the parameter Z represents the continuous value of delay along the tapped delay line. The delay estimate is the

value of Z corresponding to the peak of (E-3). To locate this peak, differentiate (E-3) and set it to zero, yielding the delay estimate

$$\hat{\tau} = \frac{W_{J-1} - W_{J+1}}{W_{J-1} + W_{J+1} - 2W_J} \quad \frac{T_s}{2} + JT_s \tag{E-7}$$

Note that $\hat{\tau}$ is a ratio of correlated random variables with non-zero mean, and that a general determination of its density requires knowledge of the densities of the numerator and denominator. Since the weights are usually assumed to be Gaussian, the temptation is to assume that the numerator and denominator are Gaussian. This leads to an infinite variance, however, even though simulations of the quadratic interpolator indicate good performance. In fact, the densities are not Gaussian, since they are conditional on the selection of the weights in the vicinity of the peak. For example, the density of the numerator is

$$p\left(W_{J-1} + W_{J+1} - 2W_J \mid W_J > W_K,\ K \neq J\right) \tag{E-8}$$

This density is not Gaussian, and is not easily determined. However, when it can be assumed that the true peak of the weight function lies between W_{J-1} and W_{J+1}, the method of [4] can be applied to determine the variance of $\hat{\tau}$.

When the true delay between the half array outputs is in the vicinity of W_J, then the variance of $\hat{\tau}$ is given by

$$\mathrm{Var}[\hat{\tau}] = \left. \frac{\mathrm{Var}\left[\frac{df(Z)}{dZ}\right]}{\left|\frac{d}{dZ} E\left[\frac{df(Z)}{dZ}\right]\right|^2} \right| Z = Z_t \tag{E-9}$$

with Z_t the true value of delay. Based upon (E-3) through (E-6), the numerator and denominator, evaluated at Z_t, are given by

$$\frac{d}{dZ} E \left[\frac{df(Z)}{dZ}\right] = \frac{E[W_{J-1}] + E[W_{J+1}] - 2E[W_J]}{T_s^2} \qquad \text{(E-10)}$$

and

$$\text{Var}\left[\frac{df(Z)}{dZ}\right]\Bigg|_{Z=Z_t} = \frac{\sigma_w^2}{2T_s^2}\left[1 + 12\left(\frac{Z}{T_s}\right)^2\right] \qquad \text{(E-11)}$$

Here, σ_w^2 is the variance of the weights, assumed constant over all weights based upon [1]. Then

$$\text{Var}[\hat{\tau}] = \frac{\sigma_w^2 T_s^2}{2} \frac{\left[1 + 12\left(\frac{Z}{T_s}\right)^2\right]}{\left[E(W_{J-1}) + E(W_{J+1}) - 2E(W_J)\right]^2} \qquad \text{(E-12)}$$

To proceed further, statistics are needed, in particular, the input correlation function. These are available from Appendix V of [1]. Assume that

$$S_s(f) = \begin{cases} P_s, & -B_s \le f \le B_s \\ 0, & \text{otherwise} \end{cases} \qquad \text{(E-13)}$$

$$S_n(f) = \begin{cases} P_n, & -B_s \le f \le B_s \\ 0, & \text{otherwise} \end{cases} \qquad \text{(E-14)}$$

Then from [1], using the frequency domain model, the statistics of the FFT of the weight vector, where H(k) is the weight of the k^{th} FFT bin of the frequency domain model, are

$$E[H(k)] = \begin{cases} \dfrac{P_S}{P_S + P_N} e^{-j \frac{2\pi}{M} \frac{Z_t}{T_s} k} & , 0 \le k \le J-1 \\ 0 & , J-1 < k \le M-J \\ \dfrac{P_S}{P_S + P_N} e^{-j \frac{2\pi}{M} \frac{Z_t}{T_s} (M-k)} & , M-J < k \le M-1 \end{cases} \qquad \text{(E-15)}$$

and

$$Var[H(k)] = \begin{cases} \dfrac{\mu M P_N (2P_S + P_N)}{(P_S+P_N)(2-2\mu M(P_S+P_N))} & , 0 \le K \le J-1 \text{ or } M-J < k \le M-1 \\ 0 & , J-1 < k \le M-J \end{cases} \qquad \text{(E-16)}$$

The mean of the time domain weights are

$$E[W_m] = \frac{1}{M} \sum_{k=0}^{M-1} E[H(k)] e^{j \frac{2\pi}{M} m(k_1-k_2)}$$

$$= \frac{1}{M} \frac{P_s}{P_s+P_n} \frac{\sin\left[\frac{\pi J}{M}\left(\frac{Z_t}{T_s} - m\right)\right]}{\sin\left[\frac{\pi}{M}\left(\frac{Z_t}{T_s} - m\right)\right]} \left[\cos\left(\frac{J-1}{M}\right) \pi \left(\frac{Z_t}{T_s} - m\right)\right] \qquad \text{(E-17)}$$

and

$$E\left|W_m\right|^2 = \frac{1}{M^2}\sum_{k_1=0}^{M-1}\sum_{k_2=0}^{M-1} E\left[H(k_1)\,H^*(k_2)\right] e^{j\frac{2\pi}{M}m(k_1-k_2)}$$

$$= \frac{1}{M^2}\sum_{k=0}^{M-1} \mathrm{Var}\left[H(k)\right] + \frac{1}{M^2}\left(\frac{P_s}{P_s+P_n}\right)^2 \frac{\sin^2\left[\frac{\pi J}{M}\left(\frac{Z_t}{Ts}-m\right)\right]}{\sin^2\left[\frac{\pi}{M}\left(\frac{Z_t}{T_s}-m\right)\right]}$$

$$\cdot \cos^2\left[\left(\frac{J-1}{m}\right)\pi\left(\frac{Z_t}{T_s}-m\right)\right] \qquad \text{(E-18)}$$

Therefore,

$$\mathrm{Var}\left[W_m\right] = \frac{2J}{M^2}\,\frac{\mu M P_N(2P_s+P_N)}{(P_s+P_N)\,(2-2\mu M\,(P_s+P_N))} \qquad \text{(E-19)}$$

Substituting (E-17) and (E-19) in (E-12) gives

$$\mathrm{Var}\left[\hat{\tau}\right] = \frac{1}{2}\,\frac{\mu P_N(2P_s+P_N)(P_s+P_N)}{P_s^2\,(2-2\mu M\,(P_s+P_N))}\,K_q^2 \qquad \text{(E-20)}$$

where

$$K_q^2 = \frac{2JMT_s^2\left(1 + 12\left(\frac{Z_t}{T_s}\right)^2\right)}{\left[\sum_{m=-1}^{1} \frac{\sin\left[\frac{\pi J}{M}\left(\frac{Z_t}{T_s} - m\right)\right]}{\sin\left[\frac{\pi}{M}\left(\frac{Z_t}{T_s} - m\right)\right]} \cos\left[\frac{J-1}{M}\,\pi\left(\frac{Z_t}{T_s} - m\right)\right]\right]^2} \qquad \text{(E-21)}$$

Recall from [1] that the variance for the continuous adaptive tracker and the sin x/x interpolated adaptive tracker can be written in the same form as (E-20) with K_q replaced by K_c and K_I, respectively, where

$$K_c = \left[\frac{(2\pi B_s)^3}{3}\right]^{-1/2} \qquad \text{(E-22)}$$

and, letting $\Delta = Z_t/T_s$

$$K_I = \frac{\left[M \sum_{m_1=0}^{M-1} \sum_{m_2=0}^{M-1} f'(Z_t - m_1T_s)\, f'(Z_t - m_2T_s) \left\{\frac{\sin\left[\frac{\pi J}{M}(m_1 - m_2)\right]}{\sin\left[\frac{\pi}{M}(m_1 - m_2)\right]} \cos\left[\frac{J-1}{M}\,\pi\,(m_1 - m_2)\right]\right\}\right]^{1/2}}{\sum_{m=0}^{M-1} f''(Z_t - mT_s) \left\{\frac{\sin\left[\frac{\pi J}{M}\,(\Delta - m)\right]}{\sin\left[\frac{\pi}{M}\,(\Delta - m)\right]} \cos\left[\frac{J-1}{M}\,\pi\,(\Delta - m)\right]\right\}} \qquad \text{(E-23)}$$

$$f'(Z_t - mT_s) = \frac{\cos 2\pi B(Z_t - mT_s)}{(Z_t - mT_s)} - \frac{\sin 2\pi B(Z_t - mT_s)}{2\pi B(Z_t - mT_s)^2}$$

$$f'(0) = 0$$

$$f''(Z_t - mT_s) = \frac{2 \sin 2\pi B(Z_t - mT_s)}{2\pi B(Z_t - mT_s)^3} - \frac{2 \cos 2\pi B(Z_t - mT_s)}{(Z_t - mT_s)^2}$$

$$- \frac{2\pi B \sin 2\pi B(Z_t - mT_s)}{(Z_t - mT_s)}$$

$$f''(0) = - \frac{(2\pi B)^2}{3}$$

The variance of the peak estimate for the sin x/x and quadratic interpolators can be compared by an examination of the K_I and K_q. Therefore it is only necessary to numerically evaluate the expression for K_I, (E-23), and compare it to the expression for K_q, (E-21). Whichever term is larger has the greater variance and consequently worse performance.

The expressions for K_I and K_q were programmed on a computer and numerically evaluated. A sample frequency of 2400 Hertz was assumed with a 16 tap adaptive filter. A value of 2^{-10} was used for μ. Since the values of K_I and K_q are only dependent upon signal-to-noise ratio to the extent that they are evaluated in the vicinity of the true signal peak of the weights, an arbitrary SNR value of 20 dB was used.

The value of K_I was evaluated for signal bandwidths of 300, 600, 900, and 1200 Hz with the interpolator bandwidth parameter, B, matched to the signal

bandwidth B_s, in all cases. It was also found that K_I is dependent upon the position of the peak within the filter, so signal delays of 1, 2, 4, and 8 taps were evaluated. This dependence upon peak position only occurs when the peak is sufficiently near the end of the filter that part of the peak falls outside the filter. Table E-1 summarizes the values of K_I for these parameter selections.

The values of K_I obtained for a signal bandwidth of 300 Hertz may be suspect. By Equation (10) of [1] the value of (J-1) obtained for this signal bandwidth is,

$$(J-1) = \lfloor (300(1/2400)\ (16/2) \rfloor = 1$$

From [1] the expectation of the weights is:

$$E[H(k)] = \begin{cases} \dfrac{P_S}{P_S + P_N} e^{-j\frac{2\pi}{M}\Delta k} & , 0 \le k \le J-1 \\ 0 & , J-1 < k < M-J \\ \dfrac{P_S}{P_S + P_N} e^{-j\frac{2\pi}{M}\Delta(M-k)} & , M-J \le k \le M-1 \end{cases} \qquad \text{(E-24)}$$

Thus for (J-1) equal to 1 only 4 of the weights have nonzero expectations. This may be too few values for an accurate evaluation of K_I.

Similarly, K_q was also evaluated for signal bandwidths of 300, 600, 900 and 1200 Hertz. In the derivation of the expression for K_q it was assumed that in the worst case the center weight used for the quadratic fit would be located 1 tap away from the true peak of the weights. Therefore the value of Δ in (8) will vary

TABLE E-1. THEORETICAL VALUES OF K_I FOR VARYING SIGNAL BANDWIDTHS AND DELAYS

	Signal Delay = 1 Tap	Signal Delay = 2 Taps	Signal Delay = 4 Taps	Signal Delay = 8 Taps
Signal bandwidth = 1200 Hz	1.0221×10^{-3}	8.0756×10^{-4}	7.5334×10^{-4}	7.6028×10^{-4}
Signal bandwidth = 900 Hz	8.6724×10^{-4}	1.2009×10^{-3}	1.0969×10^{-3}	1.1584×10^{-3}
Signal bandwidth = 600 Hz	9.1604×10^{-4}	1.7065×10^{-3}	1.8678×10^{-3}	2.1715×10^{-3}
Signal bandwidth = 300 Hz	1.7928×10^{-3}	1.9906×10^{-3}	3.4006×10^{-3}	4.2747×10^{-3}

between 0.0 (for the center weight directly on the peak) and 1.0 (for the center weight one tap away from the peak). Accordingly bounds on the value of K_q were obtained by evaluating E-21 with Δ equal to 0.0 and 1.0. Table E-2 summarizes the values obtained for K_q.

Table E-3 provides a comparison of the performance of the two interpolators. By forming the ratio of K_I/K_q, the ratio of the standard deviations of the two interpolated estimates can be directly compared. If the ratio of K_I/K_q is greater than 1.0 then standard deviation of the sin x/x interpolated estimate is greater than that of the quadratic interpolated estimate. If the ratio of K_I/K_q is less than 1.0, then the sin x/x interpolator has the smaller standard deviation.

TABLE E-2. THEORETICAL VALUES OF K_q FOR VARYING SIGNAL BANDWIDTHS AND Δ

	$\Delta = 0.0$	$\Delta = 1.0$
Signal bandwidth = 1200 Hz	3.5136×10^{-4}	4.9690×10^{-4}
Signal bandwidth = 900 Hz	3.9284×10^{-4}	5.5556×10^{-4}
Signal bandwidth = 600 Hz	4.5361×10^{-4}	6.4150×10^{-4}
Signal bandwidth = 300 Hz	5.5556×10^{-4}	7.8567×10^{-4}

TABLE E-3. COMPARISON OF SIN X/X AND QUADRATIC INTERPOLATORS - THEORETICAL VALUES OF K_I/K_q FOR VARYING SIGNAL BANDWIDTHS AND DELAYS

	Signal Delay = 1 Tap		Signal Delay = 2 Taps		Signal Delay = 4 Taps		Signal Delay = 8 Taps	
	$\Delta = 0.0$	$\Delta = 1.0$	$\Delta = 0.0$	$\Delta = 1.0$	$\Delta = 0.0$	$\Delta = 1.0$	$\Delta = 0.0$	$\Delta = 1.0$
Signal bandwidth = 1200 Hz	2.9089	2.0569	2.2983	1.6252	2.1440	1.5161	2.1638	1.5300
Signal bandwidth = 900 Hz	2.2076	1.5610	3.0571	2.1617	2.7922	1.9744	2.9488	2.0852
Signal bandwidth = 600 Hz	2.0194	1.4280	3.7621	2.6602	4.1176	2.9116	4.7872	3.3851
Signal bandwidth = 300 Hz	3.2272	2.2820	3.5830	2.5336	6.1211	4.3283	7.6944	5.4408

In estimating the peak of the weights the sin x/x interpolator uses an iterative search routine to estimate the zero crossing of the interpolated derivative of the weights. Since the quadratic interpolator requires the evaluation of only a single expression in order to estimate the peak of the weights, it is both simpler to program and requires significantly fewer calculations than the sin x/x interpolator. Thus it appears that even though the quadratic interpolator is less complicated than the sin x/x interpolator, it offers advantages in both performance and implementation, at least for this selection of parameters.

As a check on this conclusion with real data and different parameters, Section 4.0 presents the results of processing acoustic data collected at sea using a line array, where both the sin (x)/x and quadratic interpolators were used. The adaptive filter used to process this taped data had 64 taps, and μ was set at 2^{-10}, 2^{-12}, 2^{-14}, and 2^{-16}. The input data bandwidth was 480 Hz, with a sample rate of 1 KHz. Using the results of this section, the theoretical performance of this tracker with broadband static targets has been computed for this range of μ. Figure E1 shows the predicted performance for the sin(x)/x interpolator, while Figures E2 and E3 show the predicted performance for the quadratic interpolator when $\Delta = 0$ and $\Delta = 1$, respectively. As above, the $\Delta = 0$ and $\Delta = 1$ case bound the theoretical bearing variance when the true peak of the weights is within one tap of the largest weight. For this set of parameter values,

$$K_I/K_q \approx 2.3 \quad \text{for} \quad \Delta = 0$$

and

$$K_I/K_q \approx .7 \quad \text{for} \quad \Delta = 1$$

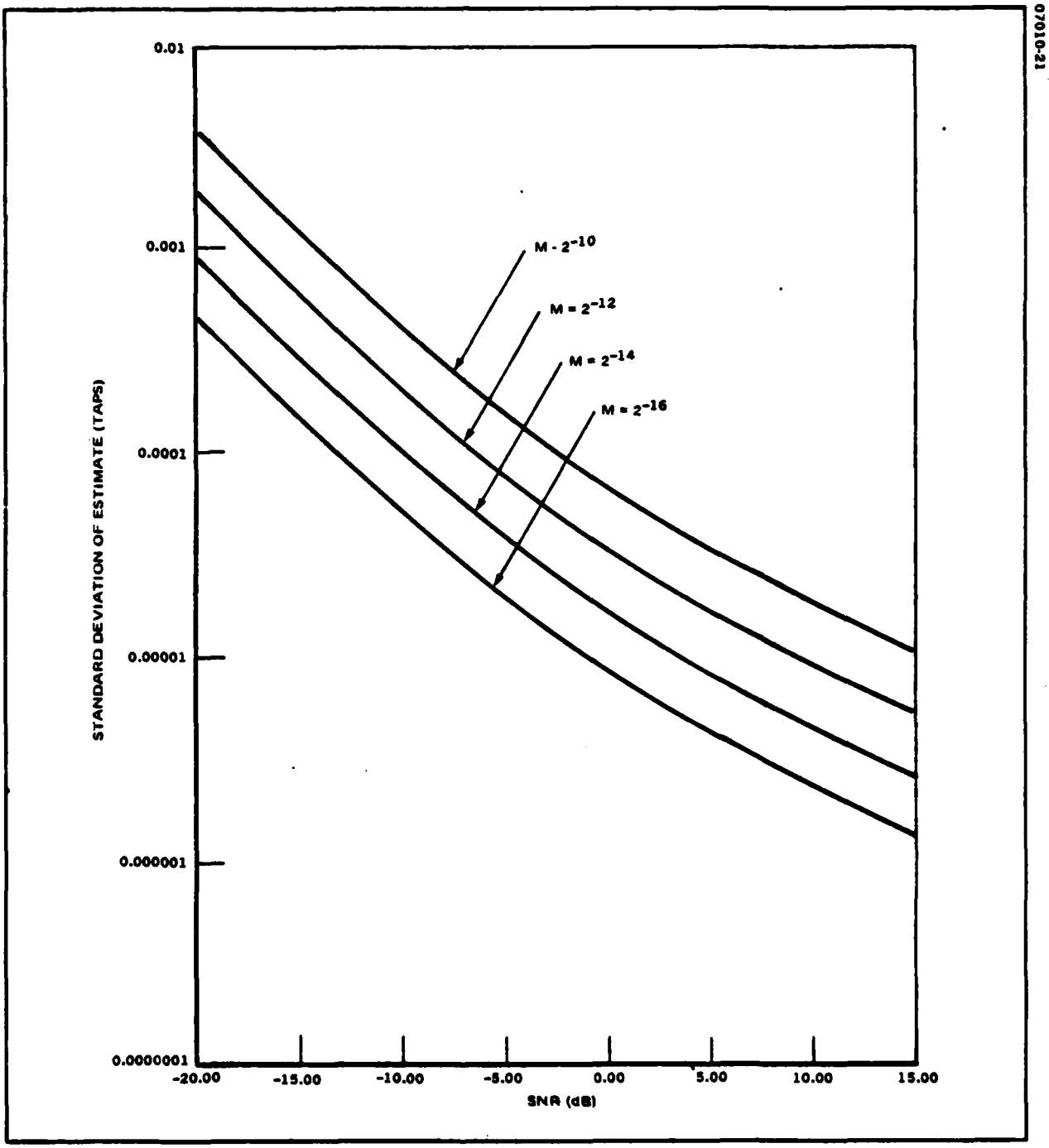

Figure E1. Predicted Standard Deviation of Bearing Estimate for Sea Tape Parameters With Sinx/x Interpolator sample frequency = 1KHz, M = 64 Taps, Bandwidth = 480 Hz

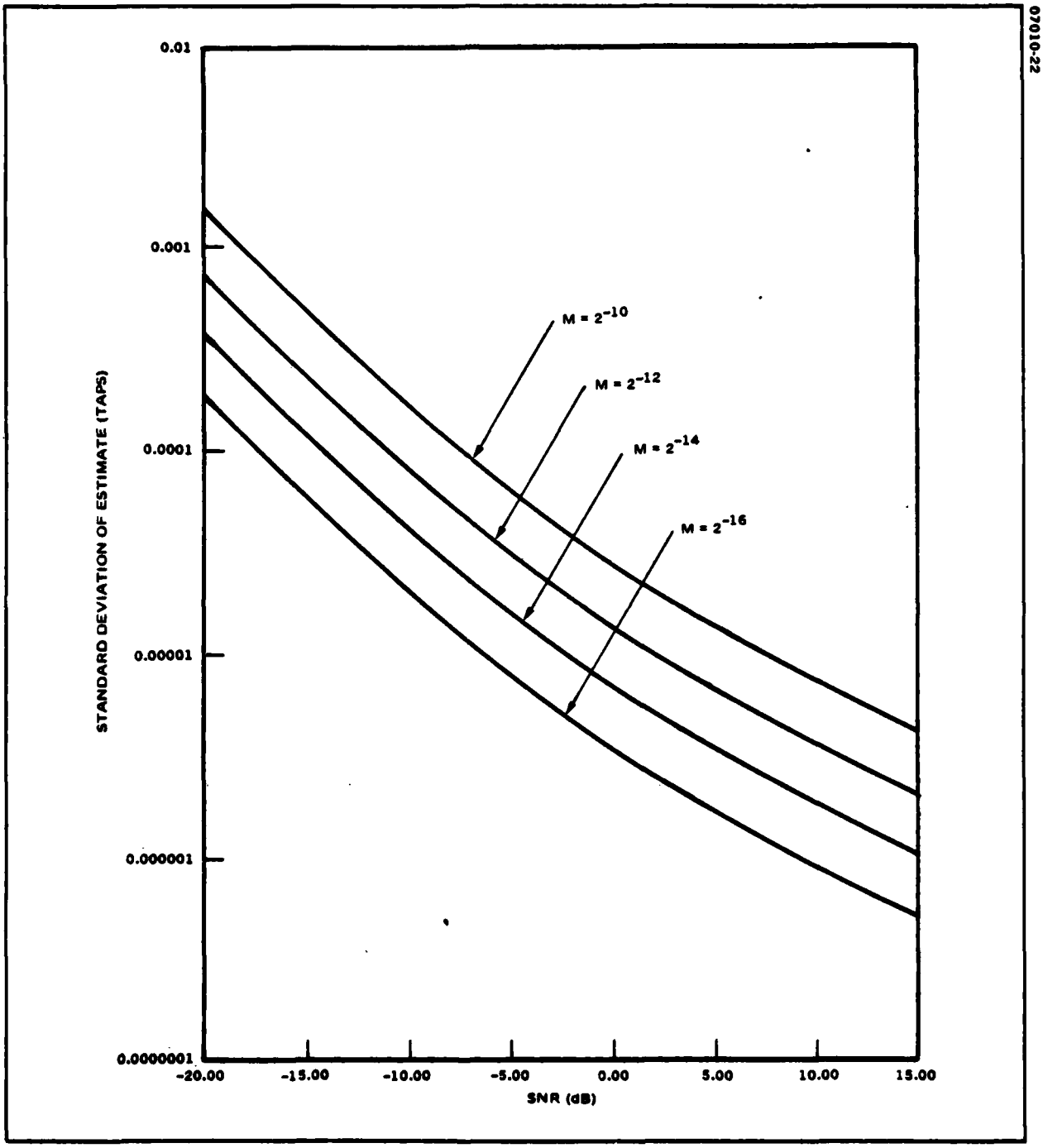

Figure E-2. Predicted Standard Deviation of Bearing Estimates for Sea Tape Parameters With Quadratic Interpolator – Sample Frequency = 1KHz, M = 64 Taps, Bandwidth = 480 Hz, $\Delta = 0$

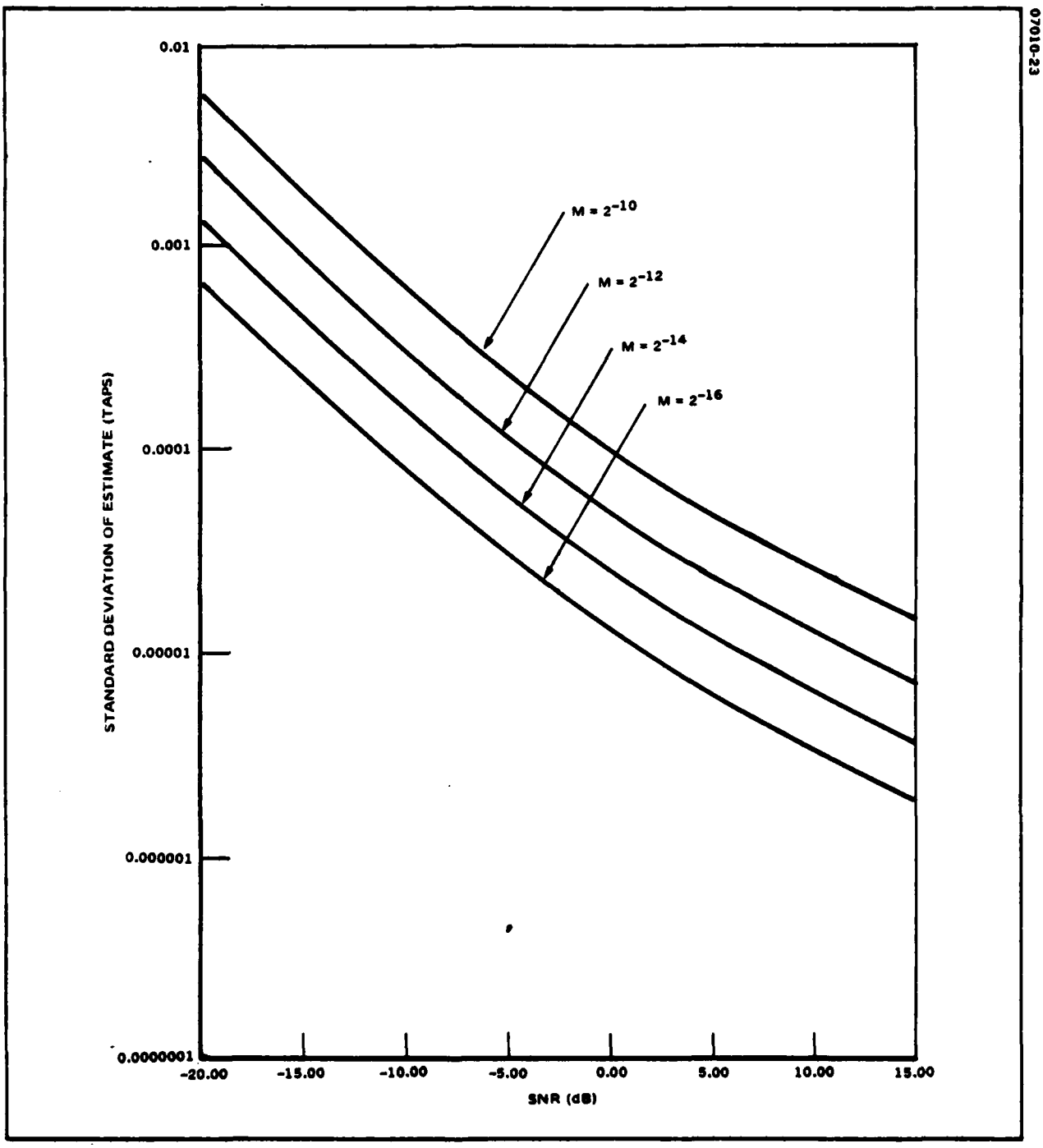

Figure E-3. Predicted Standard Deviation of Bearing Estimate for Sea Tape Parameters with Quadratic Interpolator – Sample Frequency - 1 KHz, M = 64 Taps, Bandwidth = 480 Hz, $\Delta = 1$

For this set of parameter values, the sin x/x interpolator can provide slightly better performance for some values of delay. However, the computational efficiency of the quadratic interpolator would still make it more attractive. These results are compared to those achieved with the sea tapes in Section 4.0.

APPENDIX F

CANCELLATION OF INTERFERENCE PRIOR TO TRACKING

APPENDIX F

CANCELLATION OF INTERFERENCE PRIOR TO TRACKING

There are basically two approaches to dealing with interference in the adaptive tracking system. One is to depend upon the spatial response of the split arrays and upon the adaptive properties of the tracker to provide relative immunity to the interference. The other approach is to attempt to cancel the interference from the half beam inputs to the adaptive tracker. It was shown during phase 2 of this study [2] that the primary effect of an interference is to introduce a bias in the bearing estimate, and that this bias can be quite severe when the signal-to-interference ratio is low at the split array outputs. Under these circumstances, it may be desirable to cancel the interference prior to tracking.

The adaptive noise canceller [5] is often used to eliminate an interference arriving on the sidelobes from a beam output. A reference sensor, for example an omnidirectional hydrophone that is spatially separated from the array, is used as a reference in the LMS canceller configuration of Figure F1. When the interference power dominates, the adaptive filter will spatially reject the interference from the beam output. Depending upon the spacing between the reference hydrophone and array and upon the separation of the target and interference, some rejection of the target signal will occur, but this will usually be acceptable in light of the interference rejection. Figure F2 shows this approach applied to the adaptive tracker. A reference is supplied for each half array and a canceller implemented in each half array output. A convenient choice for a reference may be a single hydrophone located in the opposite half array.

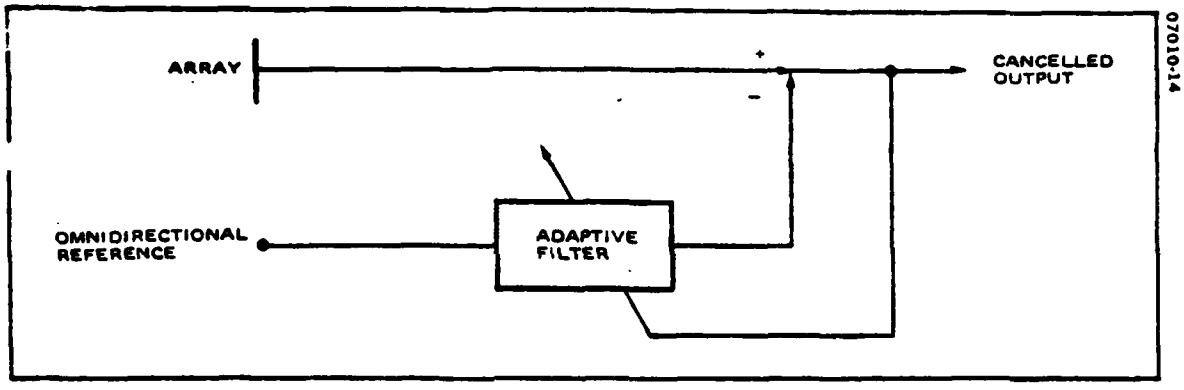

Figure F1.

LMS Adaptive Canceller

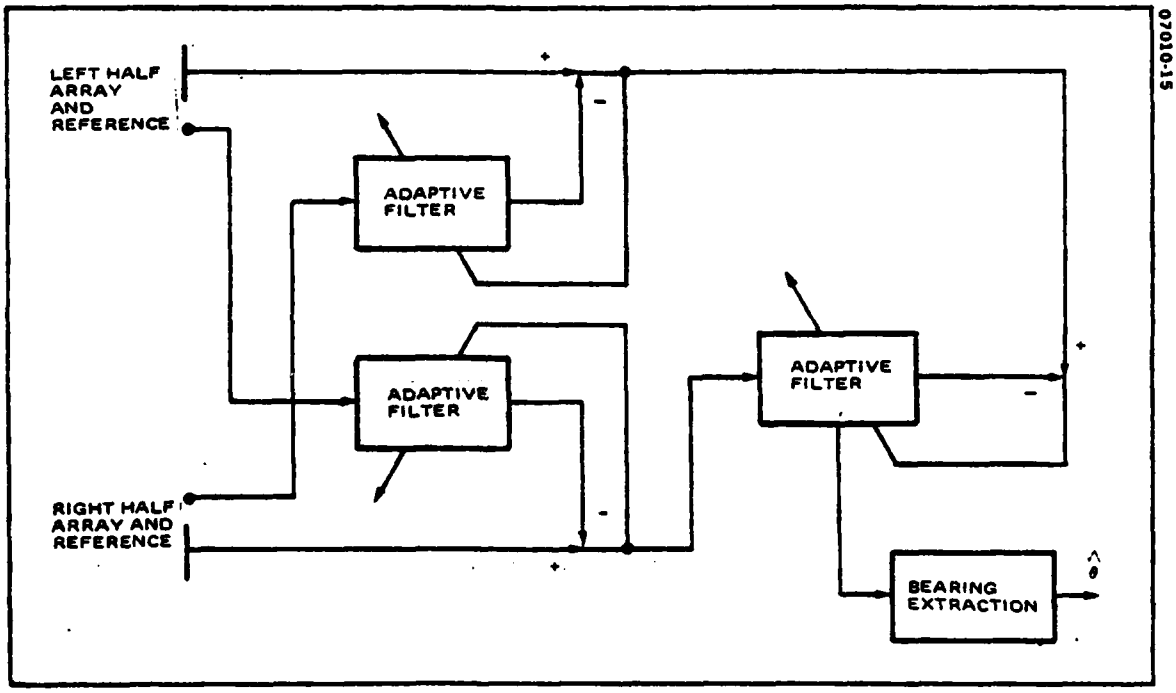

Figure F2.
Adaptive Cancellation Applied to the Adaptive Tracker

Inclusion of the cancellers of Figure F2 prior to the tracker will add the algorithm noise of the cancellers to beam outputs. In a well designed canceller, however, this noise will be negligible in comparison to the interference power rejected, and will therefore be tolerable. A more important possibility is that in inserting the transfer functions necessary to cancel the interference, the cancellers may modify the weight vector of the adaptive filter so as to bias the resulting estimate of target bearing. For broadband targets, this can be analyzed by determining the mean weight vector of the adaptive tracker with split beam cancellation and observing the effect of the cancellation on the location of the peak. With narrowband targets, a bias will be reflected in the phase of the FFT bin containing the signal.

Analysis of this effect is best performed in the frequency domain in terms of continuous Wiener filters. In steady state, the adaptive cancellers converge in the mean to discrete Wiener filters, which will approximate the continuous Wiener filters provided sample rate and filter length are judiciously chosen. Assuming that each reference is located in the opposite half array, referring to Figure F2, the inputs to the cancellers can be written

$$x_\ell(t) = \int b(\rho, \theta_s) s(t-\tau_s-\rho)\, d\rho + \int b(\rho, \theta_I)\, i\,(t - \tau_I - \rho)\, d\rho + \eta_{x\ell}(t) \qquad \text{(F-1)}$$

$$x_r(t) = \int b(\rho, \theta_s)\, s\,(t + \tau_s - \rho)\, d\rho + \int b(\rho, \theta_I)\, i\,(t + \tau_I - \rho)\, d\rho + \eta_{xr}(t) \qquad \text{(F-2)}$$

$$y_\ell(t) = s\left(t - \frac{d}{D}\,\tau_s\right) + i\left(t - \frac{d}{D}\,\tau_I\right) + \eta_{y\ell}(t) \qquad \text{(F-3)}$$

$$y_r(t) = s\left(t + \frac{d}{D}\tau_s\right) + i\left(t + \frac{d}{D}\tau_I\right) + \eta_{yr}(t) \qquad \text{(F-4)}$$

where

d = distance from split array phase center to its reference

D = distance between split array phase centers

$s(t)$ = signal

$i(t)$ = interference

$b(\rho, \theta)$ = impulse response of array to plane wave source at bearing θ

τ_s = delay between phase centers for the signal

τ_I = delay between phase centers for the interference

Here, $\eta_{x\ell}(t)$, $\eta_{xr}(t)$, $\eta_{y\ell}(t)$ and $\eta_{yr}(t)$ are zero mean and uncorrelated with each other. For plane wave signal and interference,

$$\tau_s = \frac{D}{2C} \sin \theta_s \qquad \text{(F-5)}$$

and

$$\tau_I = \frac{D}{2C} \sin \theta_I \qquad \text{(F-6)}$$

where θ_s and θ_I are bearings of the target and interference, respectively. Letting $W_\ell(t)$ and $W_r(t)$ be the impulse response of the two cancellers after convergence (i.e., the Wiener filters), then the inputs to the adaptive tracker are

$$\varepsilon_\ell(t) = x_\ell(t) - \int W_\ell(\rho)\, y_\ell(t - \rho)\, d\rho \qquad \text{(F-7)}$$

and

$$\epsilon_r(t) = x_r(t) - \int W_r(\rho)\, y_r(t-\rho)\, d\rho \qquad \text{(F-8)}$$

The Wiener filter transfer function corresponding to the adaptive tracker weight is given by

$$W_f(\omega) = \frac{S_{\epsilon_r \epsilon_\ell}(\omega)}{S_{\epsilon_\ell \epsilon_\ell}(\omega)} \qquad \text{(F-9)}$$

where

$S_{\epsilon_r \epsilon_\ell}(\omega)$ = cross spectral density between $\epsilon_r(t)$ and $\epsilon_\ell(t)$

and

$S_{\epsilon_\ell \epsilon_\ell}(\omega)$ = spectral density of $\epsilon_\ell(t)$

The functions $S_{\epsilon_r \epsilon_\ell}(\omega)$ and $S_{\epsilon_\ell \epsilon_\ell}(\omega)$ can be found from (F-7) and (F-8) using

$$S_{\epsilon_r \epsilon_\ell}(\omega) = \mathcal{F}\left\{ E\left[\epsilon_r(t)\, \epsilon_\ell(t+\tau) \right] \right\}$$

and

$$S_{\epsilon_\ell \epsilon_\ell}(\omega) = \mathcal{F}\left\{ E\left[\epsilon_\ell(t)\, \epsilon_\ell(t+\tau) \right] \right\}$$

where $\mathcal{F}[\cdot]$ denotes the Fourier transform, then

$$S_{\epsilon_r \epsilon_\ell}(\omega) = S_{x_r x_\ell}(\omega) + W_r^*(\omega)\, W_\ell(\omega)\, S_{y_r y_\ell}(\omega) - W_r^*(\omega)\, S_{y_r x_\ell}(\omega) - W_\ell(\omega)\, S_{x_r y_\ell}(\omega) \qquad \text{(F-10)}$$

where

$$S_{x_r x_\ell}(\omega) = \mathcal{F}\left\{E\left[x_r(t)\, x_\ell(t+\tau)\right]\right\}$$

$$S_{y_r y_\ell}(\omega) = \mathcal{F}\left\{E\left[y_r(t)\, y_\ell(t+\tau)\right]\right\}$$

$$S_{y_r x_\ell}(\omega) = \mathcal{F}\left\{E\left[y_r(t)\, x_\ell(t+\tau)\right]\right\}$$

$$S_{x_r y_\ell}(\omega) = \mathcal{F}\left\{E\left[x_r(t)\, y_\ell(t+\tau)\right]\right\}$$

with $W_r(\omega)$ and $W_\ell(\omega)$ the transfer functions corresponding to $W_r(t)$ and $W_\ell(t)$. Also,

$$S_{\varepsilon_\ell \varepsilon_\ell}(\omega) = S_{x_\ell x_\ell}(\omega) + \left|W_\ell(\omega)\right|^2 S_{y_\ell y_\ell}(\omega) - 2\mathrm{Re}\left[W_\ell(\omega)\, S_{x_\ell y_\ell}(\omega)\right] \qquad \text{(F-11)}$$

The Wiener filter transfer functions associated with the cancellers are given by

$$W_\ell(\omega) = \frac{S_{y_\ell x_\ell}(\omega)}{S_{y_\ell y_\ell}(\omega)} \quad \text{and} \quad W_r(\omega) = \frac{S_{y_r x_r}(\omega)}{S_{y_r y_r}(\omega)} \qquad \text{(F-12)}$$

Using expressions (F-1) through (F-4), to determine the required spectral densities, it can be shown that

$$W_\ell(\omega) = \frac{B(\omega, \theta_s) S_s(\omega) e^{-j\frac{\omega}{c}(1-\frac{d}{D})\tau_s} + B(\omega, \theta_I) S_I(\omega) e^{-j\frac{\omega}{c}(1-\frac{d}{D})\tau_I}}{P_T(\omega)} \qquad \text{(F-13)}$$

and

$$W_r(\omega) = \frac{B(\omega, \theta_s)S_s(\omega)e^{j\frac{\omega}{c}\left(1-\frac{d}{D}\right)\tau_s} + B(\omega, \theta_I)S_I(\omega)e^{j\frac{\omega}{c}\left(1-\frac{d}{D}\right)\tau_I}}{P_T(\omega)} \tag{F-14}$$

where $B(\omega, \theta) = \mathcal{F}\left[b(\tau, \theta)\right]$, $S_s(\omega)$ and $S_I(\omega)$ are the spectral densities of the signal and interference, and

$$P_T(\omega) = S_s(\omega) + S_I(\omega) + S_N(\omega) \tag{F-15}$$

with the power spectral densities of the noise $\eta_{y_e}(t)$ and $\eta_{y_r}(t)$ given by

$$S_{N_{y_\ell}}(\omega) = S_{N_{y_r}}(\omega) = S_{N_y}(\omega)$$

Similarly, it can be shown that

$$S_{x_r x_\ell}(\omega) = |B(\omega, \theta_s)|^2 S_s(\omega)e^{-j\frac{\omega}{c}2\tau_s} + |B(\omega, \theta_I)|^2 S_I(\omega)e^{-j\frac{\omega}{c}2\tau_I} \tag{F-16}$$

$$S_{y_\ell y_r}(\omega) = S_s(\omega)\, e^{-j\frac{\omega}{c}2\frac{d}{D}\tau_s} + S_I(\omega)e^{-j\frac{\omega}{c}2\frac{d}{D}\tau_I} \tag{F-17}$$

$$S_{y_r x_\ell}(\omega) = B(\omega, \theta_s)S_s(\omega)e^{-j\frac{\omega}{c}\left(1+\frac{d}{D}\right)\tau_s} + B(\omega, \theta_I)S_I(\omega)e^{-j\frac{\omega}{c}\left(1+\frac{d}{D}\right)\tau_I} \tag{F-18}$$

$$S_{x_r y_e}(\omega) = B^*(\omega, \theta_s) S_s(\omega) e^{-j\frac{\omega}{c}\left(1+\frac{d}{D}\right)\tau_s} + B^*(\omega, \theta_I) S_I(\omega) e^{-j\frac{\omega}{c}\left(1+\frac{d}{D}\right)\tau_I} \quad \text{(F-19)}$$

Combining (F-16) through (F-19) with (F-10) gives

$$S_{\epsilon_r \epsilon_\ell}(\omega) = S_s(\omega) \left[B(\omega, \theta_s) e^{-j\frac{\omega}{c}\tau_s} - W_e(\omega) e^{-j\frac{\omega}{c}\frac{d}{D}}\right]\tau_s^2 + S_I(\omega) \left[B(\omega, \theta_I)\, e^{-j\frac{\omega}{c}\tau_I} - W_e(\omega) e^{-j\frac{\omega}{c}\frac{d}{D}\tau_I}\right]^2 \quad \text{(F-20)}$$

Substituting the Wiener filter transfer functions from (F-13) and (F-14) into (F-20) gives

$$S_{\epsilon_r \epsilon_\ell}(\omega) = S_s(\omega) \left\{ B(\omega, \theta_s) e^{-j\frac{\omega}{c}\tau_s} - \frac{B(\omega, \theta_s) S_s(\omega) e^{-j\frac{\omega}{c}\tau_s} + B(\omega, \theta_I) S_I(\omega) e^{-j\frac{\omega}{c}\left[\left(1-\frac{d}{D}\right)\tau_I - \frac{d}{D}\tau_s\right]}}{P_T(\omega)} \right\}^2 + S_I(\omega) \left\{ B(\omega, \theta_I) e^{-j\frac{\omega}{c}\tau_s} - \frac{B(\omega, \theta_s) S_s(\omega) e^{-j\frac{\omega}{c}\left[\left(1-\frac{d}{D}\right)\tau_s - \frac{d}{c}\tau_I\right]} + B(\omega, \theta_I) S_I(\omega) e^{-j\frac{\omega}{c}\tau_I}}{P_T(\omega)} \right\}^2 \quad \text{(F-21)}$$

This can be simplified to

$$S_{\varepsilon_r\varepsilon_e}(\omega) = \frac{S_s(\omega)e^{-j\frac{\omega}{c}2\tau_s}}{P_T^2(\omega)} \left\{ B(\omega, \theta_s)\, S_I(\omega) + B(\omega, \theta_s)\, S_{N_y}(\omega) - B(\omega, \theta_I) S_I(\omega) e^{-j\frac{\omega}{c}\left(1-\frac{d}{D}\right)\left(\tau_I - \tau_s\right)} \right\}^2$$

$$+ \frac{S_I(\omega)e^{-j\frac{\omega}{c}2\tau_I}}{P_T^2(\omega)} \left\{ B(\omega, \theta_I)\, S_s(\omega) + B(\omega, \theta_I)\, S_{N_y}(\omega) - B(\omega, \theta_s) S_s(\omega) e^{-j\frac{\omega}{c}\left(1-\frac{d}{D}\right)\left(\tau_s - \tau_I\right)} \right\}^2$$

(F-22)

To determine the adaptive filter weight, $W_f(\omega)$, the spectral density $S_{\varepsilon_e\varepsilon_e}(\omega)$ must also be evaluated from (F-11). Evaluation of the required spectral densities yields

$$S_{\varepsilon_\ell \varepsilon_\ell}(\omega) = \frac{\left[\left[|B(\omega, \theta_s)|^2 S_s(\omega) + |B(\omega, \theta_I)|^2 S_I(\omega) + S_{N_x}(\omega)\right] P_T(\omega) \right.}{\left. - |B(\omega, \theta_s) S_s(\omega) e^{-j\frac{\omega}{c}\left(1 - \frac{d}{D}\right)\tau_s} + B(\omega, \theta_I) S_I(\omega) e^{-j\frac{\omega}{c}\left(1-\frac{d}{D}\right)\tau_s}|^2 \right]}{P_T(\omega)}$$

$$= \frac{\left[|B(\omega, \theta_s)|^2 S_s(\omega)\left[S_I(\omega) + S_{N_y}(\omega)\right] + |B(\omega, \theta_I)|^2 S_I(\omega)\left[S_s(\omega) + S_{N_y}(\omega)\right]\right.}{\left. + S_{N_x}(\omega) P_T(\omega) - 2B(\omega, \theta_s) B(\omega, \theta_I) S_s(\omega) S_I(\omega) \cos\left[\frac{\omega}{c}\left(1 - \frac{d}{D}\right)\left(\tau_s - \tau_I\right)\right]\right]}{P_T(\omega)}$$

(F-23)

Equations (F-21) and (F-23) can be used to write a general expression for the Wiener filter transfer function corresponding to the adaptive filter weight.

$$W_f(\omega) = \frac{S_s(\omega) e^{-j\frac{\omega}{c} 2 \tau_s}}{P_T(\omega)} \cdot \frac{\left[B(\omega, \theta_s) S_I(\omega) + B(\omega, \theta_s) S_{N_y}(\omega) - B(\omega, \theta_I) S_I(\omega) e^{-j\frac{\omega}{c}\left(1 - \frac{d}{D}\right)(\tau_s - \tau_I)}\right]^2}{D(\omega)}$$

$$+ \frac{S_I(\omega) e^{-j\frac{\omega}{c} 2 \tau_I}}{P_T(\omega)} \cdot \frac{\left[B(\omega, \theta_I) S_s(\omega) + B(\omega, \theta_I) S_{N_y}(\omega) - B(\omega, \theta_s) S_s(\omega) e^{-j\frac{\omega}{c}\left(1 - \frac{d}{D}\right)(\tau_I - \tau_s)}\right]^2}{D(\omega)}$$

(F-24)

where $D(\omega)$ is the numerator of (F-23)

For convenience, let $B_s = B(\omega, \theta_s)$, $B_I = B(\omega, \theta_I)$, and $\gamma = \frac{\omega}{c}\left(1 - \frac{d}{D}\right) 2\,(\tau_s - \tau_I)$. Dropping the argument, ω, define

$$A = |B_s - B_I e^{-j\gamma}| = |B_I - B_s e^{j\gamma}|$$

$$\psi_1 = \tan^{-1}\left[\frac{B_I \sin\gamma}{B_s - B_I \cos\gamma}\right]$$

and

$$\psi_2 = -\tan^{-1}\left[\frac{B_s \sin\gamma}{B_I - B_s \cos\gamma}\right]$$

In this notation, (F-24) can be written as

$$W_f(\omega) = \frac{1}{S_I S_s A^2 + S_s S_{P_y} |B_s|^2 + S_I S_{N_y} |B_I|^2 + S_{N_x} P_T}$$

$$\left\{\frac{S_s}{P_T} e^{-j\frac{\omega}{c}2\tau_s}\left[S_I A e^{-j\psi_1} + S_{N_y} B_s\right]^2 + \frac{S_I}{P_T} e^{-j\frac{\omega}{c}2\tau_I}\left[S_s A e^{+j\psi_2} + S_{N_y} B_I\right]^2\right\}$$

(F-25)

If the interference is in the sidelobes, then $B_s \gg B_I$, so that $A \approx B_s$, and

$$W_f(\omega) \approx \frac{1}{|B_s|^2 S_s\left(S_I + S_{N_y}\right) + S_I S_{N_y} |B_I|^2 + S_{N_x} P_T}$$

$$\left\{ \frac{|B_s|^2 S_s}{P_T} e^{-j\frac{\omega}{c} 2\tau_s} \left[S_I e^{-j\psi_1} + S_{N_y} \right]^2 \right.$$

$$\left. + \frac{|B_s|^2 S_I}{P_T} e^{-j\frac{\omega}{c} 2\tau_I} \left[S_s e^{j\psi_2} + \frac{B_I}{B_s} S_{N_y} \right]^2 \right\} \qquad \text{(F-26)}$$

If the interference dominates, $S_I \gg S_s$ and $S_I \gg S_{N_y}$, then $P_T \approx S_I$ and

$$W_f(\omega) \approx \frac{|B_s|^2 S_s}{|B_s|^2 S_s + |B_I|^2 S_{N_y} + S_{N_x}}$$

$$\left\{ e^{-j\left[\frac{\omega}{c} 2\tau_s - 2\psi_1\right]} + \frac{S_s}{S_I} e^{-j\frac{\omega}{c} 2\tau_I} \left[e^{j\psi_2} + \frac{B_I}{B_s} \frac{S_{N_y}}{S_s} \right]^2 \right\} \qquad \text{(F-27)}$$

where, from above, $(B_I/B_s) \ll 1$.

Now, assume that $|B_I|^2 S_{N_y} \ll S_{N_x}$, since S_{N_x} involves the noise from the entire half array and $|B_I|^2$ represents a sidelobe response. Then for high SNR at the beamformer output, $B_s S_s \gg S_{N_x}$, (F-27) reduces to

$$W_f(\omega) \approx e^{-j\left[\frac{\omega}{c} 2\tau_s - 2\psi_1\right]} + \frac{S_s}{S_I} e^{-j\left[\frac{\omega}{c} 2\tau_I + 2\psi_2\right]} \qquad \text{(F-28)}$$

Note that if the cancellers were not used on the split beams this would have been

$$W_{fo}(\omega) \approx \frac{|B_s|^2 S_s}{|B_I|^2 S_I} e^{-j\frac{\omega}{c} 2\tau_s} + e^{-j\frac{\omega}{c} 2\tau_I} \qquad \text{(F-29)}$$

On the other hand, for small SNR at the beamformer outputs, $B_s S_s \ll S_{N_x}$,

$$W_f(\omega) \approx \frac{|B_s|^2 S_s}{S_{N_x}} \left\{ e^{-j\left[\frac{\omega}{c} 2\tau_s - 2\psi_1\right]} + \frac{S_s}{S_I} e^{-j\frac{\omega}{c} 2\tau_s} \left[e^{j\psi_2} + \frac{B_I}{B_s} \frac{S_{N_y}}{S_s} \right]^2 \right\} \qquad \text{(F-30)}$$

while the transfer function in the absence of the cancellers would be as in (F-28). Therefore the overall amplitude of the weight has been reduced from the high SNR case, but the interference has still been suppressed relative to the signal.

First, consider the narrowband tracker, in which the bearing estimate is extracted from the phase of the Fourier transform of the weight sector at the signal frequency. From [2], it can be seen that if tracking is to be possible with acceptable accuracy in the absence of the interference, then $B_s S_s / S_{N_x} \gg 1$. Since S_{N_x} includes the contribution of all the phones in the array, $S_{N_x} > S_{N_y}$,

so the condition $B_s S_s \gg B_I S_{N_y}$ is met, and (F-28) is the relevant transfer function. The phase at a frequency, ω, is

$$\phi_f = \tan^{-1} \left\{ \frac{\sin\left[\frac{\omega}{c} 2\tau_s - 2\psi_1\right] + \frac{S_s}{S_I} \sin\left[\frac{\omega}{c} 2\tau_I + 2\psi_2\right]}{\cos\left[\frac{\omega}{c} 2\tau_s - 2\psi_1\right] + \frac{S_s}{S_I} \cos\left[\frac{\omega}{c} 2\tau_I + 2\psi_2\right]} \right\} \qquad \text{(F-31)}$$

As $(S_I/S_s) \to \infty$, there is a residual bias of $2\psi 1$ in the phase. Note, however, that when the interference is in the sidelobes, $B_s \gg B_I$,

$$\psi_1 \approx \tan^{-1}\left[\frac{B_I}{B_s} \sin\left[\frac{\omega}{c}\left(1 - \frac{d}{D}\right) 2\left(\tau_s - \tau_I\right)\right]\right] \approx \frac{B_I}{B_s} \sin\left[\frac{\omega}{c}\left(1 - \frac{d}{D}\right) 2|\tau_s - \tau_I|\right]$$

$$\approx \frac{B_I}{B_s} \frac{\omega}{c}\left(1 - \frac{d}{D}\right) 2|\tau_s - \tau_I| \qquad \text{(F-32)}$$

so the residual bias is very small. It can be made arbitrarily small by placing the references very close to the phase centers, so $(1 - d/D) \approx 0$.

Letting $\phi_f = \frac{\omega}{c} 2\tau_s - 2\psi 1 + C_1$, by a trigonometric identity,

$$C_1 = \tan^{-1} \left\{ \frac{\sin\left[\frac{\omega}{c} 2\left(\tau_s - \tau_I\right) - 2\left(\psi_1 + \psi_2\right)\right]}{\frac{S_I}{S_s} + \cos\left[\frac{\omega}{c} 2\left(\tau_s - \tau_I\right) - 2\left(\psi_1 + \psi_2\right)\right]} \right\} \qquad \text{(F-33)}$$

The bias in the phase, $B\phi$, is then

$$B_\phi = C_1 - 2\psi_1$$

Again, when $B_s \gg B_I$, it can be seen that

$$\psi_2 \approx \frac{\omega}{c}\left(1 - \frac{d}{D}\right) 2\,(\tau_s - \tau_I) \gg \psi_1 \tag{F-34}$$

Substituting this in (F-33) for $S_I/S_s \gg 1$ gives

$$B_\phi \quad \frac{S_s}{S_I} \sin \frac{\omega}{c} \frac{d}{D} 2\,|\tau_s - \tau_I| - \frac{B_I}{B_s} \sin \frac{\omega}{c}\left(1 - \frac{d}{D}\right) 2|\tau_s - \tau_I| \tag{F-35}$$

$$\approx 2 \quad \frac{S_s}{S_I} \quad \frac{d}{D} - \frac{B_I}{B_s} \quad (1 - \frac{d}{D}) \quad \frac{\omega}{c}\,|\tau_s - \tau_I|$$

Since both B_I/B_s and S_s/S_I are small, the bias inserted by the cancellers is small.

In the broadband adaptive tracker, a bias will appear as a time shift in the weight vector. Consider the case when signal, interference, and noise all have the same spectral shape, i.e.,

$$S_s(\omega) = P_S\, S_o(\omega) \qquad S_I(\omega) = P_I\, S_o(\omega)$$

$$S_{N_x}(\omega) = P_{N_x}\, S_o(\omega) \qquad S_{N_y}(\omega) = P_{N_y}\, S_o(\omega) \tag{F-36}$$

Substituting these into (F-27) yields the following results for the weight vector;

for $B_s P_s \gg P_{N_x}$

$$W_f(\omega) = e^{-j\left[\frac{\omega}{c} 2\tau_s - 2\psi_1\right]} + \frac{S_s}{S_I}\, e^{-j\left[\frac{\omega}{c} 2\tau_I + 2\psi_1\right]} \tag{F-37}$$

for $B_s P_s \ll P_{N_x}$

$$W_f(\omega) = \frac{|B(\omega, \theta_s)|^2 P_s}{P_{N_x}}$$

$$\left\{ e^{-j\left[\frac{\omega}{c} 2\tau_s - 2\psi_1\right]} + \frac{P_s}{P_I} e^{-j\frac{\omega}{c} 2\tau_I} \left[e^{j\psi_2} + \frac{B(\omega, \theta_I)}{B(\omega, \theta_s)} \frac{P_{N_y}}{S_s} \right]^2 \right\} \quad \text{(F-38)}$$

In either case, the interference related peak will have been sufficiently suppressed to have negligible effect on the location of the signal peak. Upon inverse transforming to obtain the mean weight vector for the tracker, using (F-32), the signal peak is seen to occur at

$$\tau_P \quad 2\tau_s - 2 \frac{B_I}{B_s} \frac{1}{c} (1 - \frac{d}{D}) 2|\tau_s - \tau_I|$$

so the bias in delay is, substituting from (F-5) and (F-6)

$$B_\tau = -2 \frac{B_I}{B_s} \frac{D}{c^2} (1 - \frac{d}{D}) |\sin \theta_s - \sin \theta_I|$$

Again, since $B_I \ll B_s$, the bias is small, and can be made arbitrarily small by placing the references at the array phase centers.

DEPARTMENT OF DEFENSE FORMS

F-200.1473 *DD Form 1473:* Report Documentation Page

UNCLASSIFIED

SECURITY CLASSIFICATION OF THIS PAGE (When Data Entered)

REPORT DOCUMENTATION PAGE	READ INSTRUCTIONS BEFORE COMPLETING FORM
1. REPORT NUMBER	2. GOVT ACCESSION NO. AD-A096 469 (9) Final
4. TITLE (and Subtitle) Final Report on Phase 3 of the Adaptive Tracking System Study (14) (14)	5. TYPE OF REPORT & PERIOD COVERED Research Report, October 1979 to October 1980 on (6) - 3, FR 81-11-70
7. AUTHOR(s) (10) P. L. Feintuch, F. A. Reed, N. J. Bershad, C. M. Flynn	8. CONTRACT OR GRANT NUMBER(s) N00024-79-C-6405 (15)
9. PERFORMING ORGANIZATION NAME AND ADDRESS Hughes Aircraft Company, PO Box 3310, Fullerton, CA 92634	10. PROGRAM ELEMENT, PROJECT, TASK AREA & WORK UNIT NUMBERS
11. CONTROLLING OFFICE NAME AND ADDRESS Naval Sea Systems Command, Code 63R, Department of the Navy, Washington, D.C. 20364 (11)	12. REPORT DATE October 1980
	13. NUMBER OF PAGES (12) 181
14. MONITORING AGENCY NAME & ADDRESS(If different from Controlling Office)	15. SECURITY CLASS. (of this report)
	15a. DECLASSIFICATION/DOWNGRADING SCHEDULE

16. DISTRIBUTION STATEMENT (of this Report)

Distribution of this document is unlimited.

17. DISTRIBUTION STATEMENT (of the abstract entered in Block 20, if different from Report)

18. SUPPLEMENTARY NOTES

19. KEY WORDS (Continue on reverse side if necessary and identify by block number)

Adaptive Filters, Adaptive Bearing Trackers, Bearing Accuracy, Broadband Bearing Trackers, LMS Adaptive Filters, Linearly Varying Bearing Narrowband Bearing Trackers, Split beam trackers

20. ABSTRACT (Continue on reverse side if necessary and identify by block number)

A specific split beam adaptive tracker using the LMS adaptive filter is investigated. Implementation of the tracker concept in an operational sonar is discussed, and a simplified time delay interpolator described and analyzed.

The report considers the effects of real world sonar phenomena on the tracker performance and the simulation of the tracker on actual sea tapes. The effects of multipath on tracker performance and the effects of array

DD FORM 1 JAN 73 1473 EDITION OF 1 NOV 65 IS OBSOLETE S/N 0102-014-6601

UNCLASSIFIED

SECURITY CLASSIFICATION OF THIS PAGE (When Data Entered)

172270

Copy

20. Abstract

size on bearing lag are analyzed. Adaptive cancellation of interferences prior to the tracker is shown to produce negligible bias in the bearing estimate. Bearing estimator structures for use with combined broadband and narrowband targets are developed. The tracker is shown to track actual sonar targets from sea tapes with variance in agreement with theoretical predictions. A single tracker structure can be used to track multiple targets using both broadband and narrowband energy.

INITIAL DISTRIBUTION LIST

Commander
Naval Sea Systems Command
Department of the Navy
Washington, D.C. 20362
Attn: D.E. Porter, 63R-11

Commander
Naval Sea Systems Command
Department of the Navy
Washington, D.C. 20362
Attn: 633X

Command
Naval Sea Systems Command
Department of the Navy
Washington, D.C. 20362
Attn: 631X

Commander
Naval Sea Systems Command
Department of the Navy
Washington, D.C. 20362
Attn: 631Y

Commander
Naval Sea Systems Command
Department of the Navy
Washington, D.C 20362
Attn: 634X

Commander
Naval Sea Systems Command
Department of the Navy
Washington, D.C. 20362
Attn: 63D

Commander
Naval Sea Systems Command
Department of the Navy
Washington, D.C. 20362
Attn: Library 09G3

Defense Documentation Center
Defense Services Administration
Cameron Station, Building 5
5010 Duke Street
Alexandria, Virginia 22314

Director
Naval Research Laboratory
Department of the Navy
Washington, D.C. 20375

Chief of Naval Research
800 N. Quincy Street
Arlington, VA 22217
Attn: Code 466

Commander
Naval Ocean Systems Center
San Diego, CA 92152
Attn: Library

Officer in Charge
New London Laboratory
Naval Underwater Systems Center
New London, Connecticut 06320

David Taylor Naval Ship Research &
Development Center
Bethesda, MD 20034

Commander
Naval Surface Weapons Center
White Oak
Silver Spring, MD 20910

Commanding Officer
Naval Coastal Systems Center
Panama City, Florida 32407

Officer in Charge
New London Laboratory
Naval Underwater Systems Center
New London, CT 06320
Attn: Library

Commanding Officer
Naval Air Development Center
Johnsville
Warminster, PA

Office of the Director of Defense
Research and Engineering
Room 3C128, The Pentagon
Washington, D.C. 20301

INITIAL DISTRIBUTION LIST (Continued)

AFPRO, Hughes Aircraft Company
Centineta and Teale Street
Culver City, CA 90230


LMED